5-2016

Performance Assessment of Deteriorated and Retrofitted Steel HP Piles

Steven T. Stauffer
University of Nebraska-Lincoln, steven.t.stauffer@gmail.com

Stauffer, Steven T., "Performance Assessment of Deteriorated and Retrofitted Steel HP Piles" (2016). *Civil Engineering Theses, Dissertations, and Student Research*. 92.
http://digitalcommons.unl.edu/civilengdiss/92

PERFORMANCE ASSESSMENT OF DETERIORATED AND RETROFITTED STEEL HP PILES

by

Steven Stauffer

A THESIS

Presented to the Faculty of
The Graduate College at the University of Nebraska
In Partial Fulfillment of Requirements
For the Degree of Master of Science

Major: Civil Engineering

Under the Supervision of Professor Joshua Steelman

Lincoln, Nebraska

May, 2016

PERFORMANCE ASSESSMENT OF DETERIORATED AND RETROFITTED STEEL HP PILES

Steven Stauffer, M.S.

University of Nebraska, 2016

Advisor: Joshua Steelman

Deterioration of aging bridges can be attributed to an assortment of mechanisms throughout the structure, with remediation policies also varying. This study focused on assessing the validity of the Nebraska Department of Roads' (NDOR) reinforced concrete encasement retrofit for corroded steel HP piles. Experiments were designed and conducted to test the capacity of the NDOR retrofit and evaluate failure limit states. Two pile locations were considered: abutment and pile bent. For each location there was a non-deteriorated, deteriorated, and retrofitted case. These cases represented the pile at key stages during its life. NDOR's concrete encasement retrofit provided the required stability and composite action to return the pile to full capacity. The key finding of the experimental study was a greater than anticipated steel-concrete bond stress. The bond stress observed was three times greater than the nominal recommended by AISC. A computational study was also conducted to investigate sensitivities and alternative configurations, such as geometric alterations, material properties, and reinforcement. The computational study emphasized the load transfer mechanism's dependence on the type of load applied. Piles governed by axial compression with relatively minor moment were observed to be more sensitive to bond. The moment dominated loads required more surface to surface pressure transfer or bearing. Further investigation is recommended to determine the bond characteristics of steel fully encased by concrete.

ACKNOWLEDGEMENTS

I am very humbled to be where I am today and I know that I have many to thank for their support and guidance to this point. There is no place like Nebraska and I am reminded of that every day. I have also been challenged by my peers to think more globally and have learned a great deal about cultures far from Nebraska. I am very grateful for the diversity in those I worked with.

I would like to specifically thank a few people starting with Dr. Steelman. I am very thankful for the opportunity to work with him on this project. He has taught me a great deal about structural engineering and challenged me to be a better engineer. Dr. Steelman's mentoring has been invaluable and I am glad I had to opportunity to work with him in my time at UNL.

For all the time spent in the lab during the summer, I have Peter Hilsabeck to thank for all of his insight and guidance. Peter was instrumental in the design and setup of the experiments. He also taught me skills that can't be learned in the classroom, and that there is great joy in life, don't stop believe.

I'd be remiss if I didn't thank, not only my parents, but also my sisters for all their support. Although they don't always understand what it is I do, they take the time to listen and show interest. Thank you Mom and Dad for instilling in me the drive, work ethic, and character that has led to my successes.

My biggest cheerleader has been my wife. Taylor has supported me throughout this entire process and has been the silver lining on the days when nothing seemed to be working. I wouldn't want anyone else right there with me, and I look forward to our future and all the good that is to come, I love you.

TABLE OF CONTENTS

LIST OF FIGURES

LIST OF TABLES

CHAPTER 1 INTRODUCTION

1.1 BACKGROUND AND NEW RESEARCH

Aging bridges experience deterioration through a range of mechanisms and at various locations within the structural system. Remediation strategies also vary, depending on the type and location of deterioration. This project specifically focuses on corrosive deterioration resulting in section loss in steel HP piles. Steel HP piles are used for abutment foundations and also for exposed pile bents at intermediate substructure locations along the bridge span. At abutments, the piles are initially protected from exposure by earth fill, but over time the fill can be eroded and the upper portions of the piles are exposed. Pile bents are constantly exposed, but typically painted to protect the steel from deterioration. As with the abutment soil, the paint on pile bents wears away over time, leaving the steel exposed to deleterious environmental influences.

When piles experience section loss, the bridge must either be evaluated and possibly posted to limit the permissible load allowed to pass over the bridge, or the piles must be retrofitted to slow the corrosion and/or to restore the capacity of the piles. Research to restore capacity of piles often addressed post-seismic repairs, rather than long-term corrosive deterioration, but the methods share similar objectives. The goal of this research project is to validate a commonly employed method in Nebraska, with reference to other department of transportation’s (DOT’s) practices, if applicable.

Nebraska Department of Roads’ current policy for repairing corroded steel HP piles is as follows:

1. Clean the corroded area by sandblasting the pile.
2. Place temporary forms and reinforcing steel.

3. With formwork and reinforcing steel in place, encase the pile from above the water line to below the mud line in concrete.

Extending the encasement above the water line and below the mud line reduces corrosion susceptibility for the steel pile. The concrete is reinforced with rebar to provide confinement and nominally develop some measure of composite action. A rebar cage is built to reinforce the boundary of the concrete, in addition to rebar doweled through the pile web. The rebar cage provides benefits of confinement for axial load transfer, in addition to acting as flexural reinforcing.

1.2 THESIS OVERVIEW

The remainder of this thesis contains discussions on the literature review and experiments conducted for the Nebraska Department of Roads (NDOR), and computational modeling developed to further assess potential changes to the NDOR standard retrofit. The literature review provides an overview of current DOT practices, proprietary products, and previous research related to steel pile retrofits. The merits of these repairs are considered with respect to their structural capacity restoration, ease of installation, and durability. The experimental portion discusses the process and results of tests conducted on specimens provided with a standard steel pile retrofit used by the Nebraska Department of Roads. Finally, a set of computational models are examined to illustrate the effect of changing both the strength of the material utilized and the geometry of the retrofit.

CHAPTER 2 LITERATURE REVIEW

2.1 INTRODUCTION

DOTs, proprietors, and researchers have been working for years to develop reliable and efficient ways to maintain and prolong the life of bridges across the United States. This section lists current practices of several DOTs and provides an overview of the state-of-practice for repair techniques in use, as well as proprietary repair methods with developing technologies.

2.2 DOT RETROFIT PROCEDURES

The individual state's DOT repair procedures that will be addressed in the following sections were identified from DOT maintenance manuals and research. Repair procedures from Delaware Department of Transportation (DELDOT), Georgia Department of Transportation (GDOT), and Florida Department of Transportation (FDOT) will be discussed, in addition to research funded by Iowa Department of Transportation (IADOT) and Wisconsin Department of Transportation (WisDOT). Many of the repair procedures follow a similar process, so in order to reduce redundancies, all details will be discussed in a comprehensive section for each repair type.

2.2.1 GENERAL RETROFIT PROCEDURES

All repair types require similar cleaning and preparation, which includes that the pile be sand blasted to near white steel. For both concrete encasement and FRP jackets, cover below the mud line and well above the high water line are required to reduce corrosion initiation. The different types of repairs are described in the following sections.

2.2.2 STEEL CHANNELS

IADOT (Wipf, 2003), GDOT (2012), and WisDOT (Wan, 2013) described a retrofit that utilizes steel channels bolted to the exterior of the flange, across the damaged area of the pile, as shown in Figure 2.1. This retrofit's installation would require minimal effort and the design capacity could be determined using current steel design techniques. Due to the susceptibility of this repair to corrosion, it would only serve as a temporary repair for strength. GDOT also permits a welded alternative to the bolted channels. The installation and capacity determination would be similar in procedure to the bolted alternative.

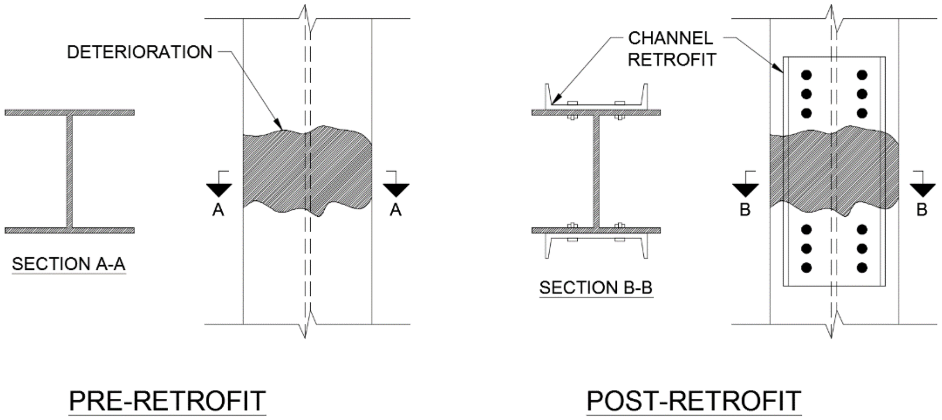

Figure 2.1 Steel channel retrofit details (GDOT, 2012)

2.2.3 STEEL PLATES

The use of welded steel plates was only found in the United States, Department of the Army (1991) repair procedure manual. This repair type is similar to the channel repair method and would have similar disadvantages of susceptibility to continued corrosion. One advantage of the retrofit is in addition to the plates welded to the flanges, steel plates are welded to the web of the pile which increases the web thickness and the stability of the cross-section.

2.2.4 CONCRETE ENCASEMENT

FDOT (2011), GDOT (2012), and WisDOT (Wan, 2013) each prescribe a type of concrete encasement procedure. Each procedure requires reinforcement in the concrete, although the requirement is nominal and prescriptive, the reinforcing provides confinement to the concrete and an increase to strength. Georgia describes both a circular and square concrete encasement retrofit, in contrast to Florida which does not prescribe a shape. Research performed for Wisconsin (Wan, 2013) showed a square encasement detail similar to that used by Ohio DOT. By using concrete, continuous bracing is provided along the deteriorated section, but also inhibits observation of the steel after the repair is made. FDOT discourages the use of jackets because it is difficult to monitor the condition of the steel after the jacket is installed.

2.2.5 FIBERGLASS JACKET

Fiberglass jackets are a newer steel pile repair based on the principle of the concrete encasement repair. The fiberglass jacket replaces the reinforcing steel used in the concrete encasement repair by providing confinement in compression and tension resistance in flexure. In addition, the FRP acts as a stay-in-place form for the concrete. Two common types of FRP available are formed and wrapped, and properties of these are dictated by the proprietor. Three DOTS, DELDOT (2012), FDOT (2011), and WisDOT (Wan, 2013) mention this method in their manuals, but offer little guidance because the material is relatively novel for civil engineering applications. This technique is similar to those previously mentioned for preparation and placement.

2.3 PROPRIETARY PRODUCTS

In addition to current DOT procedures, proprietary methods are also available. Like the DOT methods, these remediation approaches are similar in nature and can be categorized.

2.3.1 FABRIC JACKET

An alternative jacketing method uses a fabric wrap to enclose the concrete at the deteriorated location. An example of this type of retrofit was observed by the author during a site visit organized by NDOR to observe a demonstration of an FRP wrap. It was unclear whether the jacket incorporated steel reinforcing, but images available on a manufacturer’s website (Construction Techniques, Inc., 2014) suggest that internal steel reinforcing may have been installed. Little information is available for the use and effectiveness of this method in Nebraska. If reinforcing is not installed in the concrete, the product must rely heavily on the zipper and zipper/fabric connection, which would introduce an unconventional limit state for consideration, potentially resulting in premature failure. The fabric enclosure seems unlikely to be the most efficient and reliable method available to remedy pile deterioration

2.3.2 CUSTOM STEEL AND CONCRETE RETROFIT

Custom retrofits are available to fit with tight dimensional tolerances, against deteriorated sections, when complications such as secondary member connections make other methods excessively complex or costly. The Hydro-Brace (Castle Group, 2014), for example, is configured into a C shape and fabricated to fit against the web of an I-shape, in the space between the flanges. Fabrication costs will be higher for this method in comparison to simpler methods such as typical concrete jackets, except for situations which would require forms to accommodate diagonal lateral bracing members.

2.4 RETROFIT SUMMARY

Common retrofit methods identified in the literature primarily appear to have been developed in house and designed for the convenience of state repair crews. The materials are commonly available and typically utilized for bridge design and repairs. This provides DOTs with an easy means of preforming repairs, but the practice appears to be strongly prescriptive rather than analytical. Consequently, installed retrofits are generally unverified and carry unknown capacities and limitations

2.5 PREVIOUS RESEARCH

This section describes the sparse research focused on corrosion and repair of steel piles available at this time.

2.5.1 REHABILITATION OF STEEL BRIDGE COLUMNS WITH FRP COMPOSITE MATERIALS

Liu (2003) researched the benefit of FRP (Fiber Reinforced Polymer) wraps on piles with simulated corrosion. Axial testing was performed at the University of Missouri Rolla to determine capacity of the piles with varying wrap lengths and concrete fills. Test results are shown in Table 2.1 and sketches of the specimens are shown in Figure 2.2. Through axial loading tests, it was demonstrated that the varying wrap lengths had an effect on the strength. The type of concrete used also played a role in the pile strength. The test results indicated retrofitted pile strength increased with wrap length, and the strength increase was compounded using expansive concrete.

Table 2.1 Test results (Liu, 2003)

Test	Ultimate load capacity		Load capacity increase over test 1	Theoretical elastic buckling load		Difference between theoretical and experimental loads
	kips	kN		kips	kN	
1	43.8	194.9	0%	42.5	189.1	-3%
2	25.9	115.3	-41%	24.8	110.4	-4%
3	68.2	303.5	+56%	65.3	290.6	-4%
4	74.3	330.6	+70%	96.7	430.3	+30%
5	41.1	182.9	+-7%	47.8	212.7	+16%
6	77.3	344.0	+76%	67.4	299.9	-13%
7	86.4	384.5	+97%	101.6	452.1	+17%

Strength increases correlate with longer wrapped lengths because the wrapped provides improved buckling resistance for the cross section. The greater effective moment of inertia affording greater stability. The expansive concrete provides improved effectiveness of transformed section properties with improved composite action between the FRP, concrete, and steel. The findings of this research substantiate the practice of extending the retrofit repairs from above the waterline to below the mud line to provide improved stability near the deteriorated section.

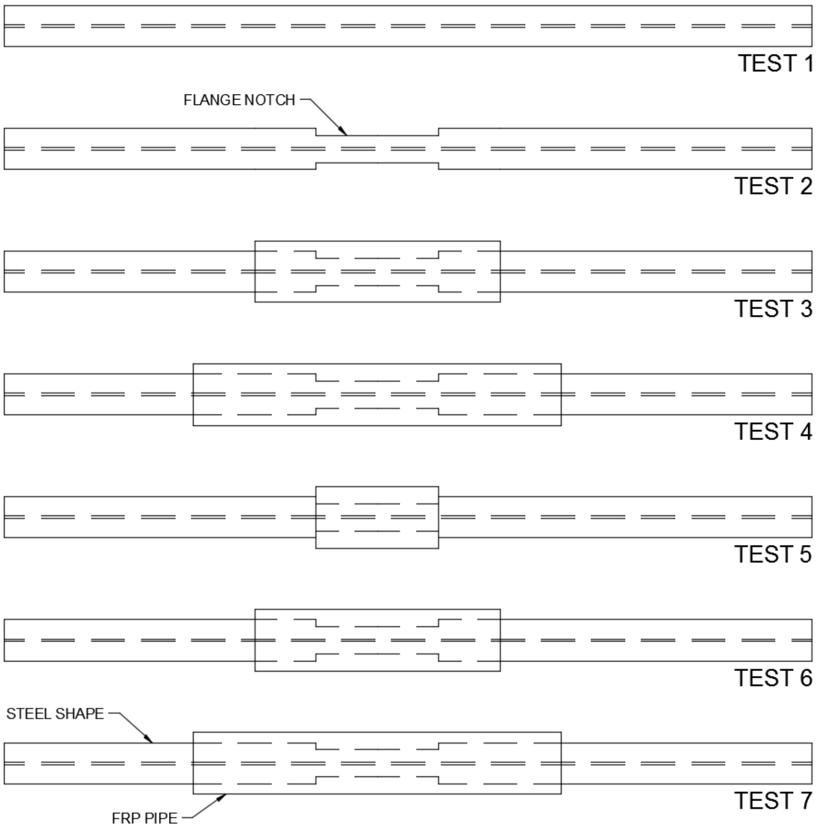

Figure 2.2 Test specimen setups (Liu, 2003

Also, as a part of this research, an analytical model was developed to calculate the pile strength. The analytical model was developed using the energy method. By setting the strain energy equal to the work done, the researchers were able to develop the buckling load equation representing the column strength of a compression element as shown in Figure 2.3. The derived equation, presented below, is only valid for pinned end boundary conditions, and in the strictest sense only when the deformed configuration follows a sine wave as assumed in the derivation.

$$P_{cr} = \frac{\dfrac{\pi^2 EL}{8L_1L_2}}{\left[\begin{array}{c} \dfrac{l}{I_1} - \dfrac{L_1}{2\pi I_2}\sin\left(\dfrac{\pi l_1}{L_1}\right) \\ + \dfrac{l_2}{I_2} + \dfrac{L_1}{2\pi I_2} * \left(-\sin\left(\dfrac{\pi(l_1+l_2)}{L_1}\right) + sin\left(\dfrac{\pi l_1}{L_1}\right) + sin\left(\dfrac{\pi(l_1+l_2+l_3)}{L_1}\right)\right) \\ + \dfrac{l_3}{2 * I_3} + \dfrac{L_1}{2\pi I_3} * \left(-\sin\left(\dfrac{\pi(l_1+l_2+l_3)}{L_1}\right) + sin\left(\dfrac{\pi(l_1+l_2)}{L_1}\right)\right) \end{array}\right]}$$

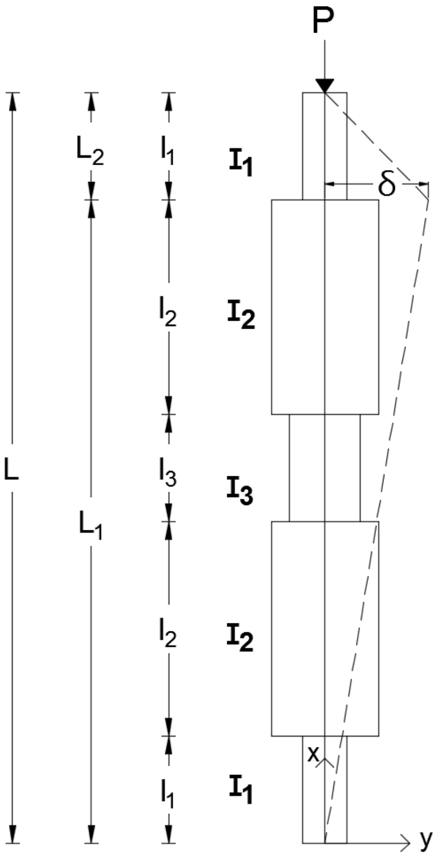

Figure 2.3 Stiffness distribution and deflected shaped (Liu, 2003)

2.5.2 FRP COMPOSITES FOR REHABILITATION OF HYDRAULIC STRUCTURES

In an effort to reduce cost of repairs, the United States Army Corps of Engineers requested research on the use of FRP material in different hydraulic structures (Vijay, Clarkson, GangaRao, Soti, & Lampo, 2014). One of these applications was a bridge with a steel substructure. All of the piles were located in the waterway and had experienced significant section loss up to 6 feet of the pile height. For the repair the piles were wrapped with a full height FRP shell and filled with 9” of epoxy grout and then self-consolidating concrete. The FRP shell was also wrapped with two layers of GFRP (Glass FRP) prior to filling. This research is still ongoing, but currently the repairs have shown a cost savings of 35% and a much shorter construction duration. Additionally, the bridge prior to repairs had been reduced to a single lane with a load rating of 6 tons. After the repairs, the bridge was reopened to two lanes and the original design capacity of 15 tons.

2.5.3 NUMERICAL INVESTIGATION OF H-SHAPED SHORT STEEL PILES WITH LOCALIZED SEVERE CORROSION

TXDOT and the University of Houston partnered to conduct research investigating corrosion effects on HP pile axial capacity (Shi, 2014). The research was an analytical parametric study, with the baseline model validated against experiments on reduced scale specimens (W4x13 x 32 in. long). The experimental and analytical work focused on piles subjected to pure axial load. The analytical study varied the location, configuration, and severity of deterioration to evaluate sensitivities of axial capacity to the various parameters.

The researchers identified three damage regions (Minor, Moderate, and Major) based on capacity. The Minor damage region is bounded by the limit at which the yield strength of the remaining pile has fallen to the original design load of the pile. Within this range, the pile requires only stiffening sufficient to prevent local and global buckling in order for a remediation measure to be successful. Load sharing with the retrofit is not required in the Minor damage region. The Moderate damage region indicates the yield strength of the remaining pile is below the original design load of the pile. The pile would require load sharing with the retrofit to reach the design capacity. The Major damage region would require the pile to be heavily retrofitted or replaced. The transition from Moderate damage to Major damage is largely influenced by owner policy.

In addition to the damage classifications, it was determined that flange deterioration was the single factor that most significantly affected the remaining axial capacity of the pile. It was also established that the location of the deterioration along the pile did not have a significant effect on the axial capacity. The information gathered by the University of Houston could provide a useful guideline to DOTs on how to effectively rehabilitate deteriorated piles. By knowing what capacity still remains, an appropriate retrofit can be applied to the pile. This would allow DOTs to make efficient use of their resources and rank pile repairs based on their damage category.

2.6 LITERATURE REVIEW SUMMARY

There are numerous repair procedures and even a few proprietary products available to aid in the rehabilitation of deteriorated steel piles. What is lacking is the research to prove the effectiveness of these repair options. As more research is conducted on this subject, a greater understanding and awareness can be created for these repair procedures. This will give DOTs more confidence in the repairs they use and more cost effective repairs for taxpayers. For this reason, testing will be performed in conjunction with this literature review. The testing will help validate the current repair process used by the Nebraska Department of Roads and provide suggestions for future use and development.

CHAPTER 3 EXPERIMENTAL DESIGN

3.1 INTRODUCTION

The experimental testing for this project evaluated the prevalent repair method employed by the Nebraska Department of Roads for deteriorated steel HP piles: reinforced concrete encasement. The experiments demonstrated capacities for piles in three conditions: as-built (non-deteriorated), deteriorated without retrofit, and deteriorated with retrofit. Additionally, two different pile locations were considered: abutment, and pile bent. The experimental investigation was intended to not only validate the restoring capacity of the concrete encasement retrofit employed by NDOR, but to also provide additional information pertaining to failure mechanisms. The repair is applied with the purpose of protecting the remaining portions of the pile, slowing the rate of corrosion, and restoring some or all of the pile's capacity. The following subsections will discuss the theoretical capacities of each component of the retrofit and the loading ratio which was used for the experimental investigation, followed by the design and layout of the experiments and the procedure used during the tests.

3.2 TEST SPECIMENS

For this project, HP 10x42 (AISC, 2011), steel piles were obtained with a minimum yield strength of 50 ksi. The HP 10x42 is a historically common pile size utilized by NDOR for steel piling. It is more common to see 36 ksi steel in the bridges that were built during this time, while today 50 ksi is the yield strength that is most commonly used and produced. Therefore, due to availability, it was necessary to use 50 ksi steel in place of 36 ksi steel.

The experimental investigation consisted of six total piles: three abutment simulations, and three pier simulations. Figure 3.1 shows a schematic of a bridge indicating scenarios where each simulation case applies.

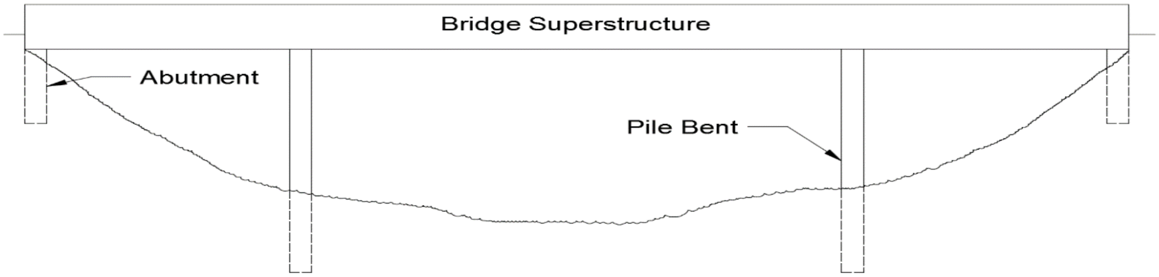

Figure 3.1 Simplified bridge elevation view

Simulated pile lengths and an assumed depth of fixity of five feet were established based on expert opinion supplied by the Technical Advisory Committee for the project at NDOR. The ground elevation was assumed to be at the bottom of the pile cap for the abutment case and nine feet six inches below the pile cap on the pier case. Additional plate steel was added to each specimen to distribute end loads and to stiffen and stabilize the cross-section where concentrated transverse loads were applied, see Appendix C. Additional modifications specific to individual tests are described in the following sections

3.2.1 NON-DETERIORATED CASE

Non-deteriorated tests established a baseline for the ultimate load that an undamaged specimen could resist and provided a reference for comparison of capacity, failure mechanism, and instrumentation readings to the deteriorated and retrofitted cases. No special modification were required for non-deteriorated cases other than those previously indicated. Schematic representations for the two cases are presented in Figure 3.2.

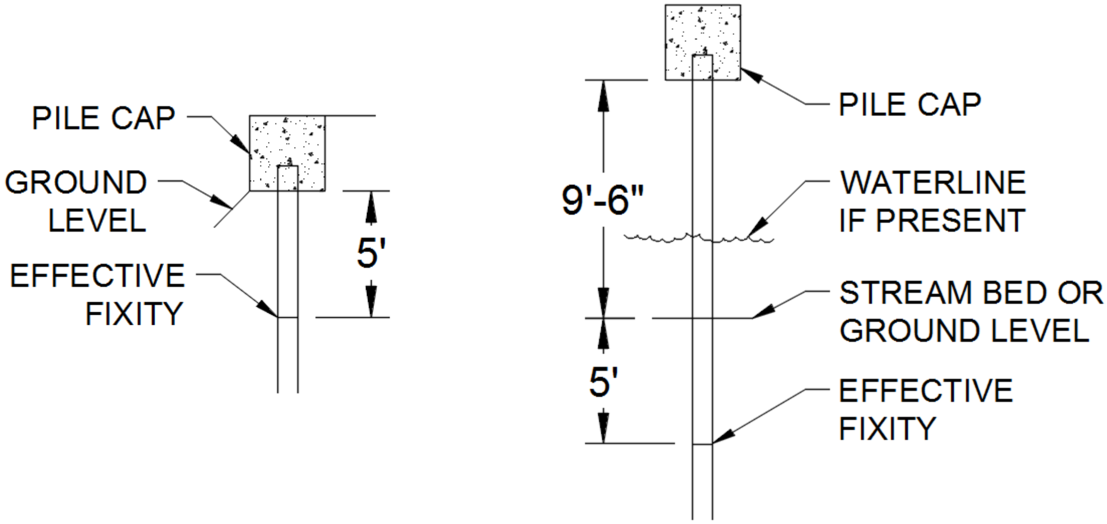

Figure 3.2 Non-deteriorated test cases

3.2.2 DETERIORATED CASE

The deterioration level (thickness reduction of flanges and web) selected for the experimental program was 45%. At a 45% reduction of the steel cross-section, the nominal yield strength of the remaining section was slightly (approximately 10 kips) less than the safe operating capacity of the test setup (350 kips). Bond was ignored for this estimation, because it is implied to be negligible both in AASHTO (2012) and in AISC (2010). Additionally, the yield strength of the pile specimens was assumed to be 50 ksi, but steel tensile coupon tests showed that this assumption underestimated the actual steel strength. Delayed delivery of the testing coupons led to this discovery after the milling had been completed and the concrete placed.

Corrosive section loss was simulated by milling flanges to reduce thickness. Although a uniform reduction in thickness would have been preferable, a compromise was designed such that holes cut through the web provided a reduced cross-section with similar capacity and cross sectional area to a uniform thickness loss. The theoretical strength of a uniformly deteriorated cross section was calculated and set as a target capacity. Two separate analyses were conducted to determine the location of the holes to provide a capacity equal to the target capacity. The demands for the analyses were based on the intersection of the axial-to-moment loading ratio and the combined axial-moment capacity interaction diagram of a cross section reduced by 45%.

First, the reduced cross section was evaluated assuming that moment induced by shear would form a couple acting on flanges (similar to WTs with holes cut in the section). The axial force was partitioned to the WT flanges and the rectangular bar (the remaining web between the holes) proportionately based on area. After preliminary design (placement of holes), a second corroborating analysis was performed utilizing SAP2000 software. The initial approximate analysis neglected flexural stiffness and frame action of the WT and rectangular bar components. In SAP2000, the structure was modeled to capture frame action by using beam elements with appropriate axial and flexural stiffness at the deteriorated section. The portion outside of the deteriorated section was modeled with rigid elements connecting the ends of the deteriorated segments and axial and shear loads were applied to simulate test conditions. The Bar dimension indicates the interior portion of the web that would remain, and the WTs' dimension is the portion of the web under the flange that would remain. The Demand values in Table 3.1 correspond to loading that would theoretically cause failure for a uniformly deteriorated section. From the two separate analyses, the remaining web portion should be approximately 2.65 inches and the stem of the flange should be 0.875 inches. The resulting cross section is shown in Figure 3.3.

Table 3.1 Deterioration analysis results

			Excel Calculations		SAP2000	
Wt (Stem Height) in.	Bar (Width) in.	Capacity (k)	Demand (k)	Remaining (k)	Demand (k)	Remaining (k)
0.875		87.89	87.49	0.41	86.68	1.21
	2.65	45.77	30.32	15.45	30.59	15.18
1.25		102.06	91.99	10.07	91.76	10.30
	1.9	32.82	21.74	11.08	21.93	10.89
1.5		107.23	95.03	12.20	94.73	12.50
	1.4	24.18	16.02	8.16	16.16	8.02

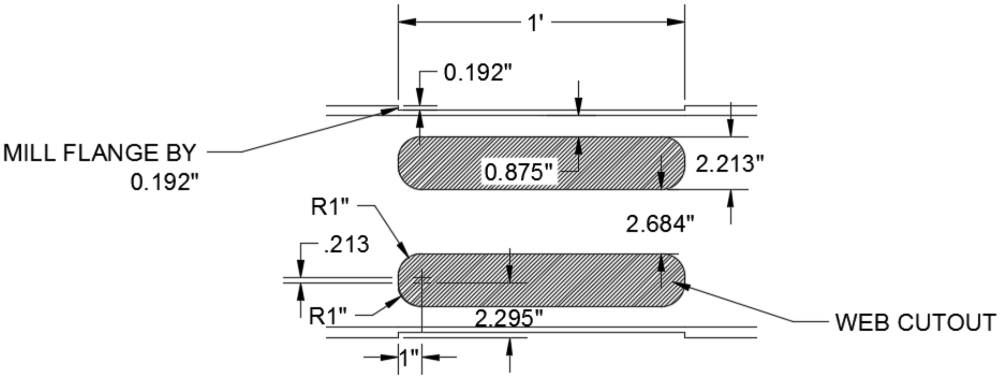

Figure 3.3 Deteriorated section milling detail

The deterioration was located as shown in Figure 3.4, based on field conditions inferred from previous repair scenarios. For the abutment case, it was assumed that the back fill would erode, exposing the pile just below the pile cap, and that the most severe corrosion would occur 2’-3” below the bottom of the pile cap. A deteriorated location 3’-7” above ground level (or the stream bed) was assumed for the pile bent experiments, based on typical stream conditions in Nebraska and documentation for a previous repair project provided by NDOR. After the milling was completed, the deteriorated pile specimens were provided with identical plate steel at ends and transverse loading locations similar to the non-deteriorated specimens.

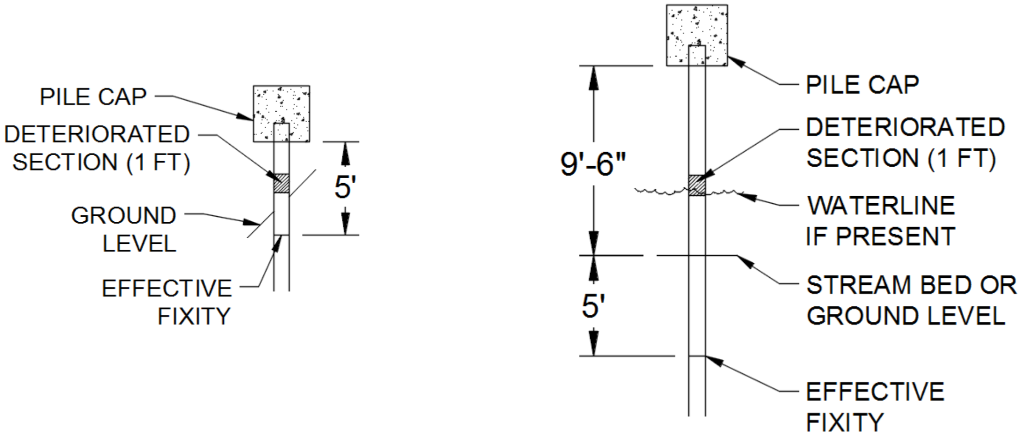

Figure 3.4 Deteriorated test cases

3.2.3 RETROFITTED CASE

Retrofitted specimens were milled and prepared with plate steel similarly to the deteriorated specimens prior to placing reinforced concrete consistent with NDOR’s standard detail. Four 1” diameter holes (two on either side of the deteriorated section) were also cut through the web for doweled rebar as shown in Figure 3.5. The dowel holes were spaced at 12 inches on center, with the farthest dowels installed 18 inches from the boundary of the deteriorated section. Embedded instrumentation was installed with protective covering for both the strain gages and lead wires prior to placing concrete around the deteriorated steel section.

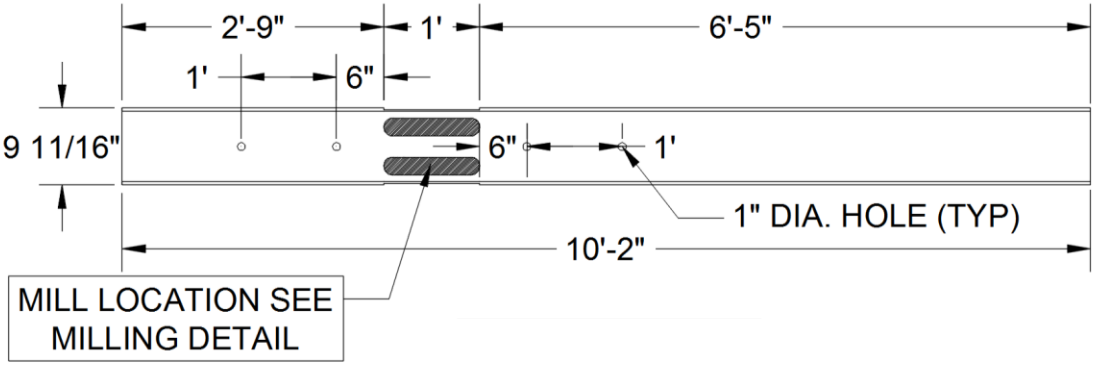

Figure 3.5 Elevation view of retrofitted test case milling

Rebar was placed within the form to create a cage, as illustrated in repair plans supplied by NDOR, see Appendix B. Finally, the concrete was placed and vibrated to consolidation, resulting in test specimens that represented the two scenarios presented in Figure 3.6. Instrumentation to be installed outside the concrete was deferred until after the concrete had been placed, while the concrete was curing.

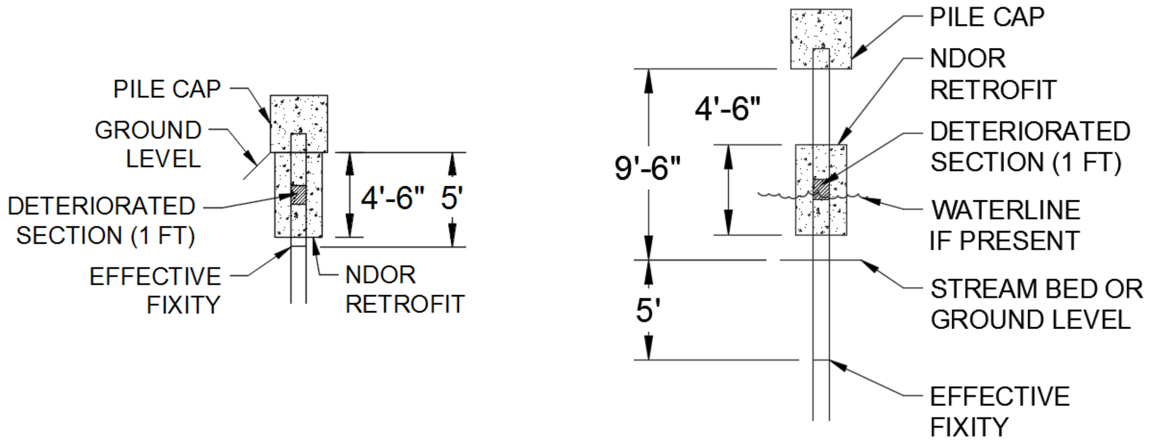

Figure 3.6 Retrofitted test cases

3.3 LOADING RATIO PROTOCOL

Prototype bridges and loading scenarios, considering sequences and combinations of vertical dead and live loads together with horizontal braking and thermal effects, were considered and presented to the Technical Advisory Committee. Additional details on the loading scenarios presented to the Committee are outlined in Appendix A. The Committee ultimately recommended an internal loading combination comprised of 80% axial and 20% moment. The author interpreted this 80/20 loading ratio to correspond to a plastic condition, for which 80% of the area resists axial load, and 10% at the outer edge of each flange resists flexure. Moment was induced for the experimental program by applying a shear load at the end of the specimens simulating braking or thermal effects from the pile cap. The following sections present and describe the equations used to calculate the capacity of steel structural elements subjected to combined axial and moment demand.

3.3.1 INTERACTION DIAGRAMS

Equations from AISC (2010) and AASHTO (2012) were utilized to develop interaction diagrams envelopes for combined loading capacity. A number of the equations were only available in AISC. The AASHTO (2012) equations were located by first consulting section 6.15 for piles and following the references to the appropriate sections in 6.9 and 6.10. AASHTO Equations (6.9.2.2-1) and (6.9.2.2-2) and AISC (H1-1a) and (H1-1b) are the typical approximate envelopes used by default, based on plastic capacity and validated by stub-column tests. AISC (H1-2) provides an alternative equation which is allowed to be used for out-of-plane buckling limit states, in conjunction with (H1-1) for in-plane buckling. AISC (C-H1-3a) and (C-H1-3b) provide analytical formulations for plastic combined loading capacity similar to, but more exact than, (H1-1).

Ch. H1.1(a)
6.9.2.2

$$\frac{P_r}{P_c}+\frac{8}{9}\left(\frac{M_r}{M_c}\right)\leq 1.0$$

(H1-1a) (AISC)
(6.9.2.2-2) (AASHTO)

Ch. H1.1(b)
6.9.2.2

$$\frac{P_r}{2P_c}+\left(\frac{M_r}{M_c}\right)\leq 1.0$$

(H1-1b)
(6.9.2.2-1)

Ch. H1.3
No equivalent

$$\frac{P_r}{P_{cy}}\left(1.5-.5\frac{P_r}{P_{cy}}\right)+\left(\frac{M_{rx}}{C_bM_{cx}}\right)^2\leq 1.0$$

(H1-2)

Comm. H1.1
No equivalent

$$\frac{M_{pc}}{M_p}=1-\frac{A^2\left(\frac{P}{P_y}\right)^2}{4t_wZ_x}$$

(C-H1-3a)

Comm. H1.1
No equivalent

$$\frac{M_{pc}}{M_p}=\frac{A\left(1-\frac{P}{P_y}\right)}{2Z_x}\left[d-\frac{A\left(1-\frac{P}{P_y}\right)}{2b_f}\right]$$

(C-H1-3b)

Deteriorated sections were assumed to undergo uniform thickness loss at flanges and webs. The flange width was held constant. Corresponding P_c and M_c values were determined using the radius of gyration for a non-deteriorated section when evaluating Euler buckling stress, F_e, but reducing axial capacity with Q factors to address local instability associated with reduced flange and web thickness, according to the following equations

Ch. E3, E7 $P_n = F_{cr}A_g$ (E3-1), (E7-1)
6.9.2.1 (6.9.2.1-1)

Ch. E3(a) $F_{cr} = \left[0.658^{\frac{F_y}{F_e}}\right]F_y$ (E3-2)
6.9.4.1.1 (6.9.4.1.1-1)

Ch. E7(a) $F_{cr} = Q\left[0.658^{\frac{QF_y}{F_e}}\right]F_y$ (E7-2)*
6.9.4.1.1 (6.9.4.1.1-1)
*Where Q is a function of Q_a and Q_s.

Ch. E3(b), E7(b) $F_{cr} = 0.877F_e$ (E3-3), (E7-3)
6.9.4.1.1 (6.9.4.1.1-2)

Sections F2 and F3 of AISC (2010) were used to determine pile flexural capacity. The AISC equations are functionally identical to AASHTO (2012) Chapter 6 when accounting for the web plastification factor, R_{pc}, which scales elastic to plastic capacity in Appendix A. The presentation is significantly more simplified in AISC, which focuses on steel I-sections with compact webs and compact or noncompact flanges and characterizes bending capacity in terms of moment rather than stress.

Ch. F2.1 $$M_n = M_p = F_y Z_x \quad \text{(F2-1)}$$

Ch. F2.2(b) $$M_n = C_b \left[M_p - \left(M_p - 0.7 F_y S_x \right) \left(\frac{L_b - L_p}{L_r - L_p} \right) \right] \leq M_p \quad \text{(F2-2)}$$

Ch. F3.2(a) $$M_n = M_p - \left(M_p - 0.7 F_y S_x \right) \left(\frac{\lambda - \lambda_{pf}}{\lambda_{rf} - \lambda_{pf}} \right) \quad \text{(F3-1)}$$

Ch. F3.2(b) $$M_n = \frac{0.9 E k_c S_x}{\lambda^2} \quad \text{(F3-1)}$$

Figure 3.7 and Figure 3.8 show the interaction diagrams for both pile types. The limits of the pile capacities were calculated based on equation H1-1 for strong and weak axis column buckling as well as equation H1-2. For the deteriorated pile, equation H1-1 for strong axis column bucking was utilized to predict the capacity. The line labeled “Plastic: 80% P, 20% M” represents the load ratio at the critical section (the depth of fixity) for the non-deteriorated pile. The line labeled “Loading at Deteriorated Section” accounts for the reduced moment arm to the deteriorated section relative to the depth of fixity, and the corresponding reduction in moment relative to axial load. The non-deteriorated loading ratio is based on the calculations preceding Figure 3.9. The rectangular retrofit envelope is described in a subsequent section

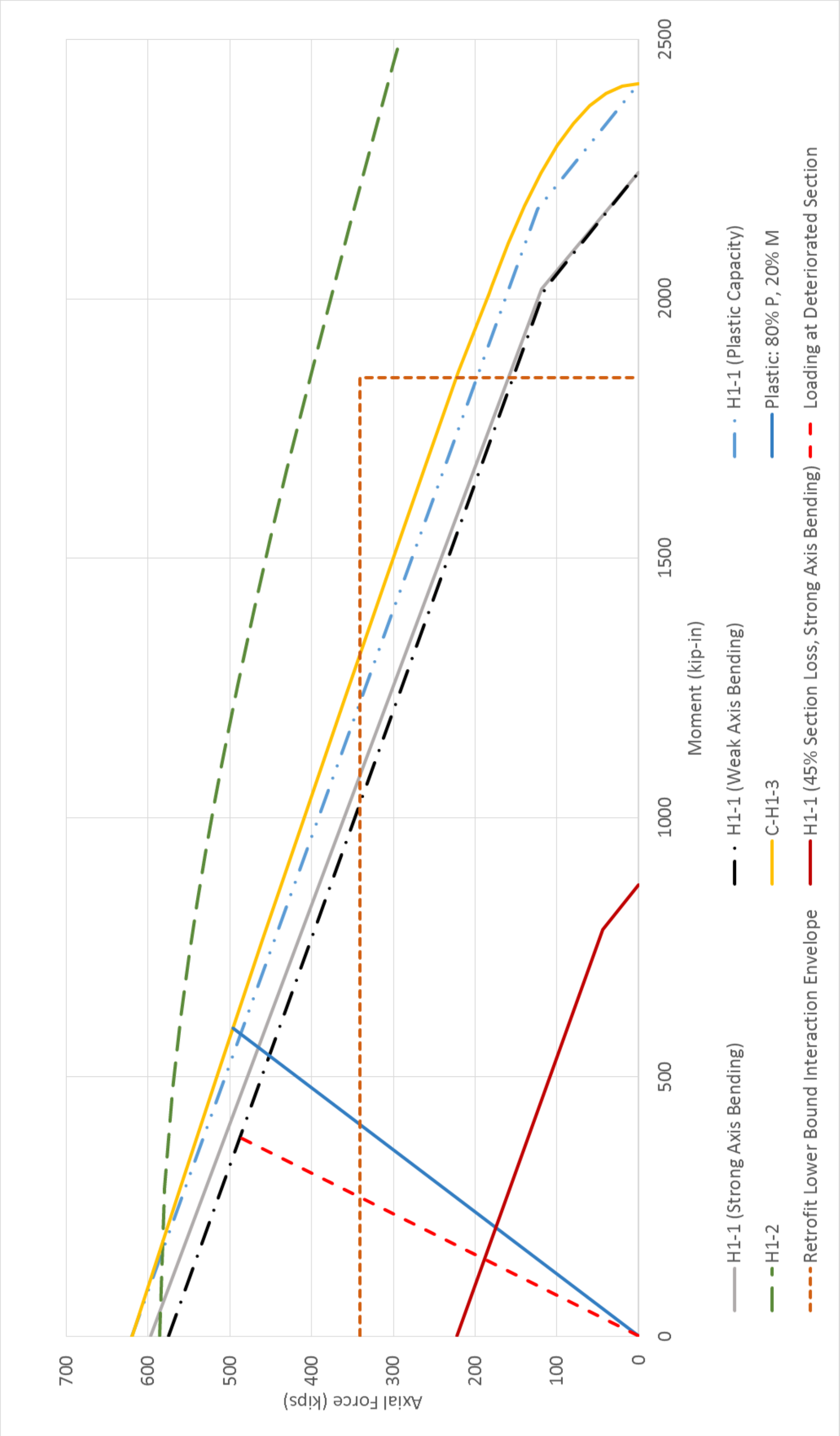

Figure 3.7 Abutment interaction diagram

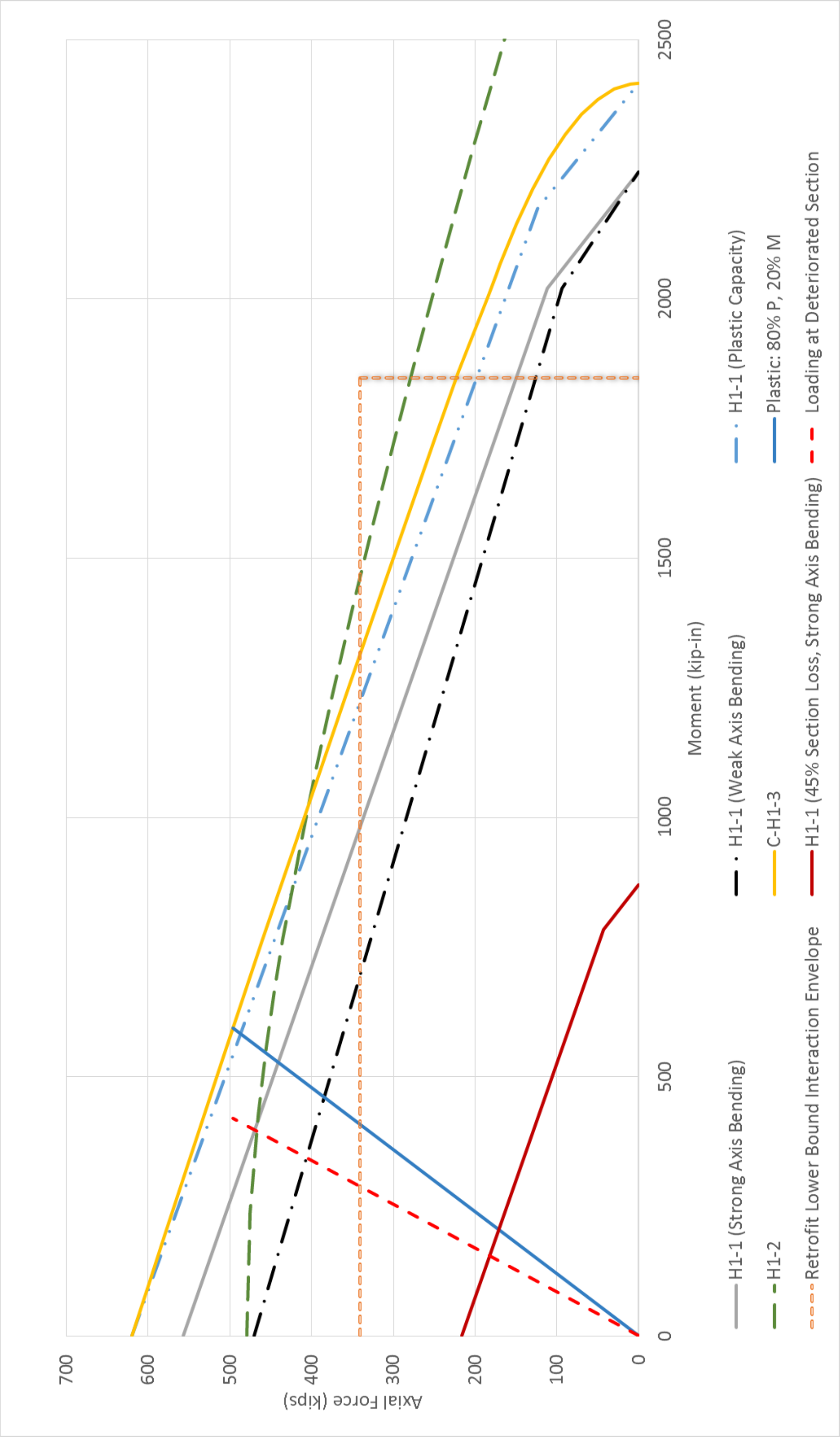

Figure 3.8 Pile bent interaction diagram

The slope of the loading ratio line in the preceding figures conforms to the 80/20 axial-moment ratio previously mentioned, as recommended by the project TAC. Anchor values at the plastic capacity were determined as follows. Figure 3.9 illustrates how the forces were converted to stress on the cross section.

$$Depth\ of\ flange\ utilized\ for\ moment = A_g * 20\% = 2.48\ in^2 \rightarrow \frac{2.48}{10.1 * 2}$$

$$= .12\ in = w$$

$$x = Moment\ arm = D - w = 9.7 - .12 = 9.6\ in$$

$$M = x * F_y * A_{flange\ utilized\ for\ moment} = 9.6 * 50 * (.12 * 10.1) = 582\ k - in$$

$$P = (A_g - A_{flange\ utilized\ for\ moment} * 2) * F_y = (12.4 - (.12 * 10.1 * 2)) * 50$$

$$= 499\ k$$

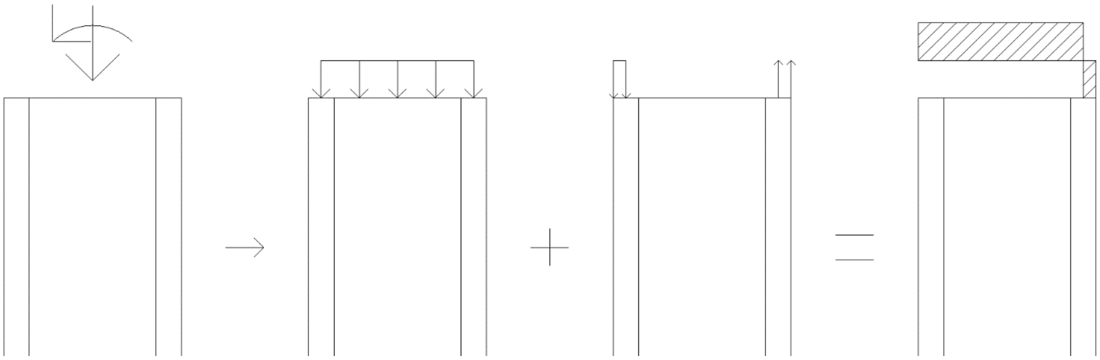

Figure 3.9 Ultimate pile loading stress distribution

3.3.2 RETROFIT CAPACITY

The retrofit interaction envelope considers the separate capacities of the steel and the concrete jacket for axial compression and bending moment respectively. This is likely a conservative assumption as the jacket is expected to act compositely with the steel pile. The amount of composite action due to bond is implied to be negligible as mentioned earlier, but even with this consideration, this envelope is the lower bound capacity. It is anticipated that the embedded portion of the pile would carry the axial load and the steel would transfer the moment load through this embedment (much like it would in a pile cap) to the concrete. The Multidisciplinary Center for Earthquake Engineering Research (Shama, Mander, Blabac, & Chen, 2011) tested embedment depth for pile-to-cap connections and developed an equation calculating the embedment depth needed to fully transfer the shear and moment from the steel to the concrete.

$$l_{emb} = 3.4 * d_p * \sqrt{\left(\frac{f_y}{0.85 * f_c'}\right)\left(\frac{t_f}{d_p}\right)} = 3.4 * 9.7 * \sqrt{\left(\frac{50}{0.85 * 3}\right)\left(\frac{0.42}{9.7}\right)} = 30.4\ in.$$

This equation resulted in an embedment of 30.4 inches, which is just over half the length of the retrofit jacket in these experiments. From material strength testing results, both the steel and concrete had greater material strengths then initially assumed, the embedment depth required was reduced to 21.8 inches. The values calculated for the remainder of this section are based on the design strengths of the material. These values are subject to change based on material testing data and for these experiments do. These changes are reflected in the experimental results section.

The steel axial capacity was taken as the maximum axial capacity of the deteriorated section with a 45% section loss, 341 kips (calculated below). The concrete jacket was expected to eliminate buckling of the deteriorated pile cross section, allowing the pile to reach its plastic limit. Based on these assumptions, the following calculation shows how the pile deteriorated section capacity was determined.

$$P_n = f_y * A_s = 50\ ksi * 0.55 * 12.4\ in^2 = 341\ kips^*$$

For the concrete jacket, calculations were performed on the moment capacity and cracking moment as shown below.

Moment Capacity (ignoring compression steel)

$$a = \frac{A_s f_y}{0.85 f_c' b} = \frac{0.31\ in^2 * 4\ bars * 60\ ksi}{0.85 * 3\ ksi * 30\ in} = 0.97\ in$$

$$c = \frac{a}{\beta_1} = \frac{0.97\ in}{0.85} = 1.14\ in$$

$$\varepsilon_s = \frac{d - c}{c} * 0.003 = \frac{26\ in - 1.14\ in}{1.14\ in} * 0.003 = 0.065 > 0.005\ (Tension\ Controlled)$$

$$M_n = A_s f_y \left(d - \frac{a}{2}\right) = 0.31\ in * 4\ bars * 60\ ksi * \left(26\ in - \frac{0.97\ in}{2}\right)$$

$$= 1898.3\ k - in = 158.2\ k - ft$$

Cracking Moment

$$M_{cr} = \frac{f_r I_g}{y_t} = \frac{7.5 * \sqrt{f_c'} * \frac{b^4}{12}}{y_t} = \frac{7.5 * \sqrt{3000}\ psi * \frac{30^4}{12}\ in^4}{15\ in} = 1848563.63\ lb - in$$

$$= 1848.7\ k - in = 154\ k - ft$$

Cracking moment is the calculated limiting state for the concrete jacket. The flexural strength of the jacket exceeds the maximum moment capacity of the pile by 15 k-ft. The difference in moment capacities is not significant, but for a pile only carrying 50% of its capacity at design loads, it is less of a concern.

The NDOR standard jacket retrofit includes #6 rebar (yield stress, f_y of 60 ksi) doweled through the web of the pile to provide improved composite action. For the experimental study, four 30 inch pieces of rebar were doweled through the pile's web and spaced vertically above and below the deteriorated section. Details from NDOR indicate a bar located in the deteriorated section, this bar was assumed to not contribute significantly to the retrofit's capacity and was eliminated. With two bars above the deterioration and two below, the load theoretically flows into the first two bars, is transmitted through the concrete and flows back out through the last two bars. Therefore, the capacity is based on the first two bars with two shear planes or hinges per bar, depending on the limit state considered. The next set of calculations check the rebar's shear capacity and plastic limit.

Shear Capacity

$$P_n = 0.6F_yA_wC_v = 0.6 * 60\ ksi * \left(\frac{\left(\frac{6}{8}\right)^2}{4} * \pi\right) in^2 * 1 = 15.9\ k$$

$$For\ 2\ bars\ P_{n_{total}} = 63.6\ k$$

Plastic Limit

$$M_p = F_yZ_x \qquad Z = \frac{d^3}{6} = \frac{\left(\frac{6}{8}\right)^3}{6} = 0.0703\ in^3$$

$$M_p = 60\ ksi * 0.0703\ in^3 = 4.22\ k - in = 0.35\ k - ft$$

$$\text{Distributed load} = \frac{4.22\ \text{k} - \text{in}}{15\ in * \frac{15}{2}\ in} = 0.038 \frac{\text{k}}{\text{in}}$$

$$Stress\ on\ rebar\ per\ side = \frac{0.038 \frac{k}{in}}{\frac{6}{8}\ in} = 0.51\ ksi$$

$$For\ 2\ bars\ P_{n_{total}} = 2.3\ k$$

The considered limit states indicate that the formation of plastic hinges will be the controlling limit for the doweled rebar. The force required to achieve this limit state is minimal in comparison to the overall axial load. Along with the negligible anticipated bond, the shear transfer from the doweled rebar indicates minimum axial load transfer to the concrete. The low calculated capacity of the rebar and the limited confidence in the steel-concrete bond stress presented in AASHTO (2012) and AISC (2010), validate the conservatism in the retrofit envelope.

3.4 FAILURE CASES

For the retrofitted pile, three possible failure cases were established. The first two failure cases considered the failure of the pile in the jacket, and the third failure case considered the failure of the pile outside the jacket.

The first failure case (Failure Case 1) predicted local buckling of the reduced section due to the axial load. Failure Case 1 considered the pile to be loaded beyond its axial capacity and as a result would begin to exhibit local buckling. The deteriorated section would buckle causing localized crushing of the concrete within the jacket. This would indicate a low bond between the steel and concrete as the pile would carry significant load through the deteriorated section. Figure 3.10 illustrates Failure Case 1.

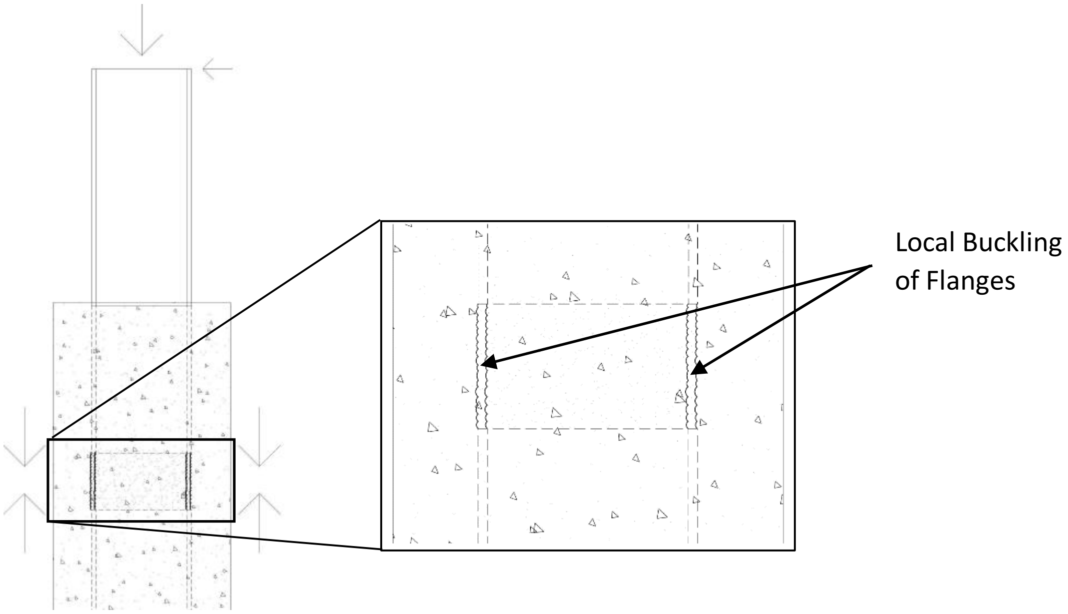

Figure 3.10 Failure Case 1

The second failure case (Failure Case 2), represents a bond significant enough to transfer the axial load into the concrete around the steel, but not sufficient enough to transfer the full moment. Again local buckling would be the failure mechanism, but this would be due to the shear-induced moment. The deteriorated section of the pile would buckle locally in one flange. Crushing of the concrete at the deteriorated section and near the end of the jacket with the larger moment would be expected in Failure Case 2. Figure 3.11 below shows Failure Case 2.

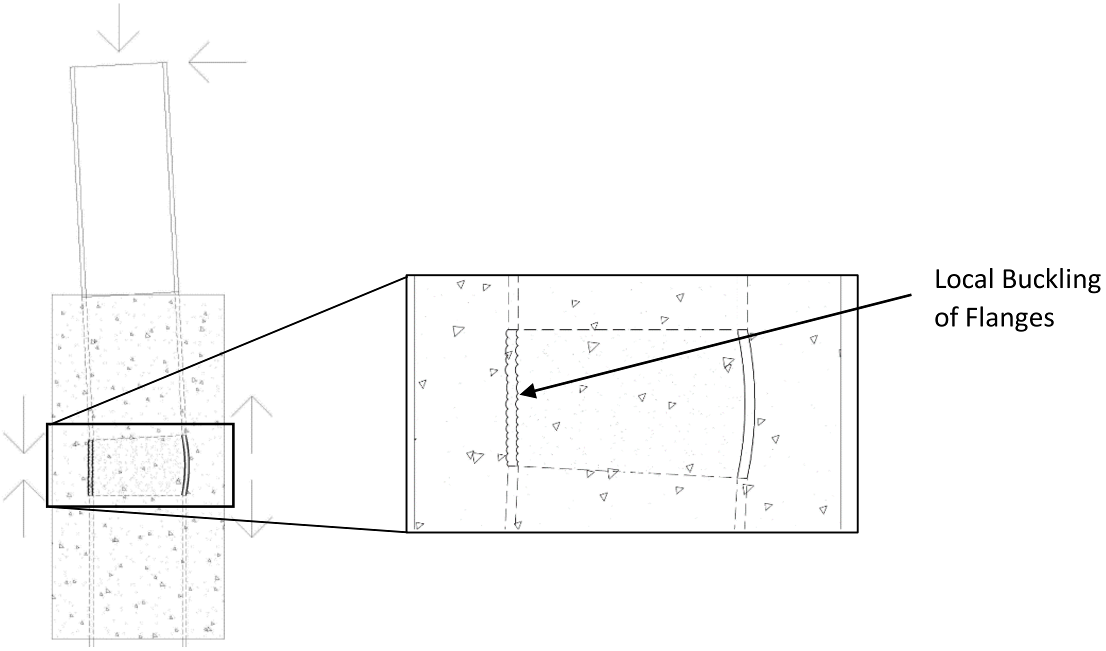

Figure 3.11 Failure case 2

The final failure case (Failure Case 3) shown in Figure 3.12, considered the jacket acting compositely with the pile, preventing local buckling of the steel within the jacket, leading to a yielding failure of the pile outside the jacket.

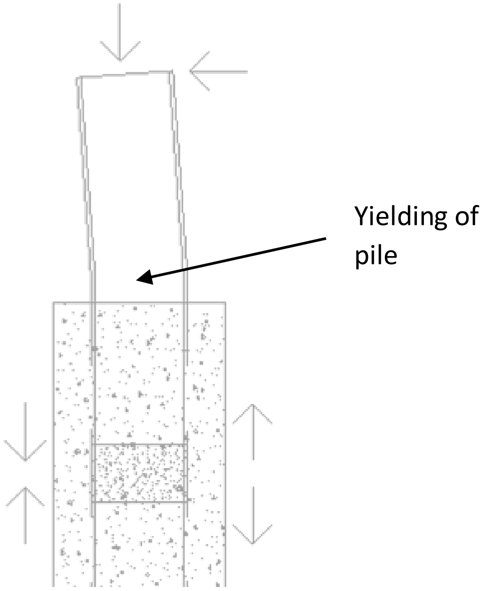

Figure 3.12 Failure Case 3

The first two failure cases considered limit states within the concrete jacket. These failure cases represented a steel-concrete interaction less than that of the load applied. Failure Case 3 assumed a bond strength sufficient enough to transfer the load and a retrofit capable of carrying that transferred load. This would lead to the pile failing outside the jacket.

Based on commentary from both AISC (2010) and AASHTO (2012), bond strength is considered to be negligible. AASHTO (2012), section 6.12.2.3.1 of the code, provides a moment equation for the encased shape, but does not state the bond stress available. From AISC (2011), for filled members, the direct bond interaction can be taken as 0.06 ksi with a reduction factor of 0.45. With a perimeter of 56.25 in^2 and a length of 1 ft - 9 in per side of the deteriorated section, the bond based on the AISC's values should be able to transfer approximately 71 kips (32 kips after the reduction by the phi factor). This, along with the pile's fully braced deteriorated section capacity, would indicate that the pile should be capable with the bond to carry 453 kips in compression. From the National Cooperative Highway Research Program's (NCHRP, 1998) *Bridge Rating through Nondestructive Load Testing* Technical Report, a bond stress of 100 psi is recommended as a conservative amount. The report goes on to state that bond stresses of 145 psi have been observed. With a bond stress of 145 psi the pile would be able to transfer 171 kips to the concrete, which would result in a compression capacity of 553 kips.

3.5 SETUP

Simulating representative field conditions and the loading ratio prescribed by NDOR required that the test setup apply both an axial and shear load. The pile was orientated horizontally with the flange face parallel to the floor, and placed on spacers, which were sitting on a steel encased concrete block (termed base block) that supported the pile's base. Small spreader beams were placed on top of the pile and anchor the pile to the base by Dywidag bars tensioned through the strong floor. A self-reacting frame was utilized to apply the axial load, and consisted of four RCH-1506 hollow core rams, each acting on a 1-3/4" cold rolled Dywidag all thread bar. The bar and ram reacted against custom built spreader beams. These spreader beams consisted of two channels spaced and connected by one inch thick steel plates. A single ram reacting against the strong floor applied the shear load. The shear load was opposed by the two smaller spreader beams used to tension down the pile. This setup is shown in Figure 3.13.

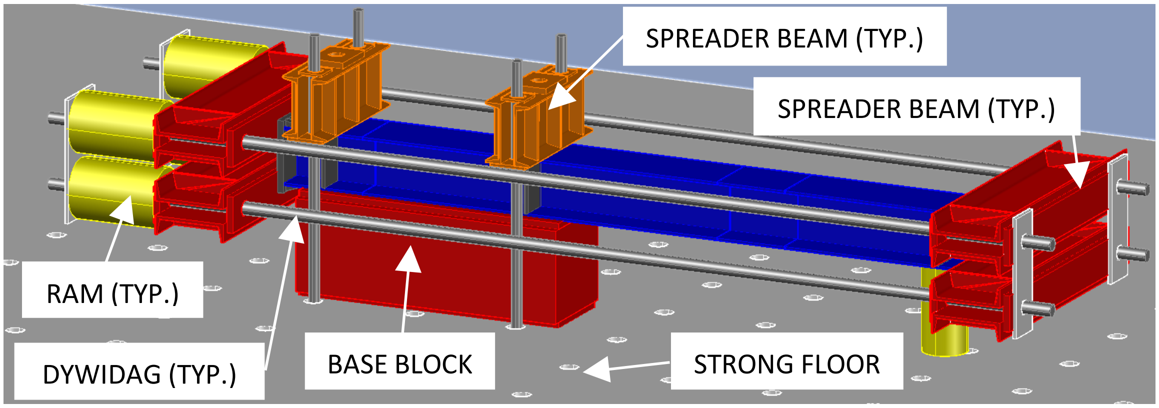

Figure 3.13 AutoCAD drawing of test setup

Each component of the testing frame was analyzed to find the load rating. The component with the lowest load rating determined the ultimate load that could be applied to the specimens. The spreader beams were determined to be the limiting component of the setup and required that the maximum axial force applied be no greater than 350 kips. This limitation required that the shear (moment inducing) force be increased in order to reach a failure limit state.

3.6 DATA ACQUISITION

Data was collected for measured strains, displacements, and pressures, using linear pattern strain gages, string pots, and pressure transduces. Data was observed and collected during the experiments, and exported and post-processed using Matlab.

For all specimens, strain gages were located at what were termed the base and deteriorated sections as shown in Figure 3.14. Both locations were instrumented with five gages as illustrated in Figure 3.15, one centered in the height of the web, and one centered in each half of the exterior flange face for both flanges.

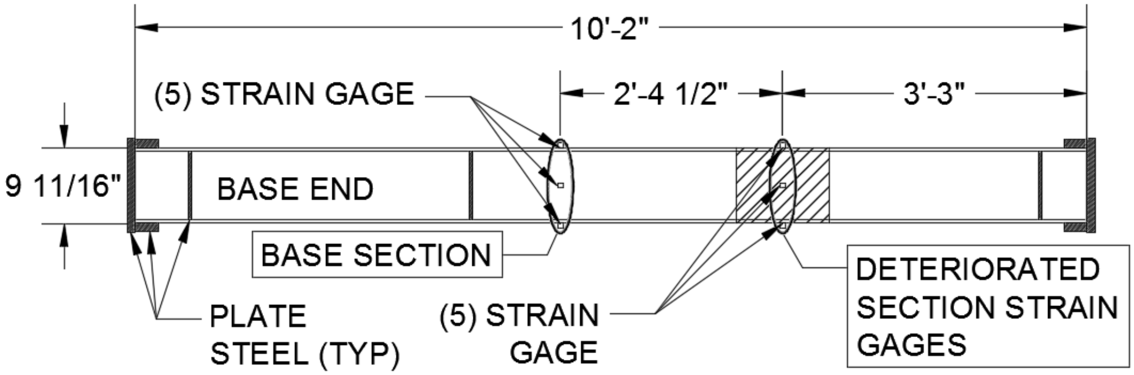

Figure 3.14 Elevation view of strain gage locations

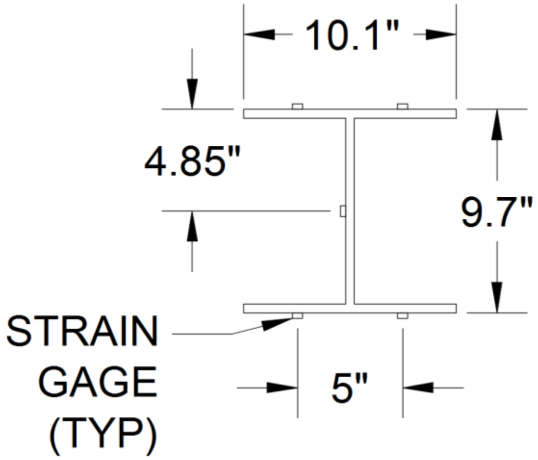

Figure 3.15 Cross section view of strain gage locations

All of the test specimens were also instrumented with two gages located near the tie down location on the top flange with the same spacing as the other gage locations. These gages near the tie down location were used to monitor yield initiation at the fixity location. Additional strain gages were installed for the retrofitted cases to provide greater detail of the piles response and to allow for accurate load tracking and application. For the retrofitted abutment case, the additional gages were applied to the web to allow for improved moment load monitoring during the test. For the retrofitted pile bent case, the additional gages were applied to the pile outside of the retrofit. This allowed for comparison of the loading before and after the encasement. The following tables provide the location at which each strain gage was located. The left table (Table 3.2) shows the gage locations used in all of the test and the right table (Table 3.3) shows the additional gages for the retrofitted tests. The location from fixity is given for the abutment case and pile bent case respectively (only one number is given if it’s the same for both cases).

Table 3.2 Strain gage locations

Gage Name	Location from Fixity Point	Distance from Center
BB-TF-L	4-3/8"	2.5"
BB-TF-R	4-3/8"	2.5"
B-TF-L	10-1/4"	2.5"
B-TF-R	10-1/4"	2.5"
B-W-R	10-1/4"	0"
B-BF-L	10-1/4"	2.5"
B-BF-R	10-1/4"	2.5"
D-TF-L	3' 2-3/4" / 8' 5-3/4"	2.5"
D-TF-R	3' 2-3/4" / 8' 5-3/4"	2.5"
D-W-R	3' 2-3/4" / 8' 5-3/4"	0"
D-BF-L	3' 2-3/4" / 8' 5-3/4"	2.5"
D-BF-R	3' 2-3/4" / 8' 5-3/4"	2.5"

Table 3.3 Additional strain gage locations

Gage Name	Location from Fixity Point	Distance from Center
B-W-R(A)	10-1/4" / N/A	1-7/8"
B-W-R(U)	10-1/4" / N/A	1-7/8"
U-TF-L	N/A / 5' 11-1/4"	2.5"
U-TF-R	N/A / 5' 11-1/4"	2.5"
U-W-R	N/A / 5' 11-1/4"	0"
U-BF-L	N/A / 5' 11-1/4"	2.5"
U-BF-R	N/A / 5' 11-1/4"	2.5"
A-TF-L	N/A / 11' 1/4"	2.5"
A-TF-R	N/A / 11' 1/4"	2.5"
A-W-R	N/A / 11' 1/4"	0"
A-BF-L	N/A / 11' 1/4"	2.5"
A-BF-R	N/A / 11' 1/4"	2.5"

The gages were given acronyms to help quickly identify them during and after the test. The general idea behind the acronym was location (along the length - vertical placement - horizontal placement). Table 3.4 presents the abbreviation, label, and descriptions for the three parts of the acronym.

Table 3.4 Strain gage acronyms

Location along the length		
BB	Base Block	Location closest to the fixity point
B	Base	Non-deteriorated section expected failure location
U	Under	Location before the retrofit (when applicable)
D	Deteriorated	Deteriorated section location
A	Above	Location after the retrofit (when applicable)
T	Top	Location of the pile top
Vertical Placement		
TF	Top Flange	Exterior face of the top flange
W	Web	Either face of the web
BF	Bottom Flange	Exterior face of the bottom flange
Horizontal Placement		
L	Left	Left of center looking from the base towards the top
C	Center	Center of the section
R	Right	Right of center looking from the base towards the top

The displacements were measured at the same general locations (distances varied for the two cases) for the abutment and pile bent cases. Vertical displacements (from the floor up) were taken at the tie down point, base section, deteriorated section, and top of the pile. Horizontal displacements were taken from the base section, deteriorated section, and two from the top. The first horizontal top displacement was taken for out of plane movement and the second for shortening of the pile along its length. Table 3.5 gives a summary of the locations where displacement measurements were taken.

Table 3.5 String pot locations

Gage Name	Location from Fixity Point	Measured
BB-BF-C	4-3/8"	Vertical
B-BF-C	10-1/4"	Vertical
D-BF-C	3' 2-3/4" / 8' 5-3/4"	Vertical
T-BF-C	6' 5-3/4" / 15' 5-3/4"	Vertical
B-W-L	10-1/4"	Horizontal
D-W-L	3' 2-3/4" / 8' 5-3/4"	Horizontal
T-W-L	6' 5-3/4" / 15' 5-3/4"	Horizontal
T-W-C	6' 5-3/4" / 15' 5-3/4"	Horizontal

In order to monitor the load from the hydraulic rams, pressure transducers were installed on the advanced side of each ram, shown in Figure 3.16 (four for the axial load application, and one for the shear load application). One additional pressure cell was located just before a 4-way splitter for the axial load hydraulic lines as a reference to monitor the main hydraulic line pressure. The load readings from the pressure transducers served as a validation of the strain gage readings.

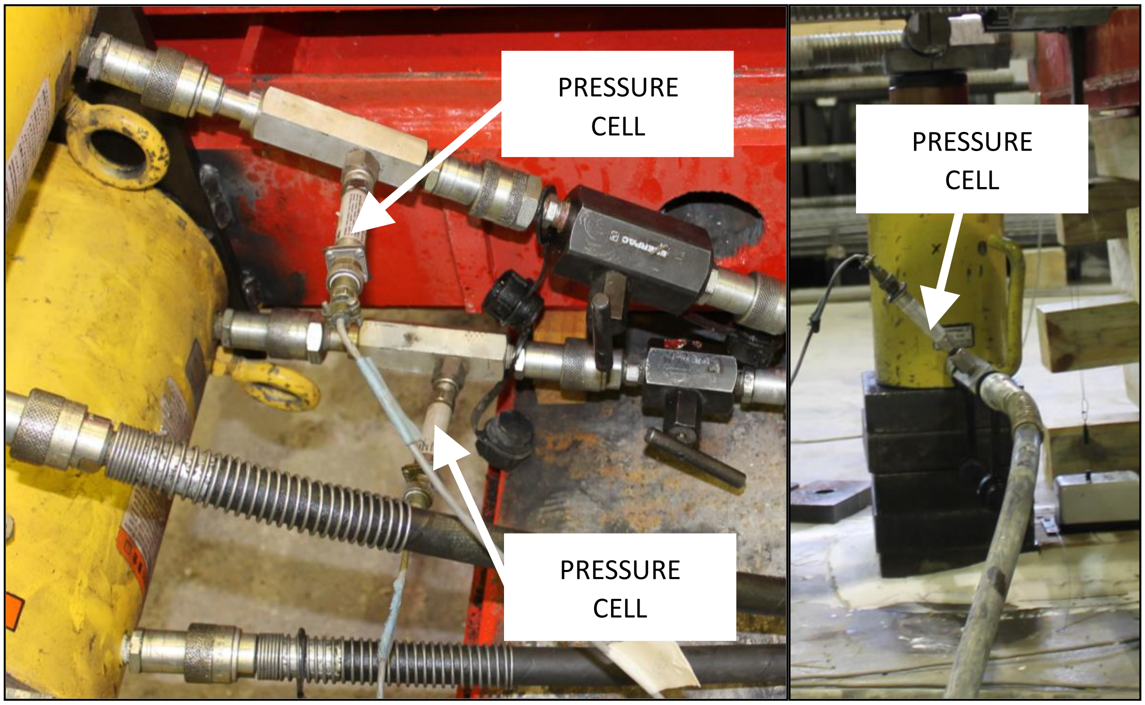

Figure 3.16 Pressure cell locations

3.7 PROCEDURE

For each test, the instrumentation was powered and offset to zero through a National Instruments Data Acquisition Chassis using a user interface developed by a third party. Once the instrumentation was set, the axial and shear forces were applied in a stepped fashion. The application of the axial force was controlled via a pendent that connected to the large stationary hydraulic pump. The shear force application was controlled by a trigger on a portable hydraulic pump. This stepped approach allowed for the loading to follow as closely to the intended loading ratio as possible. If the maximum axial load of 350 kips was reached, the hydraulic lines to the stationary pump were held constant with a check valve, and the loading continued with the single ram applying additional shear load. This load was applied at a rate of a trigger pull approximately every four seconds, this is consistent with ASTM E8.

During this loading, the axial load would begin to decrease as the flexural load increased and the pile softened, once the axial load fell below 330 kips it was increased again to 350 kips.

This process of shear loading and maintaining 350 kips axial load was continued until an appreciable amount of softening was detected. This was determined by observing the shear loading values and tracking the maximum shear achieved, noting fall off after each load application. Once the pile was considered failed, the load was carefully backed off and the test was concluded.

CHAPTER 4 DATA PROCESSING

Data collected was evaluated both during and after each test using a number equations. Axial force and moment were calculated for both the base section and the deteriorated section, in addition other key values were highlighted in the post-processing.

During the test, the axial force and moment were calculated to allow for proper monitoring of the load being applied. This was done by substituting the strain gage readings from a particular section into the following equations:

$$Axial\ Load = \frac{BTFL + BTFR + BBFL + BBFR}{4} * Modulus\ of\ Steel * Area$$

$$Moment\ Load = \frac{(BTFL + BTFR) - (BBFL + BBFR)}{2 * depth\ of\ cross\ section} * Modulus\ of\ Steel$$
$$* Moment\ of\ Inertia$$

The output from these equations determined where the test was in relation to the loading ratio desired and the load was adjusted as needed.

After the testing was complete, the data was exported and analyzed using Matlab. The strain values recorded during the test were converted into axial forces and moments for the base and deteriorated cross sections. The same equations from above were utilized for each case when the cross section being analyzed wasn't the failure section or had not been milled. When this was not the case, a more prescriptive analysis was employed. For the base a fiber analysis with linear interpolation and extrapolation of the cross section strains was utilized. The deteriorated section was analyzed by taking the measured strains and converting them into axial loads for each section based on the cross sectional area.

At the base section, the need for interpolating and extrapolating the strains was due to the buckling that occurred during the latter part of the test in the top flange. With this buckling, the readings from the top flange gages started to skew the results as they were only representative of one side of the flange. The fiber analysis was done by first determining the linear variation of the strain between the bottom flange and the middle of the web. This slope was calculated by averaging the bottom flange strain measurements and subtracting the web strain measurement, all of which was divided by half the depth of the section. The remaining strains for the section were calculated by multiplying the strain slope by the distance to that fiber and adding the average base strain.

$$Strain\ Slope = \frac{\varepsilon_{base} + \varepsilon_{middle}}{\frac{9.7}{2}}$$

$$\varepsilon_{top} = Strain\ Slope * 9.7 + \varepsilon_{base}$$

Once the strains were determined, the stress for each fiber was calculated. The stresses were capped at the yield stress of the steel that was being tested, as demonstrated in the following equations and Figure 4.1.

$$\sigma = \varepsilon * E$$

$$|\sigma| \leq f_y$$

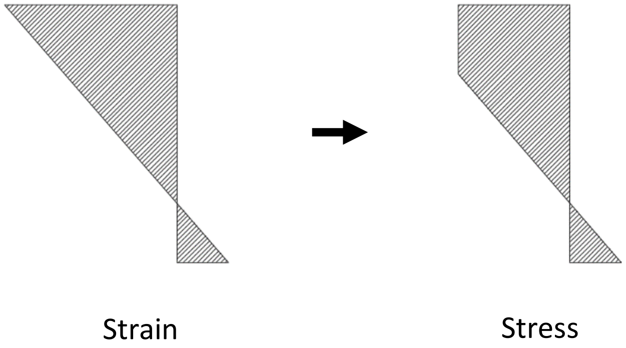

Figure 4.1 Strain diagram to stress diagram

This stress was then multiplied by the area of the fiber to get the force per fiber, shown in Figure 4.2.

$$P = \sigma * A$$

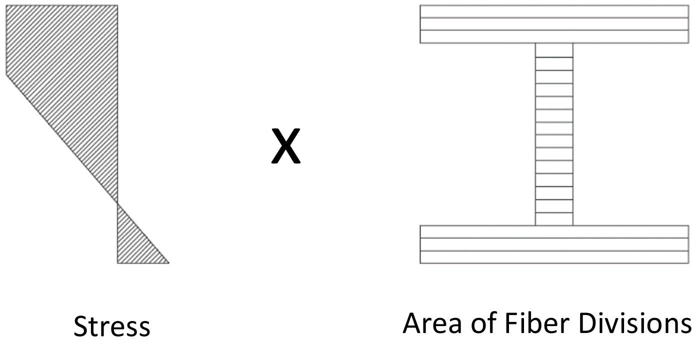

Figure 4.2 Stress diagram multiplied by the fiber areas

The axial force was then determined by summing the individual forces. The moment was determined by summing the force times the distance d (centroid of section to centroid of fiber), shown in Figure 4.3.

$$Axial\ Force = \sum P$$

$$Moment\ Force = \sum P * d$$

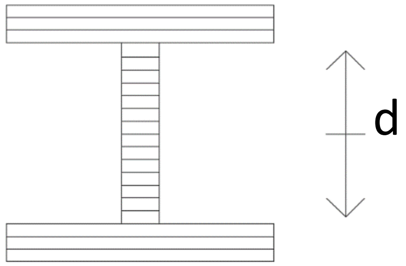

Figure 4.3 Determination of d value for base section

This extrapolation is fairly consistent over the elastic range but does start to deviate slightly towards the end of the stepped loading when compared to the measured values. This is most likely due to the actual location of the strain gages relative to the cross section. The calculations are based on dimensions of the theoretical cross section, and the placement of the gages was done with the precision of a tape measure.

For the deteriorated section, a similar concept as the fiber analysis with the base section was followed. First, the measured strains were averaged for each element. The elements shown in Figure 4.4, consisted of the top flange and stem (WT), the remaining middle portion of the web (Bar), and the bottom flange and stem (WT).

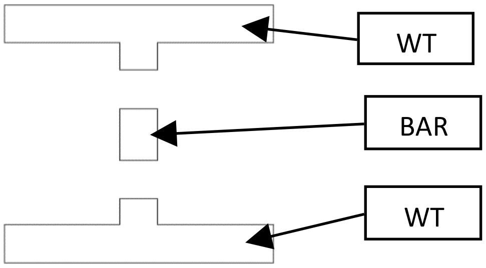

Figure 4.4 Element breakdown of deteriorated section

The three average strains were then multiplied by that element's area and the modulus of elasticity. This provided the axial force for each element.

$$\epsilon = \frac{\epsilon_{left} + \epsilon_{right}}{2}$$

$$\sigma = \varepsilon * E$$

$$|\sigma| \leq f_y$$

$$P = \sigma * A$$

Taking the axial force times the distance of that element's centroid to the centroid of the section gave the moment in that element, demonstrated in Figure 4.5. Summing the element values of the axial force and moment gave the cross section's axial force and moment.

$$Axial\ Force = \sum P$$

$$Moment = \sum P * d$$

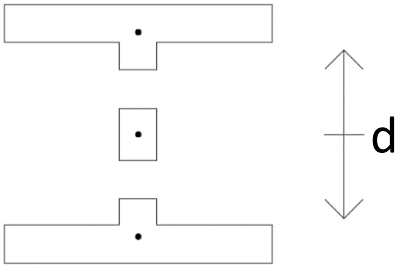

Figure 4.5 Determination of d value for deteriorated section

In addition to analyzing the strains, the first yield of the section was determined by first taking the yield stress divided by the modulus of elasticity and comparing it to the individual strain gages at each location. Once this was determined, it was plotted for comparison on graphs in subsequent sections. A similar procedure was used for the location of the end of the stepped loading, the maximum shear achieved, and web yield if it occurred.

The bond between the steel and the concrete was calculated by comparing the base section axial results to the deteriorated section axial results. The difference in the loads was taken as the amount of axial load transferred to the concrete around the deteriorated section. The axial force difference was divided by the surface area of the pile on either side of the deteriorated section, such that the load would have to be transmitted by the surface area on one side of the deteriorated section to the concrete and back to the steel on the other side of the deteriorated section, as illustrated in Figure 4.6.

$$Bond = \frac{Base\ section\ axial\ load - Deteriorated\ section\ axial\ load}{pile\ surface\ area}$$

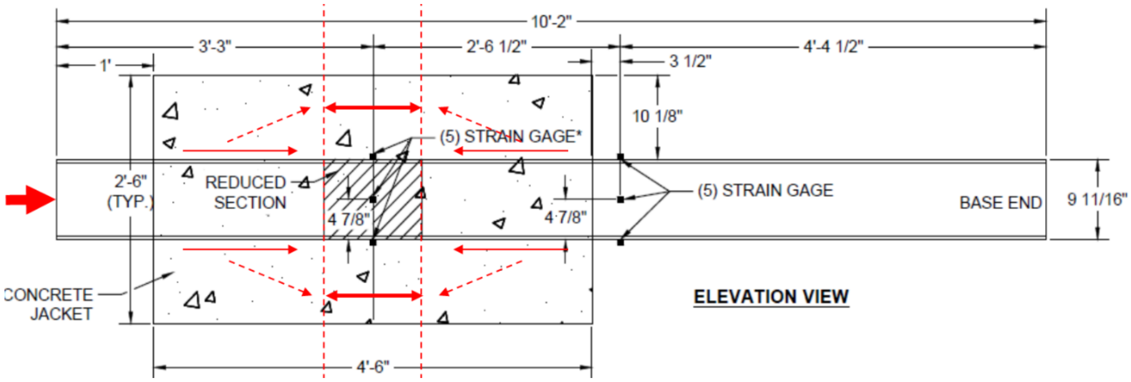

Figure 4.6 Retrofit load flow

A majority of the test data required no adjustments aside from unit conversions and calculation of axial and moments from strains. Two tests did exceeded the stroke of the shear applying ram and required that the pile be held in place by a stand and the ram reset. This occurred during the non-deteriorated and retrofitted pile bent tests. During the non-deteriorated test the ram had to be restroked two times and during the second time the string pot measuring displacement at that location was also restroked. The restroking locations are indicated on the shear vs. displacement plots by a dashed line.

CHAPTER 5 EXPERIMENTAL RESULTS

5.1 INTRODUCTION

The experimental test results are presented in this section along with a comparison of each case. Information is provided in graphical form for axial and moment load, shear and displacement, and strain measurements at the base and deteriorated sections. Furthermore, details on the tested material strengths are also presented. These material strengths were used to update the calculations from the experimental design section and used in calculations presented in the data processing section.

5.2 MATERIAL TESTING

To better represent the strength of the materials used, individual tests were performed on coupons from the steel pile and cylinders from the retrofit concrete. For the steel tensile coupon testing, there were two sample sets. The first sample set was for all of the piles except for the non-deteriorated case abutment pile. Two sample sets were required since the non-deteriorated abutment pile was from a different heat then the other five pile specimens. This was not the case for the concrete as both retrofit jackets were placed at the same time from the same batch, which allowed for one set of samples to be utilized for both.

From the tensile coupon test, the steel's yield properties were obtained, this data allowed for more accurate numerical evaluation. As can be seen in Table 5.1, the yield strength is 5 and 6 ksi above the given design strength of the steel (50 ksi). The following test average stress/strain curves in Figure 5.1 and Figure 5.2 were also obtained.

Table 5.1 Steel yield strength results

	Steel Yield Strength
Remaining Abutment Case and Pile Bent Case Piles	56 ksi
Abutment Case, Non-deteriorated Pile	55 ksi

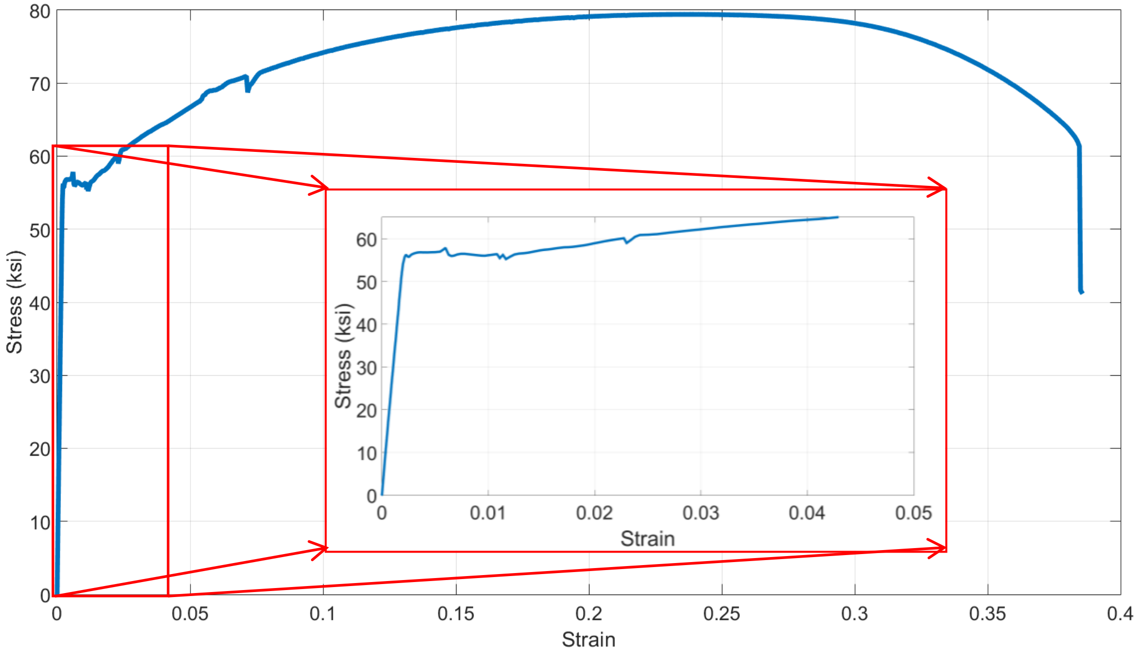

Figure 5.1 56 ksi stress vs. strain

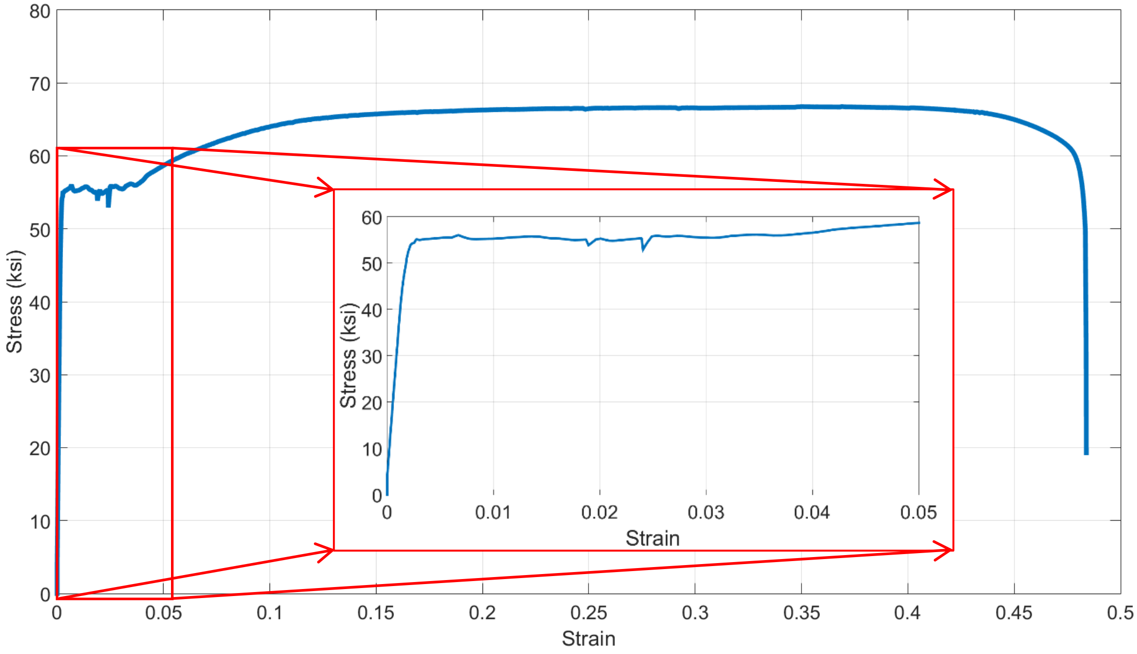

Figure 5.2 55 ksi stress vs. strain

The concrete sample cylinders were tested at three, seven, 14, and 28 days. The samples met the required strength of 3,000 psi within three days and were above double that at 28 days. These results are presented in Table 5.2 and Figure 5.3.

Table 5.2 Concrete strength results

Units (psi)	Sample A	Sample B	Sample C	Average
3 Day Break	4,240	4,460	4,040	4,250
7 Day Break	5,120	5,010	5,040	5,060
14 Day Break	5,550	5,720	5,820	5,700
28 Day Break	6,160	6,650	6,530	6,450

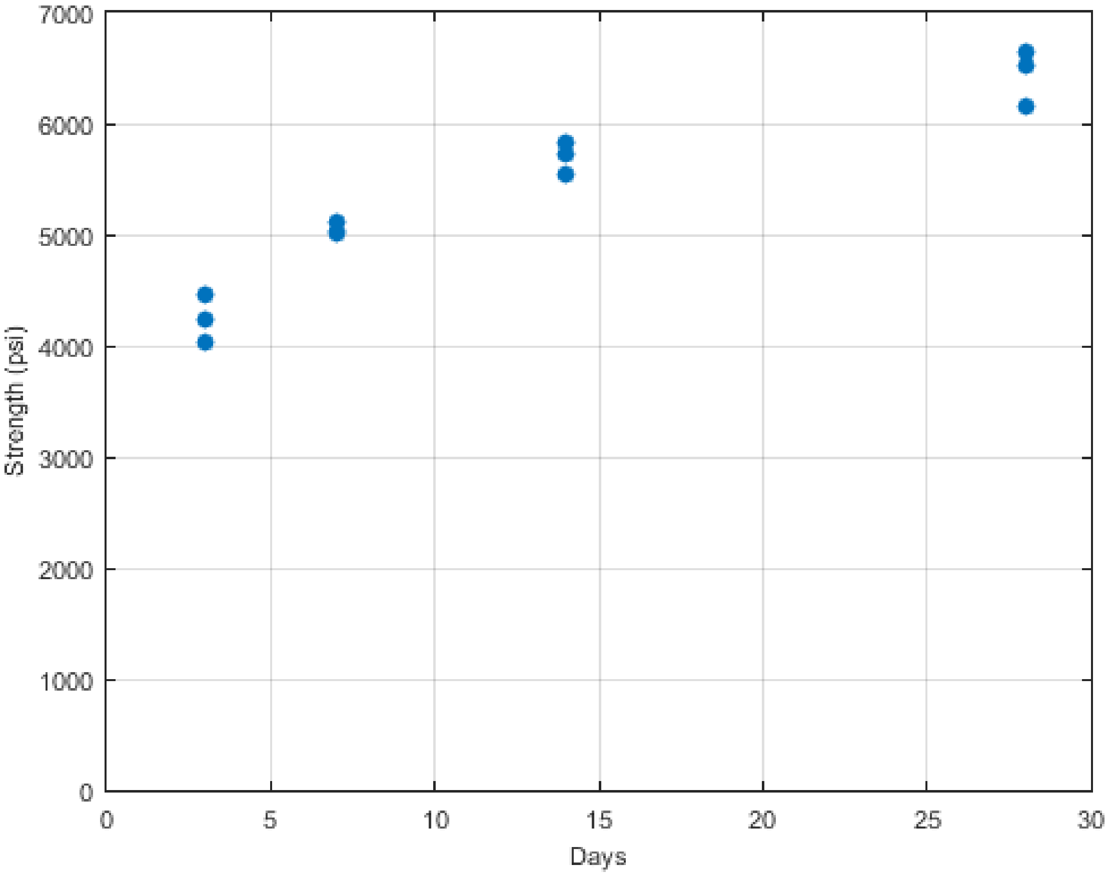

Figure 5.3 Concrete strength vs. days

5.3 ABUTMENT CASE: NON-DETERIORATED

The non-deteriorated abutment test, shown pretest in Figure 5.4, resulted in a compression flange local buckling failure as calculated. Based on calculations done using AISC (2011) equations, the pile was expected to experience compression flange local buckling in pure flexure and flange local buckling in pure compression. Since both the compression and flexure limits had similar failure cases, a local buckling failure of the top flange near the base end of the pile was anticipated, as shown in Figure 5.5 and Figure 5.6.

Figure 5.4 Non-deteriorated abutment test

Figure 5.5 Buckling of base section top flange

The failure was slow in its progression as the steel started to soften after reaching its yield limit. The stockiness of the pile’s cross section, coupled with its relatively short overall length, provided a great deal of stiffness and allowed the section to carry loads near the material’s plastic limit as illustrated in Figure 5.7. Once the pile started to trace out along its capacity envelope, each addition of load from the axial rams or shear ram resulted in a reduction of load in the other. For example, once the maximum shear was reached (see Figure 5.8), each time after the axial load was increased to maintain 350 kips, the shear would drop. This load shedding was indicative of some second-order effects taking place. The axial load was eccentric enough that it began to impact the moment reaction at the base of the pile. This

Figure 5.6 Localized failure of base section flange

effect can also be seen in Figure 5.9 from the deteriorated section. The deteriorated section measurements track out similarly to the base section measurements and as the base section begins to yield and soften, the deteriorated section shows the induced-moment beginning to decrease and the pile no longer carried additional load. Each time the axial load was adjusted, the moment decreased much more rapidly and could not be obtained again. This cycle of softening was played out a few times by the deteriorated section plot and matches with the shear load plot in Figure 5.8. This phenomena can also be seen in Figure 5.9, where after reaching the maximum shear the strain values plateau and begin to decrease.

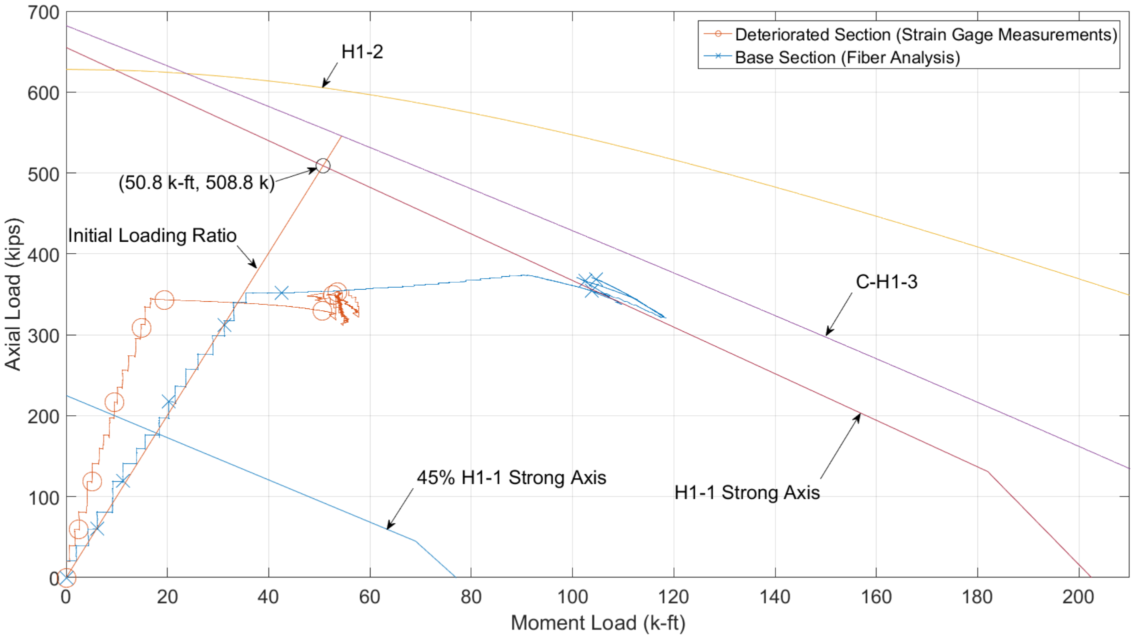

Figure 5.7 Non-deteriorated abutment case axial vs. moment

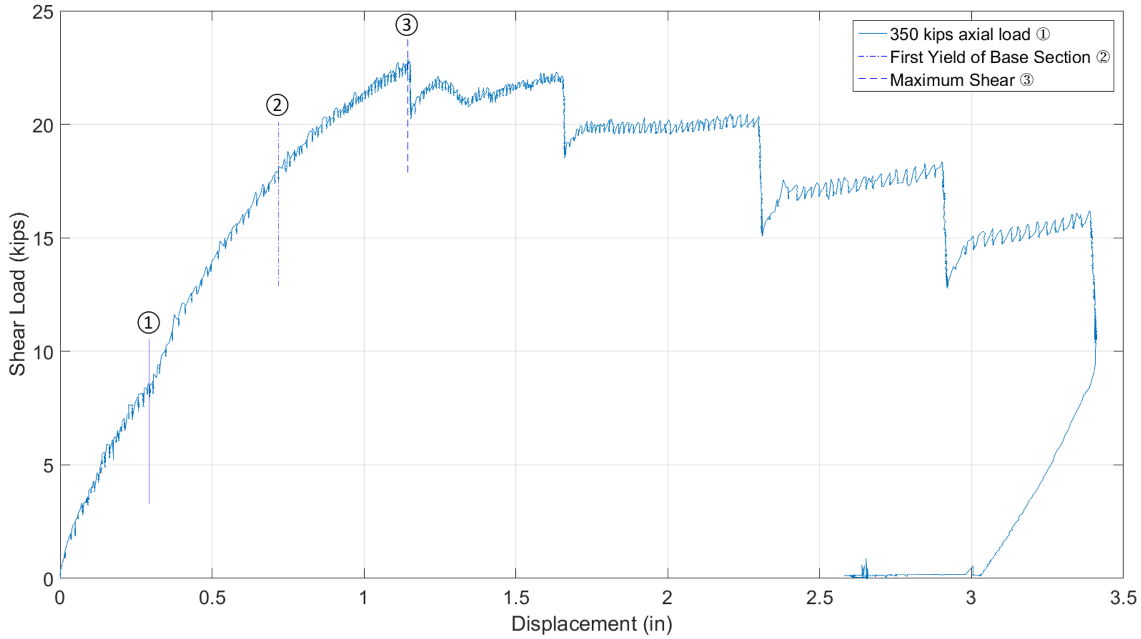

Figure 5.8 Non-deteriorated abutment shear vs. displacement

The localized failure, shown in Figure 5.6, began due to residual stresses that occur in the steel from production, and this led to the global failure of the section. Figure 5.10 provides a clear picture of the top flange of the base section reaching yield and then proceeding to buckle. This occurred after reaching the 350 kip axial load (as indicated by the encircled 1) and prior to the maximum shear (as indicated by the encircled 3) being reach. This again was the anticipated failure due to the geometry of the pile.

From the analytical calculations, the pile performed as expected and provided a solid baseline in which to compare the remaining abutment tests against. The next two sections will describe the deteriorated and retrofitted test results, and how they compare to the results just presented.

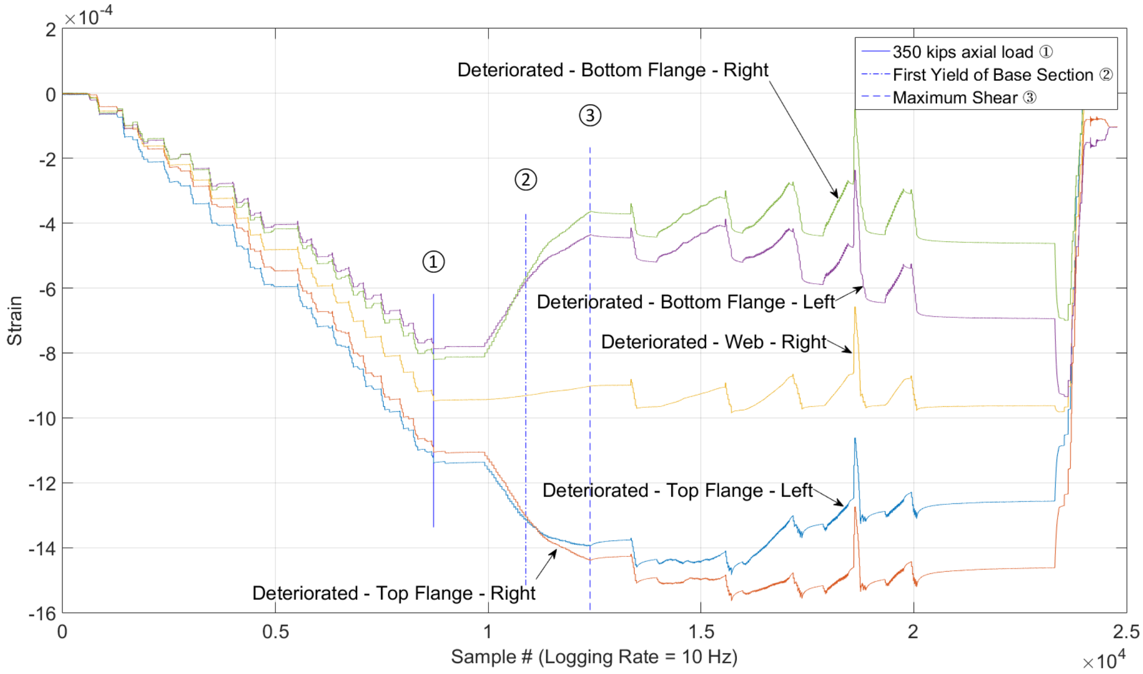

Figure 5.9 Non-deteriorated abutment deteriorated section strain vs. sample

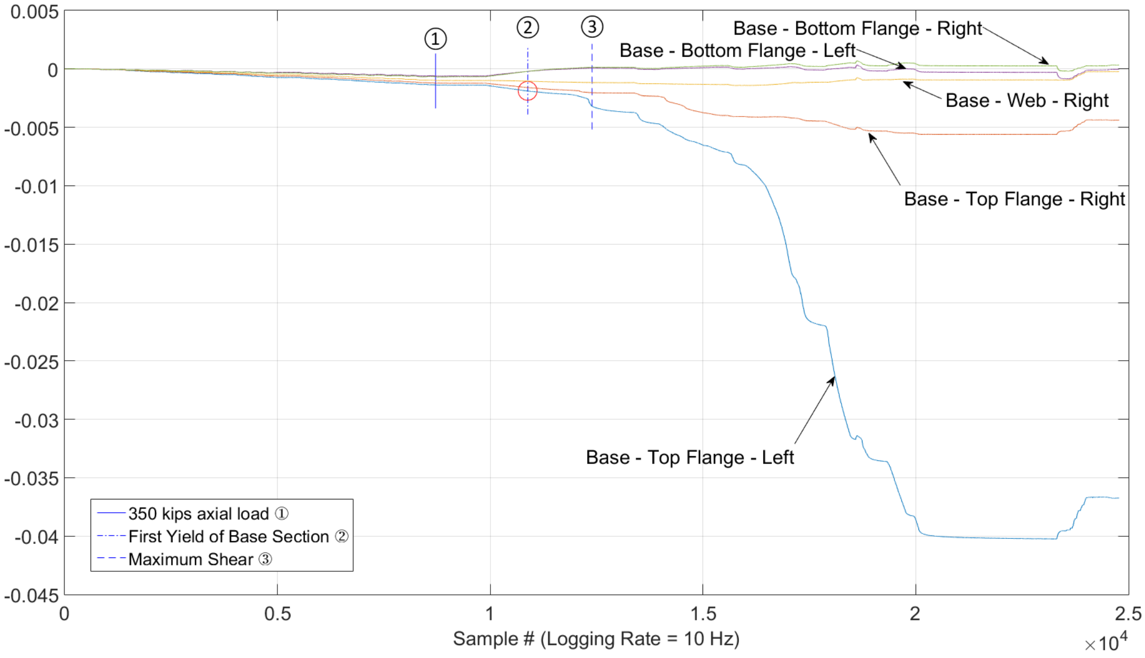

Figure 5.10 Non-deteriorated abutment base section strain vs. sample

5.4 ABUTMENT CASE: DETERIORATED

For the deteriorated abutment case (pictured in Figure 5.11) the initial failure of the deteriorated section was not as predicted, a local failure of the deteriorated section top flange, but began with buckling of the web instead. This led to load being shed to the flanges and the top flange taking control of the failure. The pile then exhibited a hinged shear failure, as illustrated in Figure 5.12, through the section as the test carried on. The section proved to be stronger then calculated and exceeded 250 kips in compression.

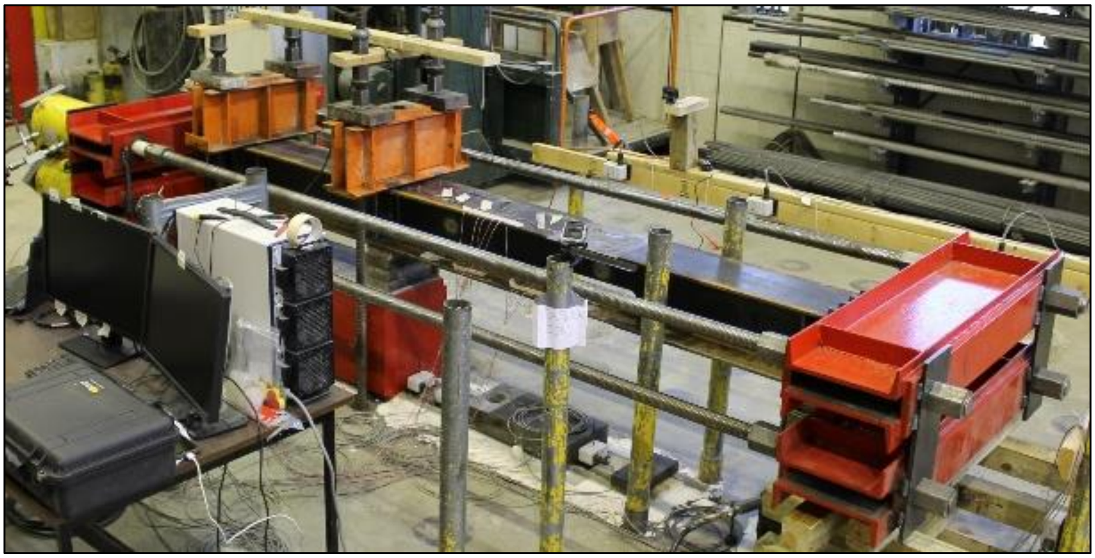

Figure 5.11 Deteriorated abutment test

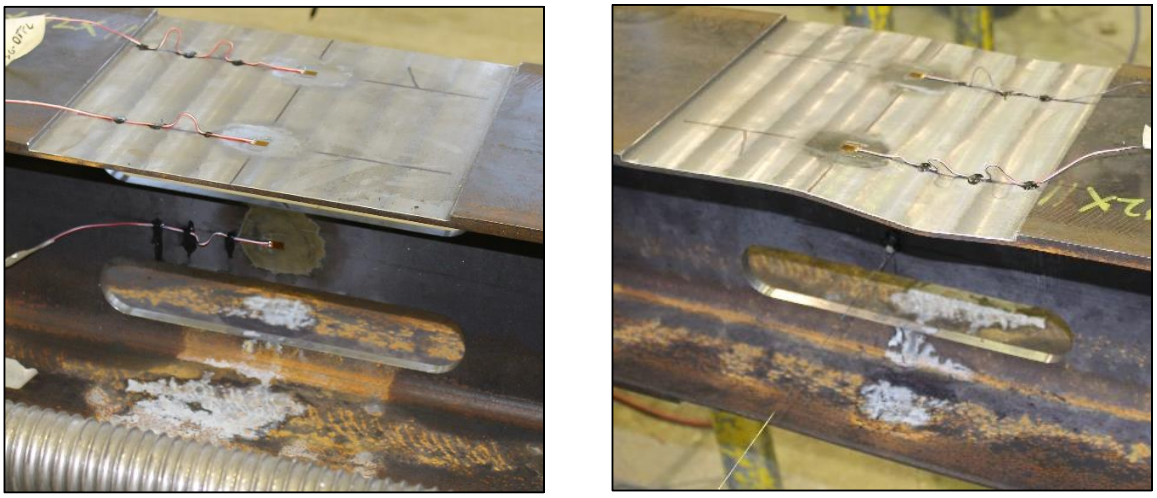

Figure 5.12 Before and after deteriorated abutment test pictures of the deteriorated section

The initial failure of the pile began with the deteriorated web section buckling slightly. This was not a perceivable event, but from Figure 5.14 the strain measurement at the web starts to deviate from the trend of the group near the 10,000 sample mark. This displacement of the web shifted load to the flanges and led to the top flange buckling. The overloading of the top flange caused an initial local buckling of the left side of the top flange but then progressed into a global buckling of the top flange. With the instability of top flange, the shear load began to accelerate the failure. The short distance between the shear load point and the deteriorated section resulted in the shear controlling over the small developed moment. This led to a shearing failure of the deteriorated section which can be seen visually in Figure 5.12 and Figure 5.13. From the strain measurements in Figure 5.14, the top left flange for the deteriorated section buckled causing tension at the location of the strain gage. Additionally, the hinging shear failure resulted in concentrated stresses at the end of the reduced web section as shown in Figure 5.13.

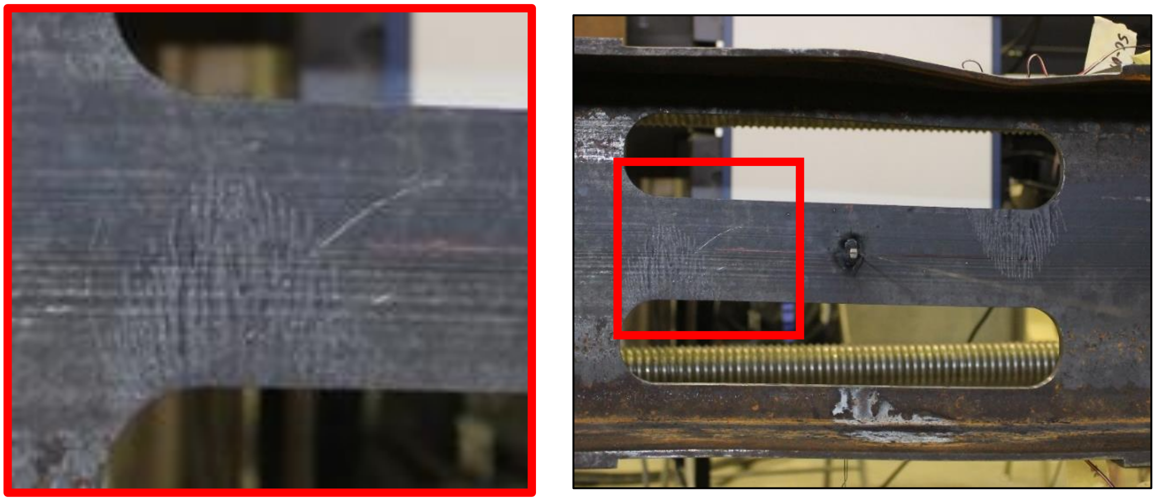

Figure 5.13 Deteriorated abutment shear failure at deteriorated section

The anticipated pile capacity is plotted in Figure 5.15 and shows that the pile performed above expectations. The geometry of the section is likely what led to such a substantial increase in capacity over expected values. In calculating the capacity, the section was treated as individual elements and analyzed using AISC (2011) equivalent sections. The rounded hole opening likely provided increased load sharing between elements and resulted in a stronger cross section. Figure 5.16 and Figure 5.17 provide addition data on the shear load and the base section strains respectively.

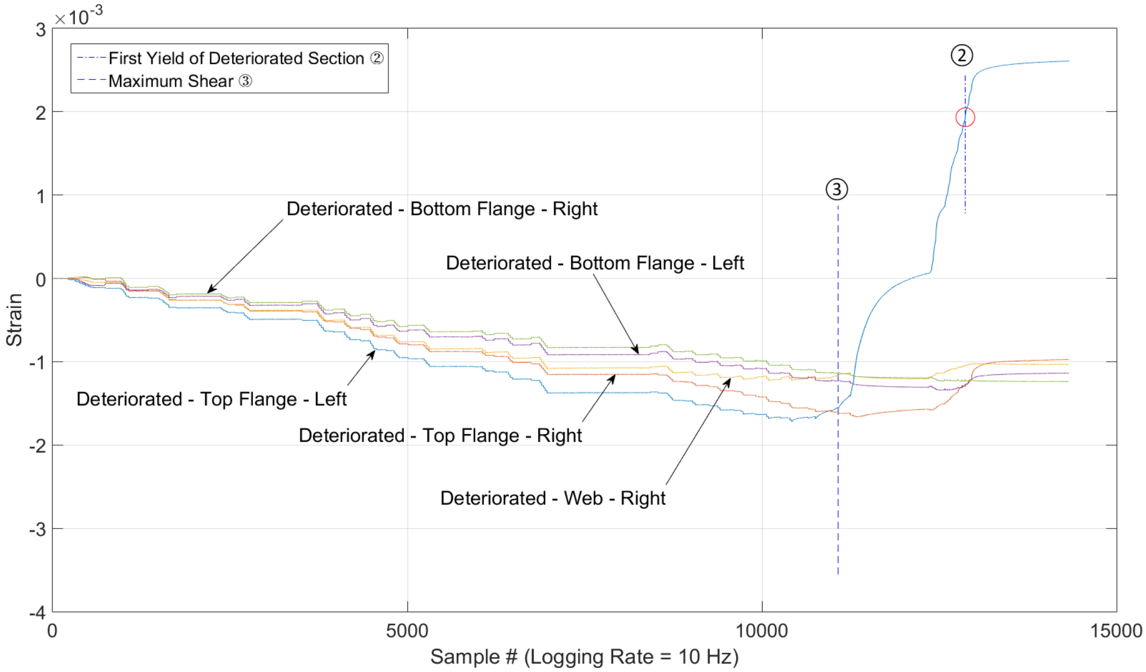

Figure 5.14 Deteriorated abutment deteriorated section strain vs. sample

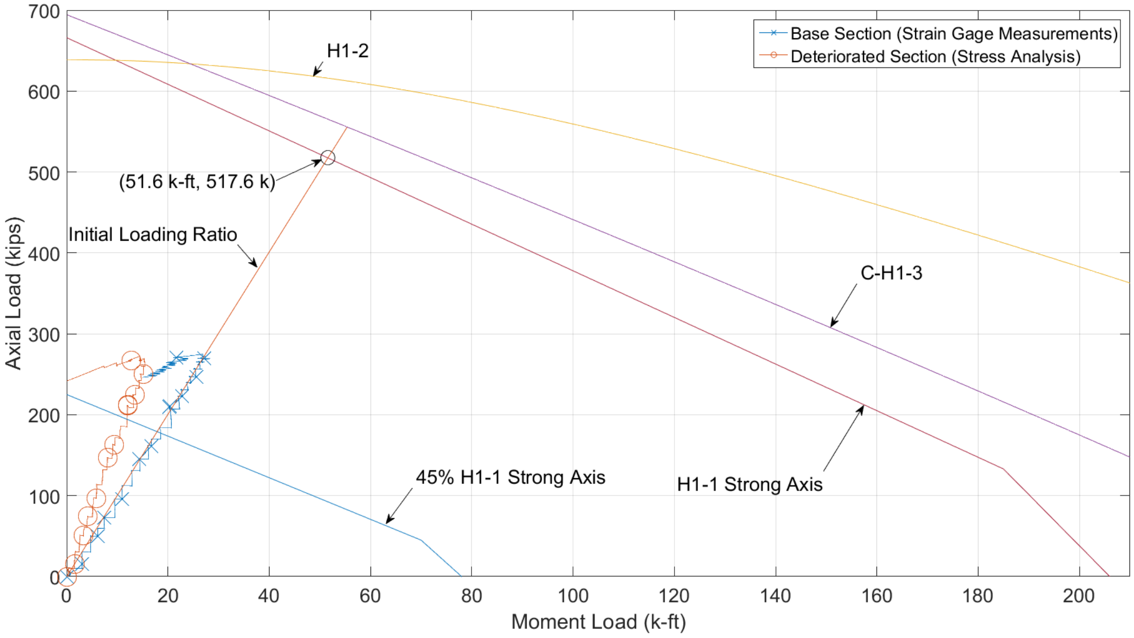

Figure 5.15 Deteriorated abutment axial vs. moment

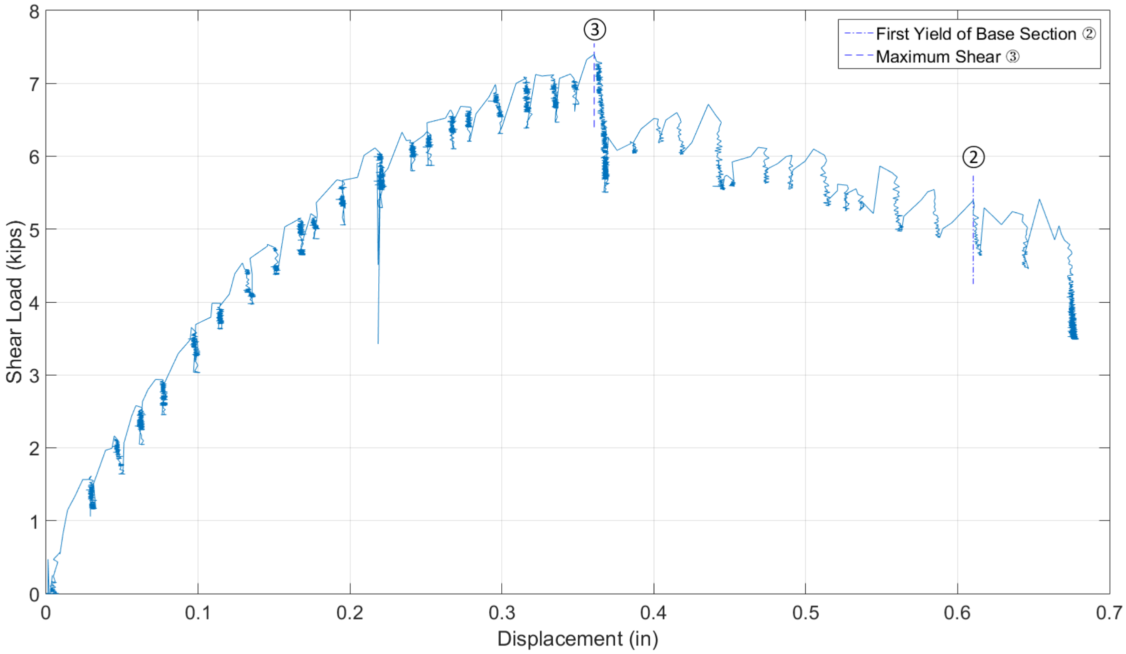

Figure 5.16 Deteriorated abutment shear vs. displacement

Figure 5.17 Deteriorated abutment base section strain vs. sample

5.5 ABUTMENT CASE: RETROFITTED

Figure 5.18 Retrofitted abutment test

The outcome of the abutment retrofit test was positive. The retrofit (pictured in Figure 5.18) performed as intended by stabilizing the deteriorated section and restoring the pile back to its original non-deteriorated strength. The pile was able to withstand the same loading as the non-deteriorated pile and even carried a slightly higher shear load. A small increase in stiffness was an additional benefit, and the buckling failure seen in the deteriorated test was eliminated.

Figure 5.19 Retrofitted abutment buckling of base section

The pile failed in a similar manner to the non-deteriorated pile and the third failure case presented above. As a reminder, the Failure Case 3 was a local buckling failure outside of the retrofitted section. The pile buckled locally in the top flange on either side of the web as illustrated in Figure 5.19. This buckling was limited in the distance along the pile that it could propagate by the tie down and the concrete. The retrofit provided bracing for the cross section of the pile and held it rigidly in place, causing the buckling zone to be shorter than in the non-deteriorated test.

The redistribution of forces within the retrofit were of particular interest in establishing the amount of composite action was being obtained. The results from this test indicate that the concrete bond was substantial and the retrofit transmitted a considerable amount of load around the deteriorated section. As can be seen in Figure 5.20, the load applied to the deteriorated section was less than 100 kips and 10 k-ft. With the reduced force, the buckling seen in the deteriorated case, at the deteriorated section, was not detected in the retroffited test. With the concrete jacket, it was not possible to directly observe the reaction of the deteriorated section to the loading, but based on the measured strains in Figure 5.21, the section did not undergo enough strain at the measured locations to reach a yielding limit of 56 ksi.

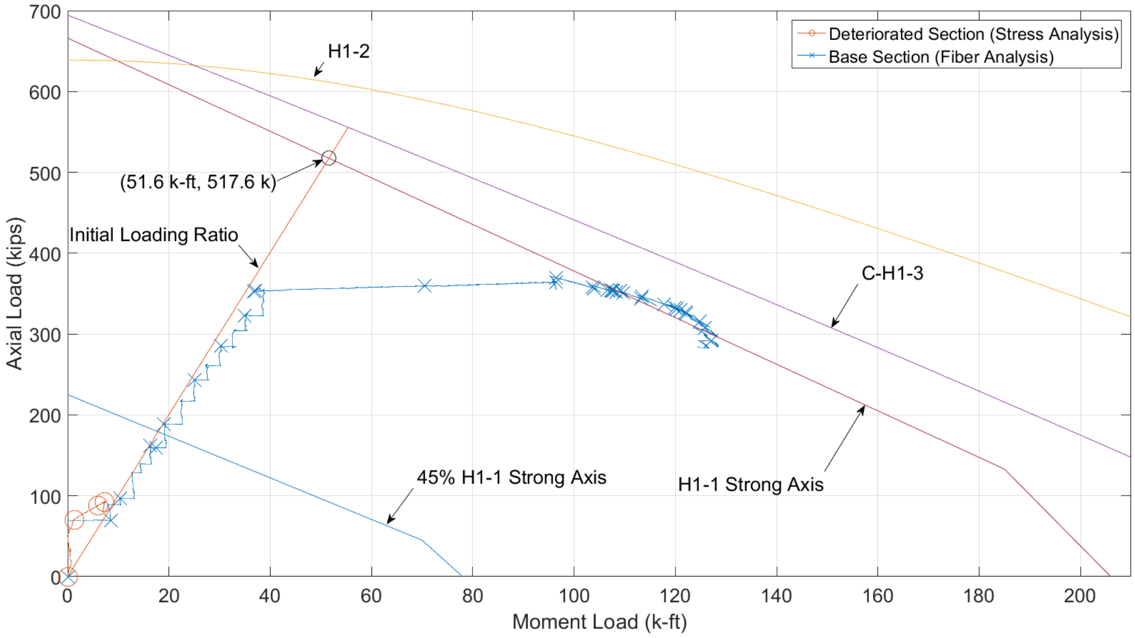

Figure 5.20 Retrofitted abutment axial vs. moment

In addition to the elimination of buckling at the deteriorated section, the pile saw less displacement in comparison to the non-deteriorated case (see Figure 5.22). This demonstrated an increase in the overall stiffness of the pile. This added stiffness allowed the pile to carry more load prior to softening in comparison to the non-deteriorated case. The resulting increase in shear load applied to fail the pile was 2 kips, which is a 9% increase over the non-deteriorated case.

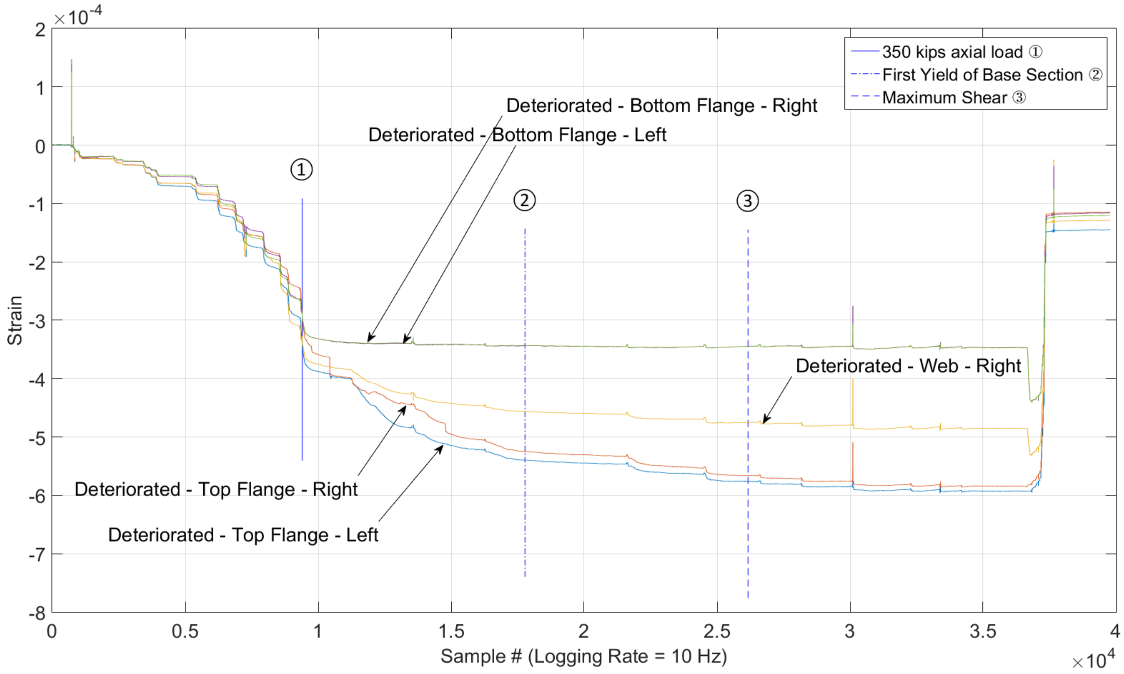

Figure 5.21 Retrofitted abutment deteriorated section strain vs sample

The amount of load that was transferred to the concrete prior to the deteriorated section was unexpected when compared to the bond strength recommended in AISC (2010) for steel to concrete. The bond strength that was anticipated for this retrofit was 71 kips (NCHRP data was not discovered until after the experimental study was completed), as presented in the experimental design section. From the strain gage data within the concrete jacket, the maximum axial load carried by the pile was 93 kips of the 333 kips applied at that same time. The remaining 240 kips was then carried by the jacket through the concrete/steel bond. This gave a minimum bond of 203 psi, which is 3.38 times greater than the AISC (2010) recommended value.

As was the case for the non-deteriorated test, the top flange buckled and yielded first in the cross section. Figure 5.23 shows the top right flange yielding first and then the top left flange yielding next. The top left flange then experienced the greatest buckling between the two locations.

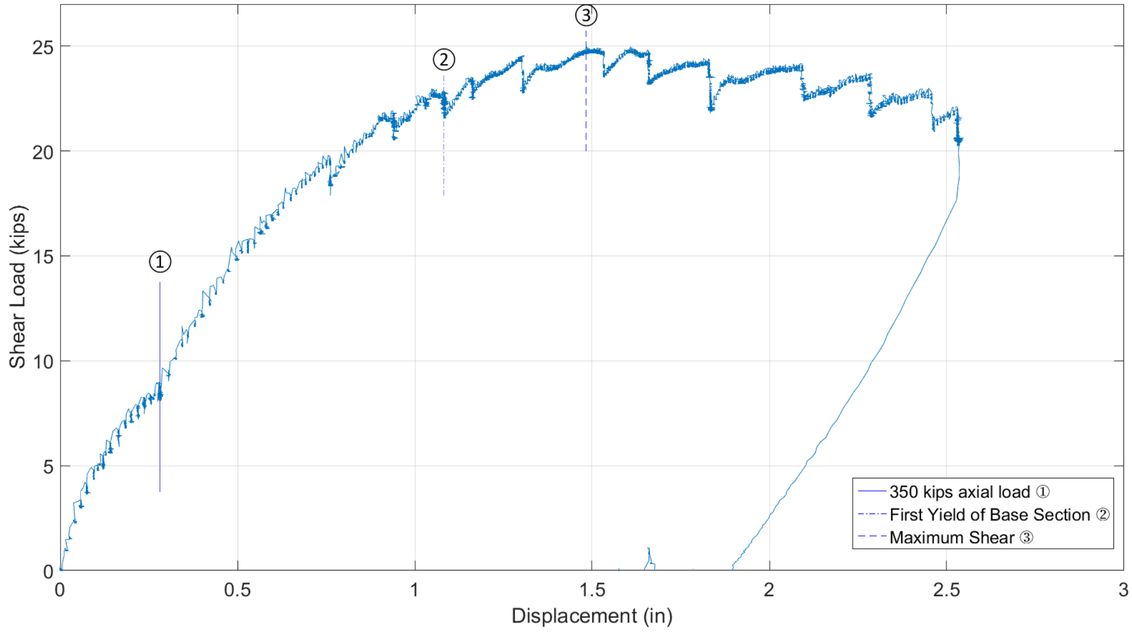

Figure 5.22 Retrofitted abutment shear vs. displacement

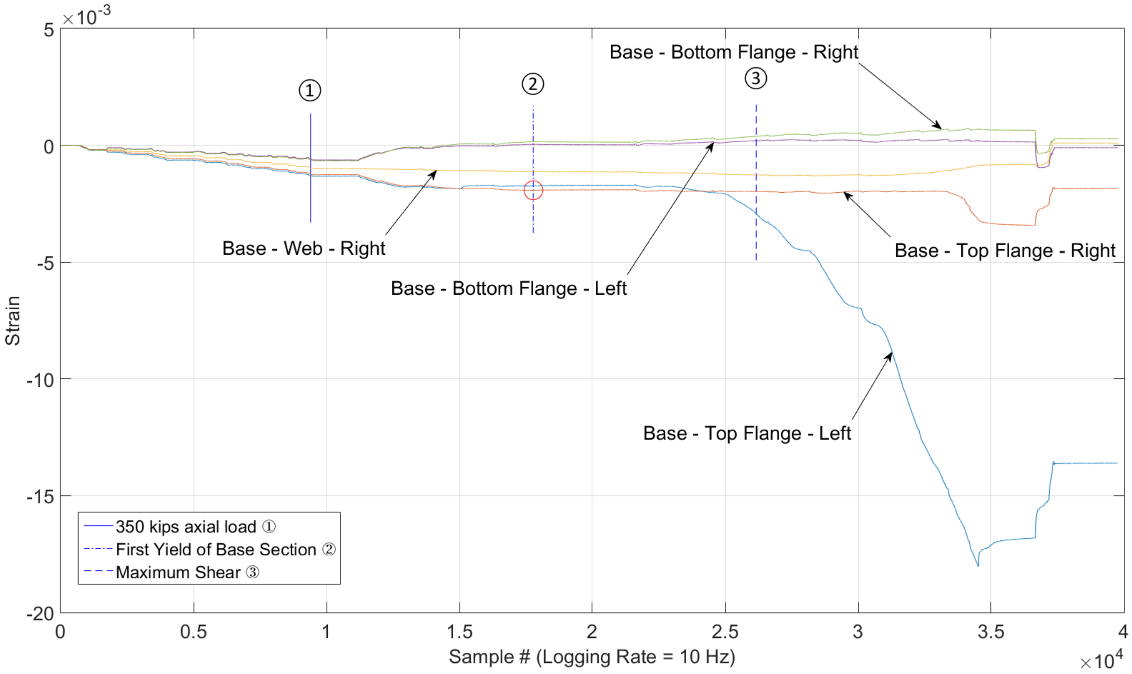

Figure 5.23 Retrofitted abutment base section strain vs. sample

5.6 ABUTMENT CASE: OVERVIEW

As mention in the previous section, the results from the abutment case provided satisfying data to compare between the three tests. The end product of the retrofitted test was a demonstration that the retrofit exceeded expectations. From this testing, the repair appears to be a reasonable repair option for NDOR to return strength to deteriorated piles.

The abutment case was different from the pile bent case in that it had one pile with a different steel strength. The difference was 1 ksi and does not appear to have adversely affected the results. Looking at the base section results, Figure 5.24, it can be seen that the non-deteriorated case and the retrofitted case under went similar loading but differed during the softening of the pile. The difference does not appear to be one that gives one pile an advantage over the other.

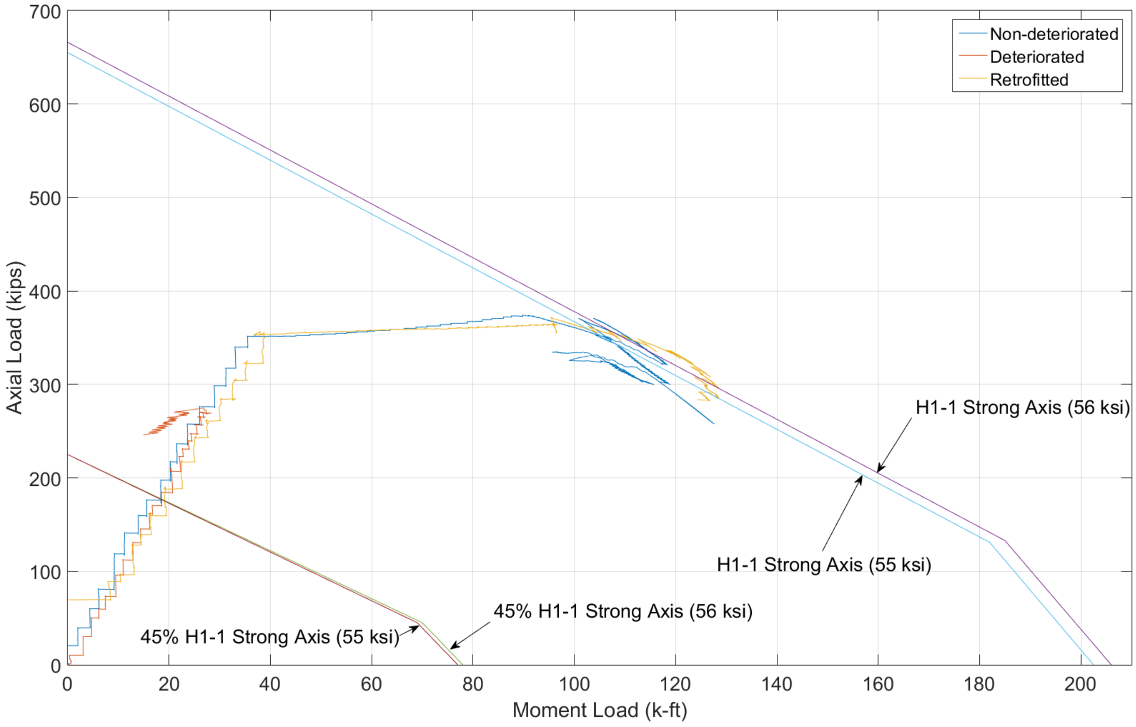

Figure 5.24 Abutment case base section axial vs. moment

The deteriorated section benefitted greatly from the retrofit, as shown in Figure 5.25. Prior to the retrofit, the deteriorated section carried a significant amount of load. The retrofit reduced that load to less than a third of the non-deteriorated test and eliminated the buckling seen in the deteriorated test.

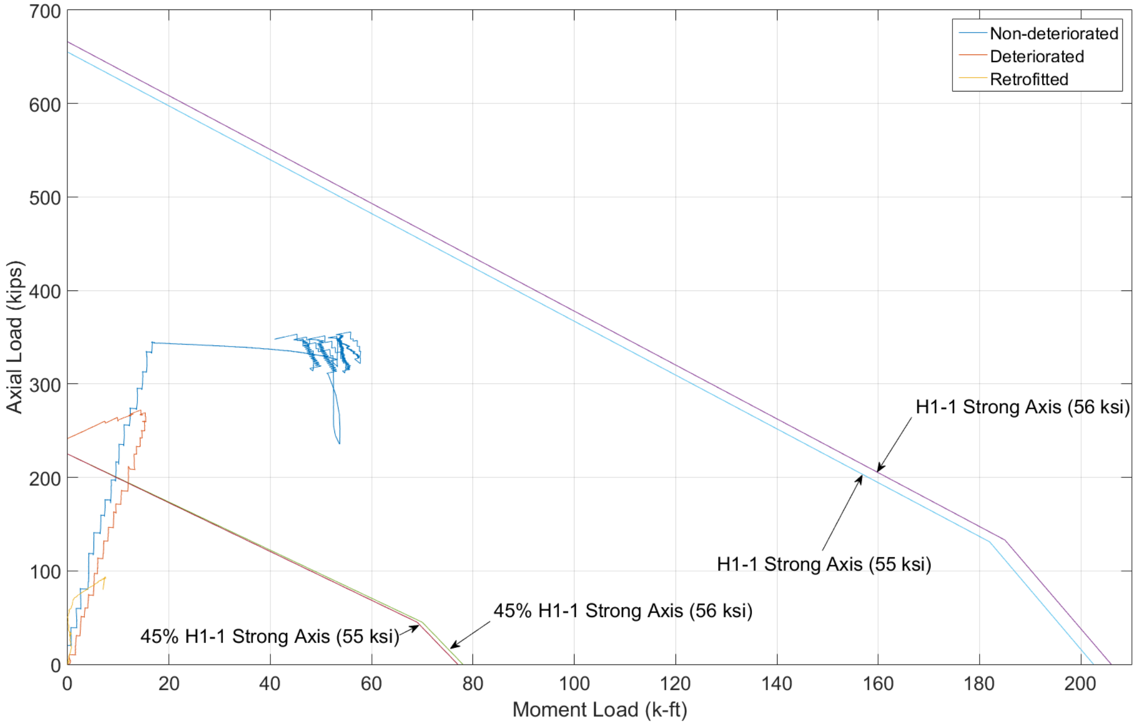

Figure 5.25 Abutment case deteriorated section axial vs. moment

5.7 PILE BENT CASE: NON-DETERIORATED

Of the four test without concrete, the non-deteriorated pile bent case pile (pictured in Figure 5.26) experienced the greatest combination of failures. There were two localized failures, as well as a global failure. The first localized failure was of the top flange behind the tie down location, and the second was a local failure of the top flange at the base section. The final failure the pile experienced was an out of plane failure. The localized failure behind the tie down was not expected but did not impact the test outcome. The other failures where predicted and matched the analytical limit states.

Figure 5.26 Non-deteriorated pile bent test

The initial buckling of the pile, along its top flanges behind the tie down spreader beam, was caused by rotation of the spreader beam. The moment was strong enough at the base to cause the tie down spreader beam to pivot on top of the pile and deform the flange behind it. Further into the loading, the pile began to locally buckle in a similar manner to the abutment non-deteriorated case at the base location, which is visible in Figure 5.27. The pile's stocky geometry and length still indicated that the full plastic moment was the calculated capacity at which the pile should

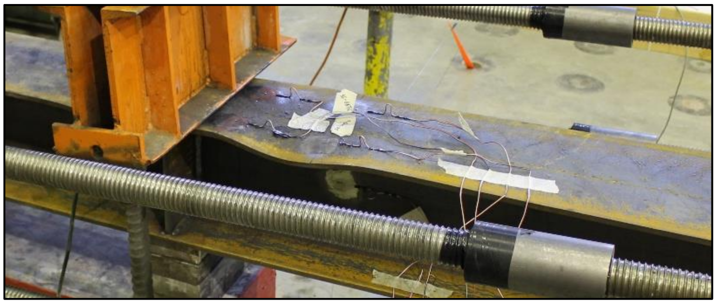

Figure 5.27 Non-deteriorated pile bent local buckling of base section

fail, but the unbraced length was approaching that of the Inelastic Lateral Torsional Buckling (LTB) limit. Once the pile began to buckle, the instability allowed the pile to start twisting and displacing laterally. This lead to a notable LTB failure between the deteriorated section location and the base, as shown in Figure 5.28. This could also be seen in the strain measurements for the deteriorated section shown in Figure 5.29.

Figure 5.28 Non-deteriorated pile bent LTB failure

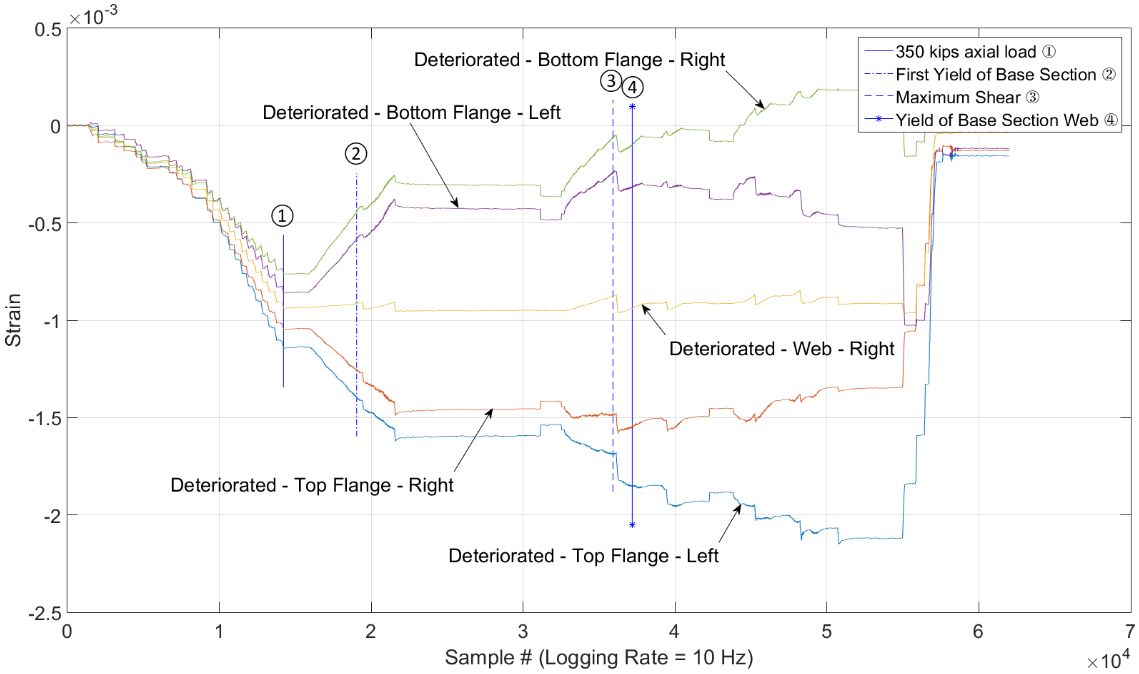

Figure 5.29 Non-deteriorated pile bent deteriorated section strain vs. sample

The displacement and deformation that the pile underwent resulted in the first test with yielding that occurred in the web. As can be seen in Figure 5.31, and Figure 5.32, the pile reached its maximum shear and shortly after, as the section was softening from the top down, the web yielded through its mid-depth. Like the non-deteriorated abutment case, the pile exceeded the H1-1 Strong Axis envelope and failed prior to the H1-1 Strong Axis (Plastic) envelope in Figure 5.30.

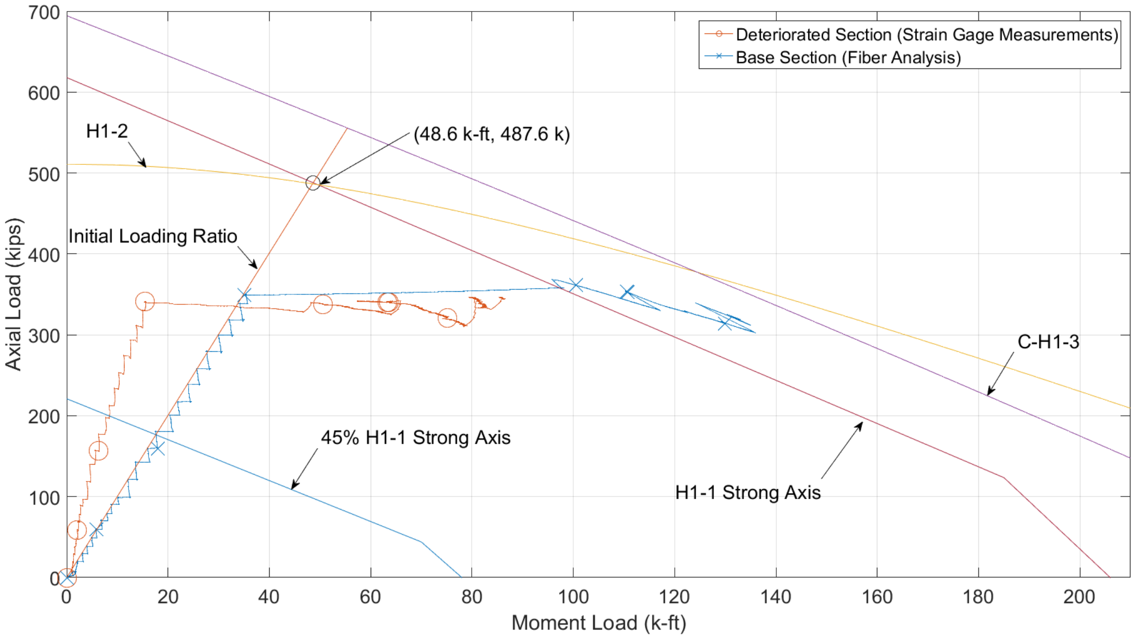

Figure 5.30 Non-deteriorated pile bent axial vs. moment

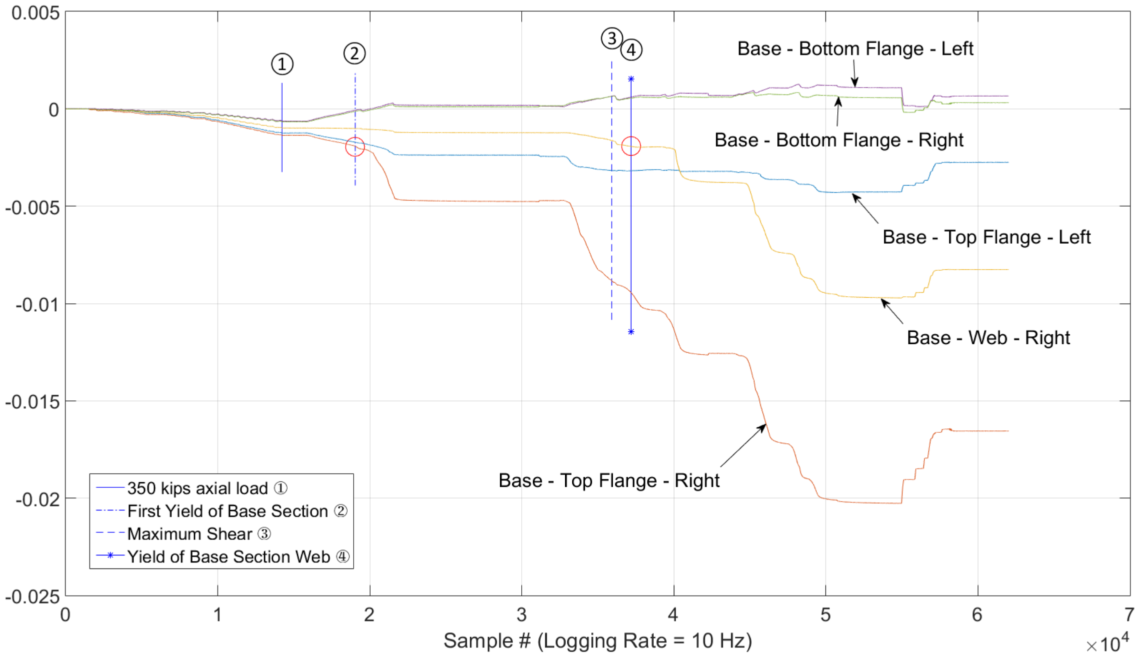

Figure 5.31 Non-deteriorated pile bent base section strain vs. sample

In comparison to the abutment case, the non-deteriorated pile bent test was expected to have a similar failure but with less shear. This was due to the overall height of the pile bent being greater than the abutment case. As mentioned before, the length of the pile was still short enough that the theoretical limit should have been the plastic limit in flexure, but the pile was only a few feet from qualifying for the LTB limit state. With the initial local buckling of the pile, the instability in the section allowed for the LTB limit state to take effect. The additional length also allowed the pile to deflect a greater distance which gave the largest displacement from all of the tests at approximately 11 inches, see Figure 5.32.

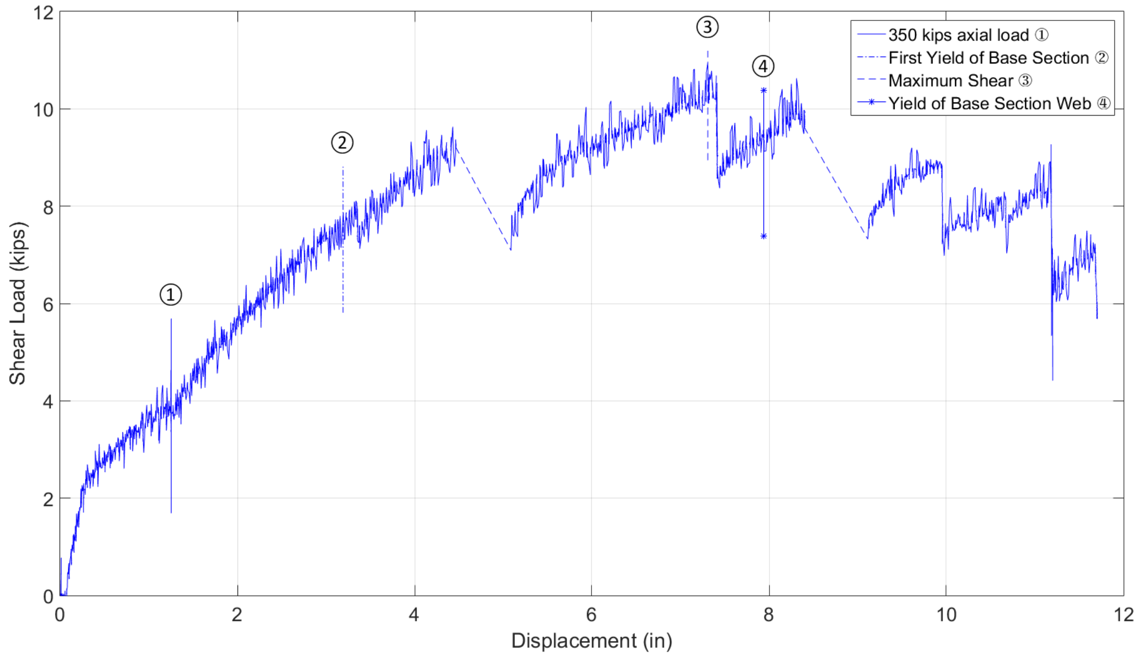

Figure 5.32 Non-deteriorated pile bent shear vs. displacement

This non-deteriorated test, like the abutment case, matched well with the theoretical limit states and provided a satisfactory baseline to which the remaining pile bent tests could be compared too.

5.8 PILE BENT CASE: DETERIORATED

The deteriorated pile bent case (pictured in Figure 5.33) underwent the most sudden failure that was observed during the pile testing. Local buckling in the web of the deteriorated section preceded a global buckling (pictured in Figure 5.34) of the cross section at the deteriorated location. The pile buckled in plane in the upper flange and out of plane in the web. The deteriorated section shortened by half an inch in the top flange, and the web buckled out approximately 7/8 of an inch. Overall, the pile displaced vertically 5.5 inches, 4.4 inches of which were gained during the sudden failure, as shown in Figure 5.35. The pile still carried some load after the buckling as shown in Figure 5.36, but any additional load would have resulted in continued deformation.

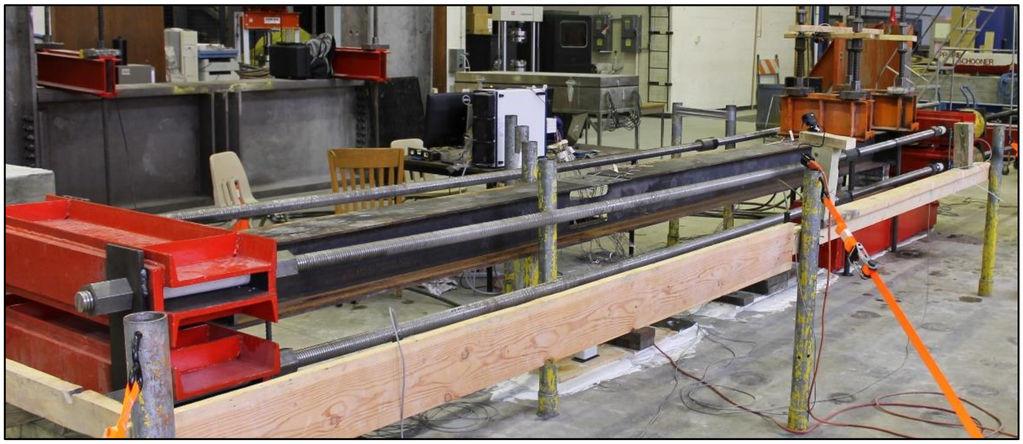

Figure 5.33 Deteriorated pile bent test

Figure 5.34 Deteriorated pile bent deteriorated section global section failure

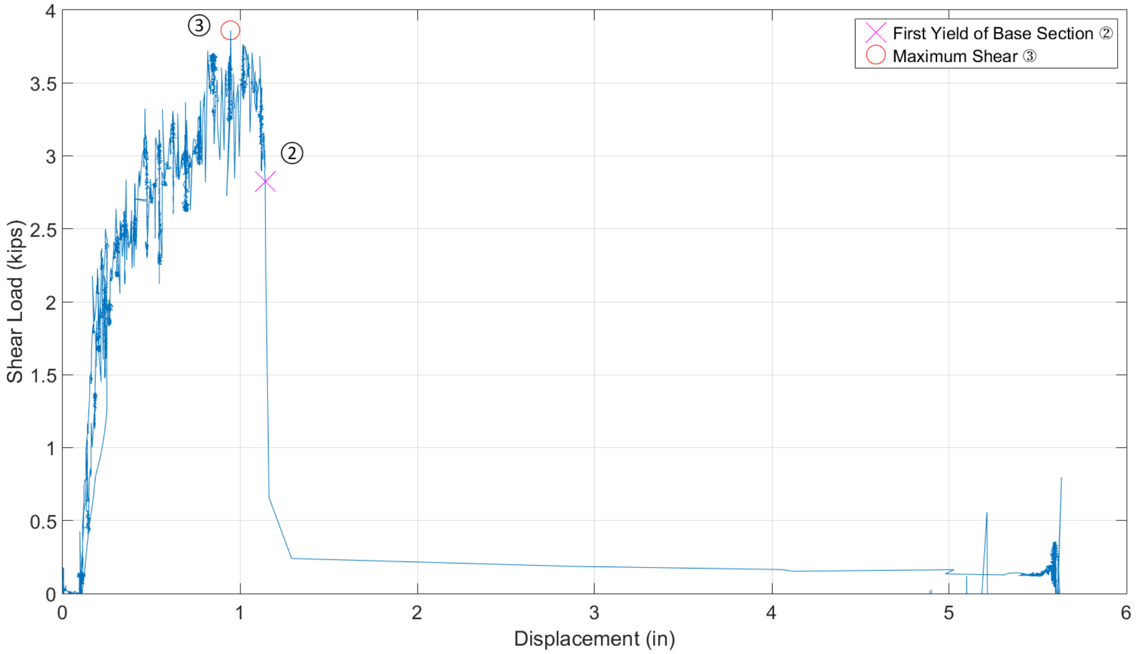

Figure 5.35 Deteriorated pile bent shear vs. displacement

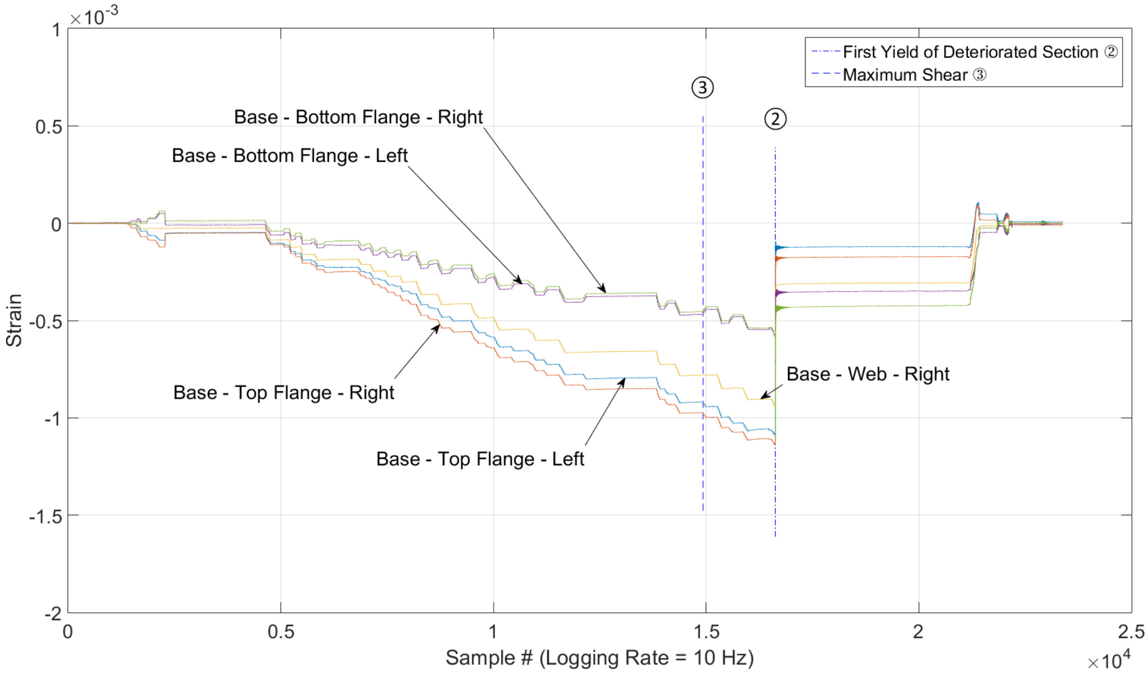

Figure 5.36 Deteriorated pile bent base section strain vs. sample

Like the deteriorated abutment case, the pile in this test was stronger than anticipated and exceeded the 45% H1-1 Strong Axis envelope of Figure 5.37 by nearly 100 kips in compression. This again was most likely due to the analysis assumptions and the actual geometry of the section. Unlike the abutment case though, this test ended in an abrupt buckling of the top flange and web. The strains were noticeably more polarized in this test then the others. Figure 5.39, which is a magnified view of the initial loading portion of Figure 5.38, shows the web paralleling the top flange strains closely through the test prior to its buckling. Unlike the abutment case, the shear did not control the failure in this test. The distance from the shear ram to the deteriorated section was enough for an appreciable amount of moment to develop, resulting in larger compressive stress in the upper half of the section. The overall in plane displacement of the deteriorated section was small enough that a large amount of force was applied before the pile was displaced far enough that the section became unstable.

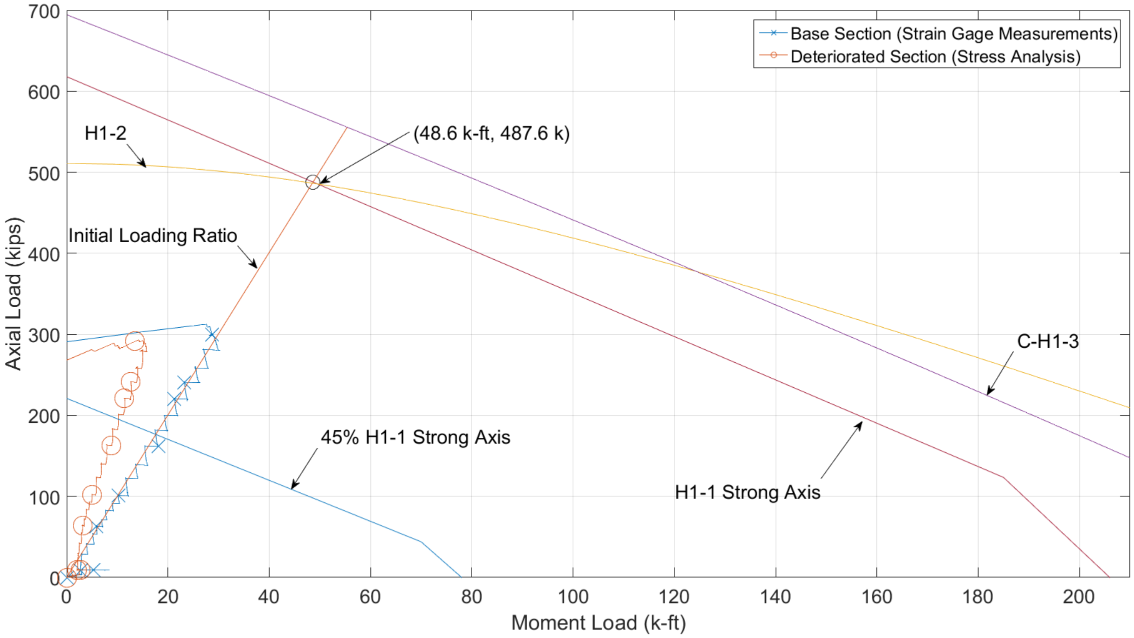

Figure 5.37 Deteriorated pile bent axial vs. moment

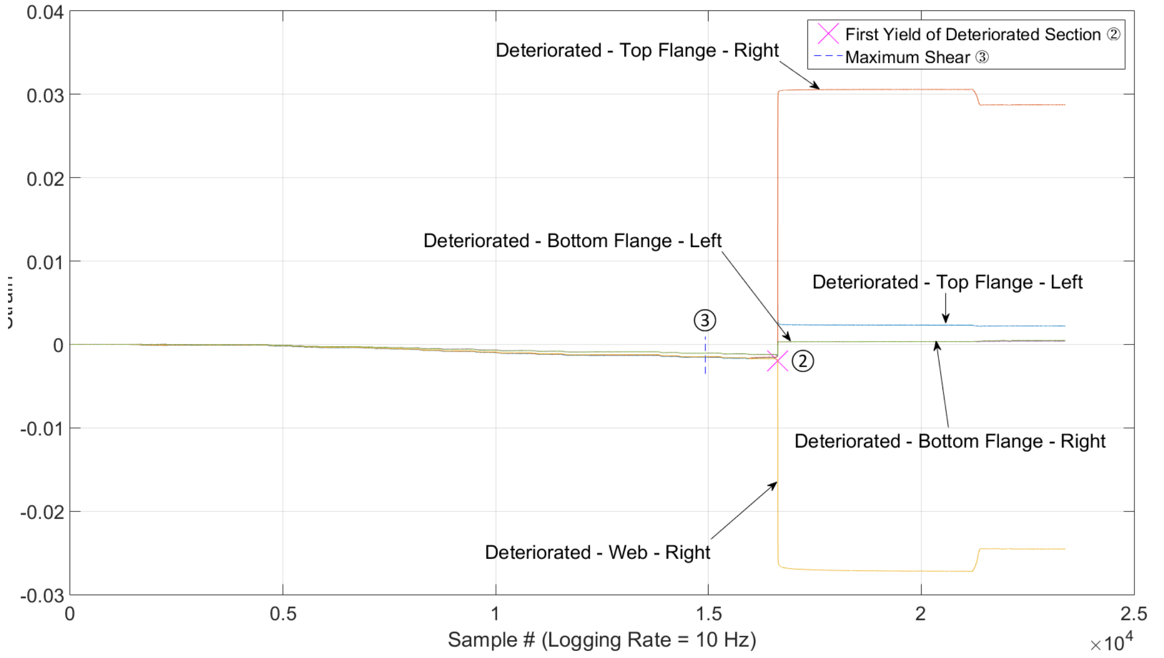

Figure 5.38 Deteriorated pile bent deteriorated section strain vs. sample

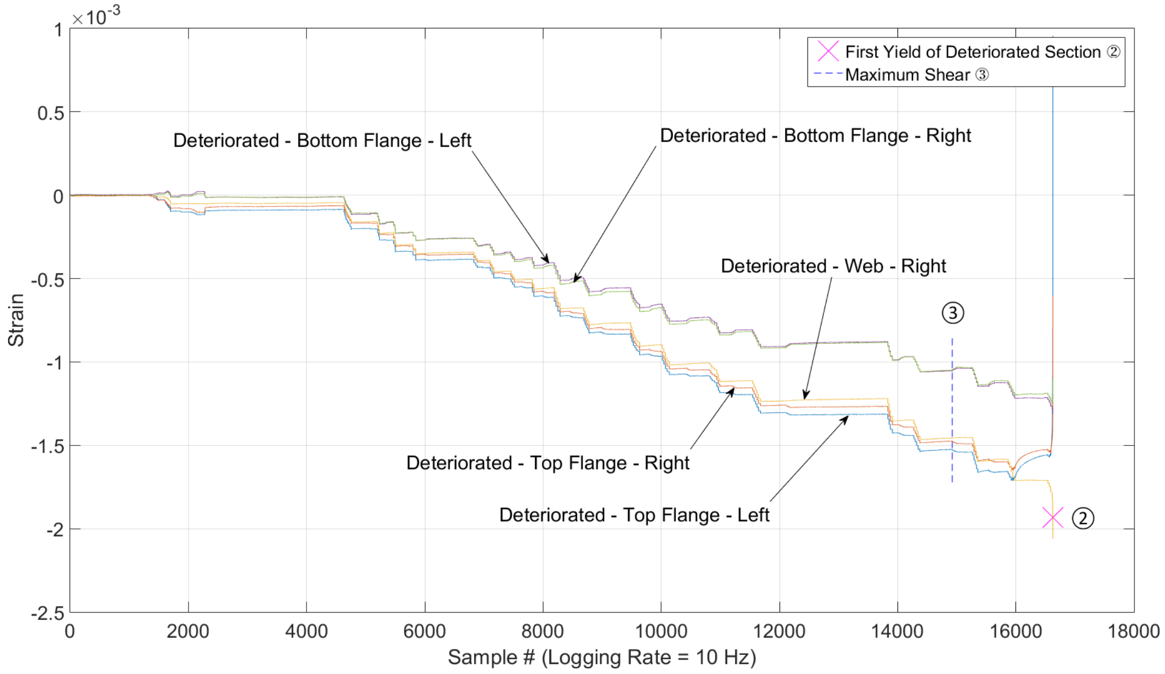

Figure 5.39 Deteriorated pile bent deteriorated section strain vs. sample zoomed in

5.9 PILE BENT CASE: RETROFITTED

Similar to the retrofitted abutment case, the pile first began to fail by buckling locally at the base. The retrofit prevented the failure of the deteriorated section that was seen in the deteriorated test. Like the abutment case, this was the intended and desired result. The pile (shown in Figure 5.40) was able to withstand the same loading as the non-deteriorated pile and resisted a slightly higher shear load.

Figure 5.40 Retrofitted pile bent test

With the deteriorated section failure eliminated, the pile buckled at the base section similarly to that seen in the non-deteriorated test. After the top flange buckled, the pile began to experience the same LTB limit state that the non-deteriorated test did, but because of the retrofit, the lateral displacement was restrained. This lead to a torsional displacement of the pile through the retrofit. This is shown in Figure 5.41, in between the tie down and a short distance from the shear loading point the pile rotated about its length. The retrofit added addition weak axis stiffness that caused the lateral displacement associated with the LTB limit state to be limited.

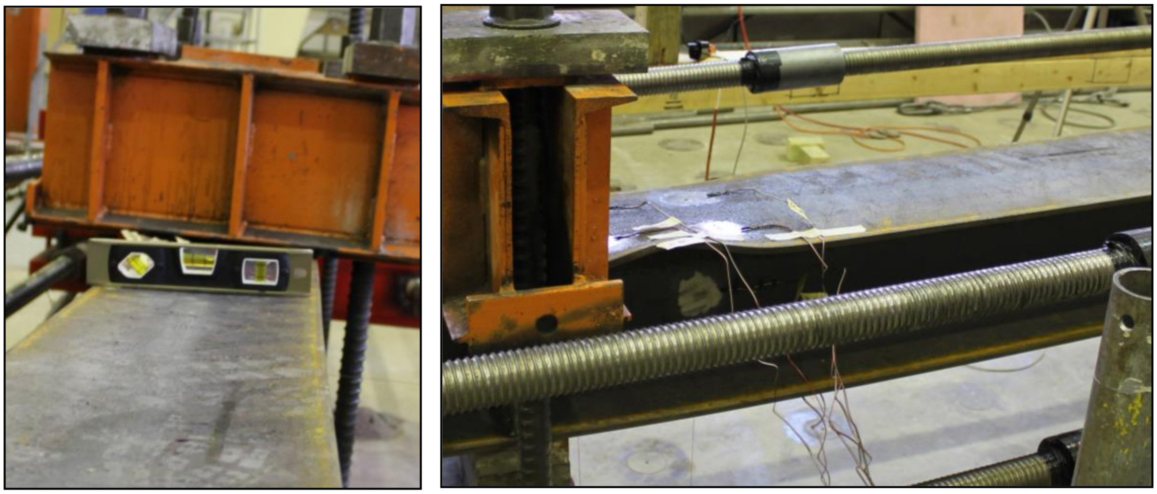

Figure 5.41 Retrofitted pile bent failure

The results from this test, like the abutment case, indicated that the concrete bond was substantial and the retrofit drew a considerable amount of load. As can be seen in Figure 5.42, the deteriorated section carried just over 100 kips of the axial force and around 10 k-ft of moment. From Figure 5.43, the deteriorated section does not experience strains near the yield limit. This data indicates that the buckling from the deteriorated test was eliminated.

The additional stiffness added by the retrofit resulted in an inch less deflection at the maximum shear load, as shown in Figure 5.44. The maximum shear increased by 0.7 kips over the 10.9 kips carried by the non-deteriorated test. Yielding was also measured in the web for this test and can be seen in Figure 5.45. From the strain gage data within the concrete jacket, the maximum axial load carried by the pile was 133 kips of the total 344 kips applied at that time. This corresponded to a bond 3.25 times greater than the AISC (2011) recommended value.

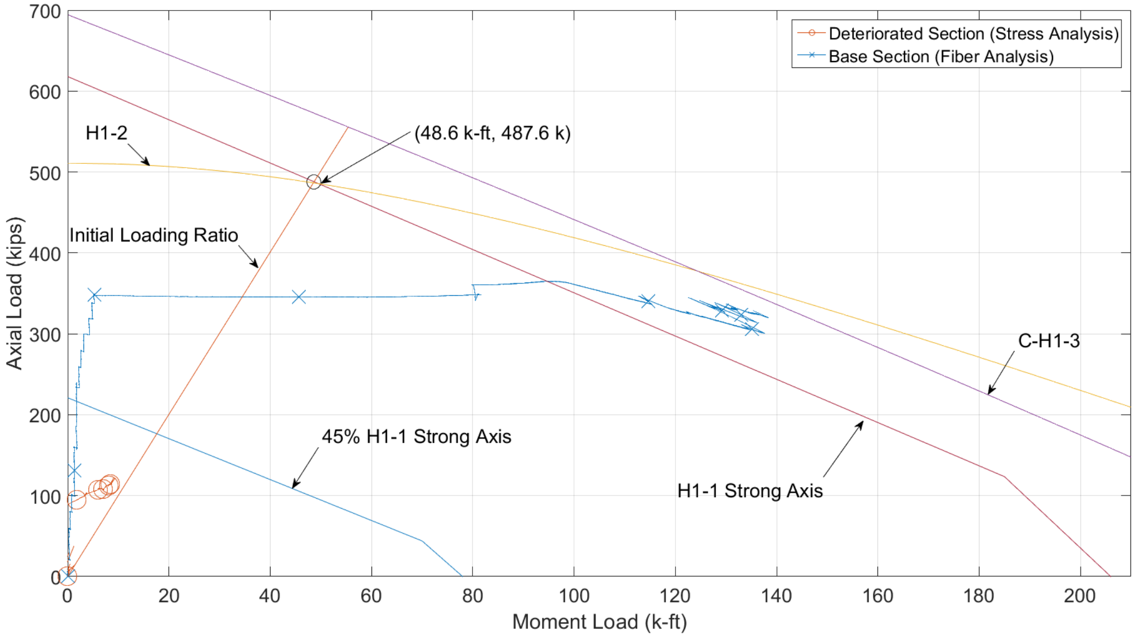

Figure 5.42 Retrofitted pile bent axial vs. moment

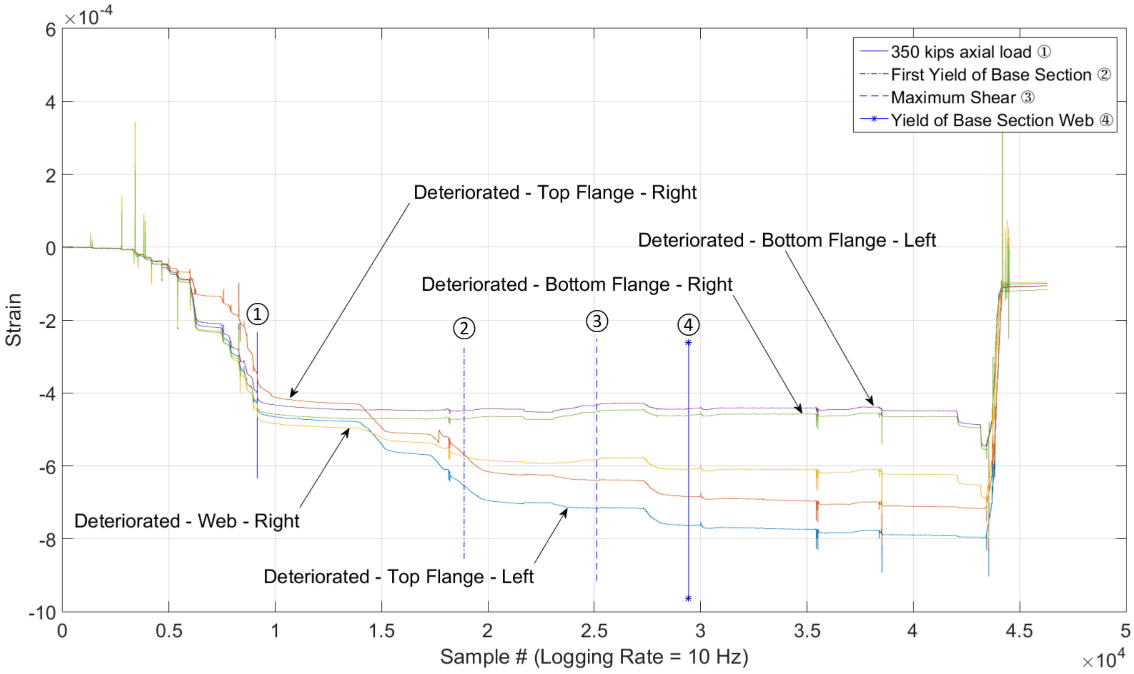

Figure 5.43 Retrofitted pile bent deteriorated section strain vs. sample

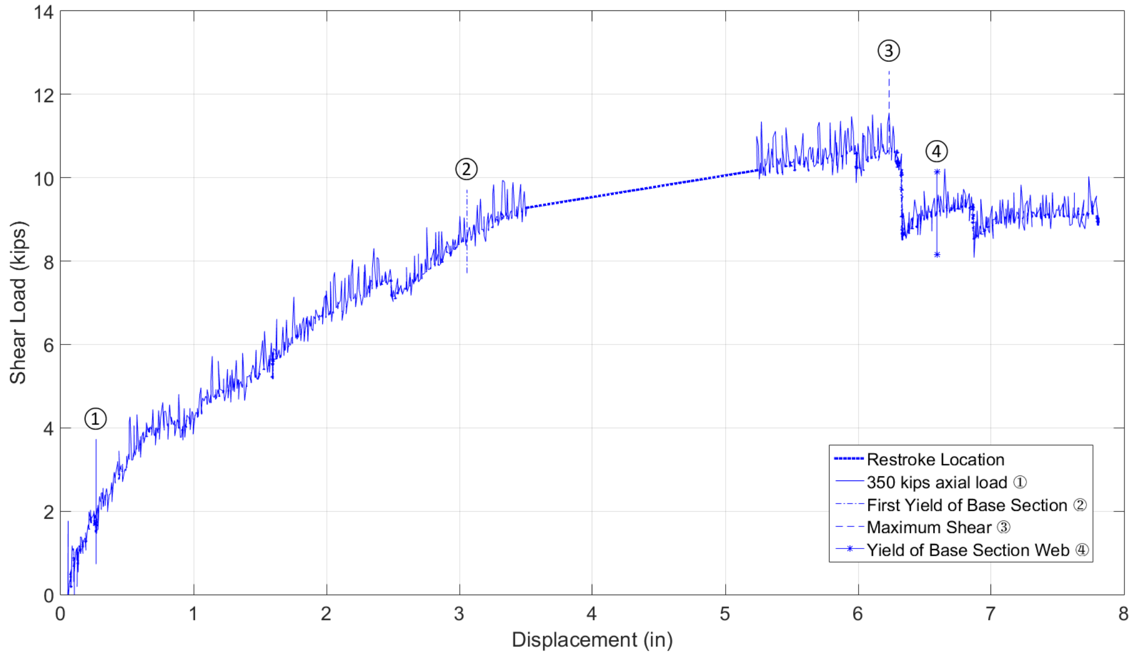

Figure 5.44 Retrofitted pile bent shear vs. displacement

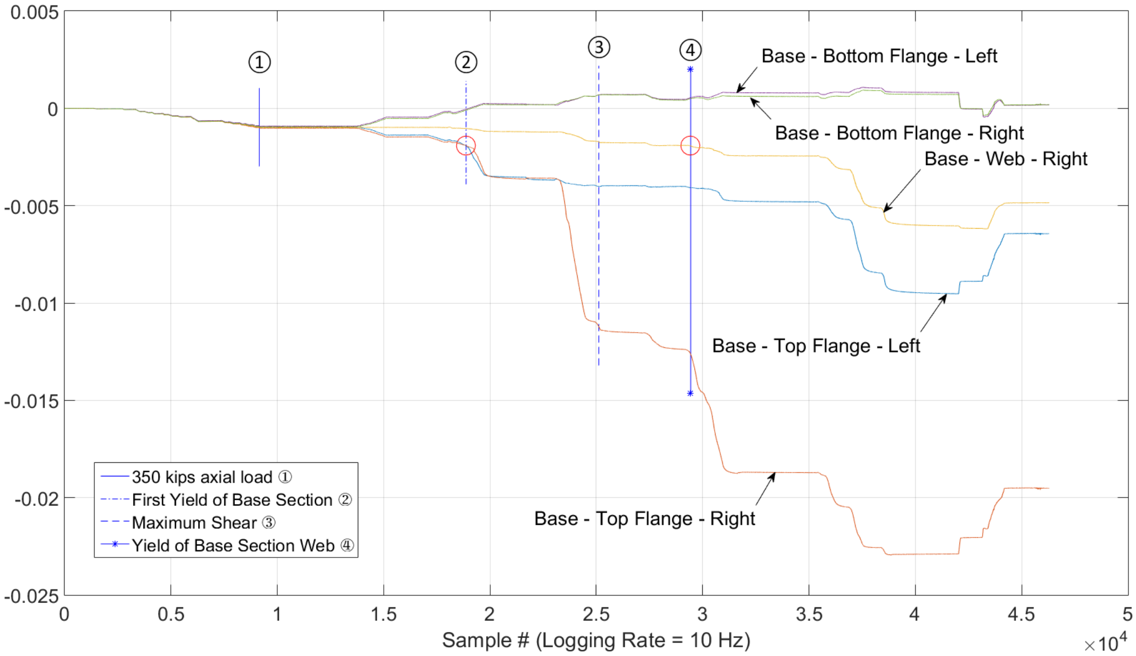

Figure 5.45 Retrofitted pile bent base section strain vs. sample

5.10 PILE BENT CASE: OVERVIEW

With all the test specimens in this case having the same steel strength, a direct comparison of the results was made. The tests provided reasonable data and positive feedback for the retrofit. The retrofit proved to be a viable option for this situation with similar material strengths.

At the base section, the results were similar for the non-deteriorated and the retrofitted tests. The initial portions of those two test follow a different loading path (shown in Figure 5.46) but once they reached the end of the initial loading ratio portion of the test the results follow each other closely. The differing load path was due to the concrete weight of the retrofitted pile. For the retrofitted pile in this case, the same shear load was applied through the stepped portion as in the non-deteriorated test (In the retrofitted abutment test, the weight was accounted for and the moment load was matched). Once the pile began to fail, the non-deteriorated and retrofitted cases appeared to have a very similar failure.

The deteriorated section results proved to be similar to the abutment case. The non-deteriorated test had the highest loading in the deteriorated section, and the retrofitted test deteriorated section carried less than a third of the overall axial load, as shown in Figure 5.47.

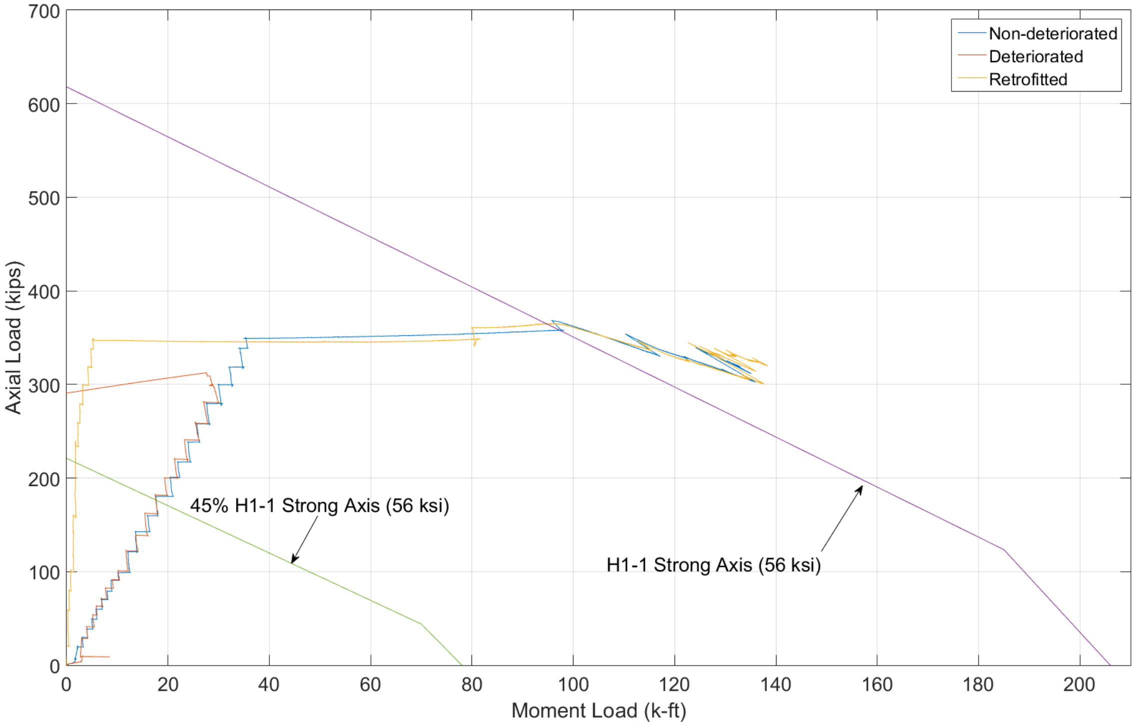

Figure 5.46 Pile bent base section axial vs. moment comparison

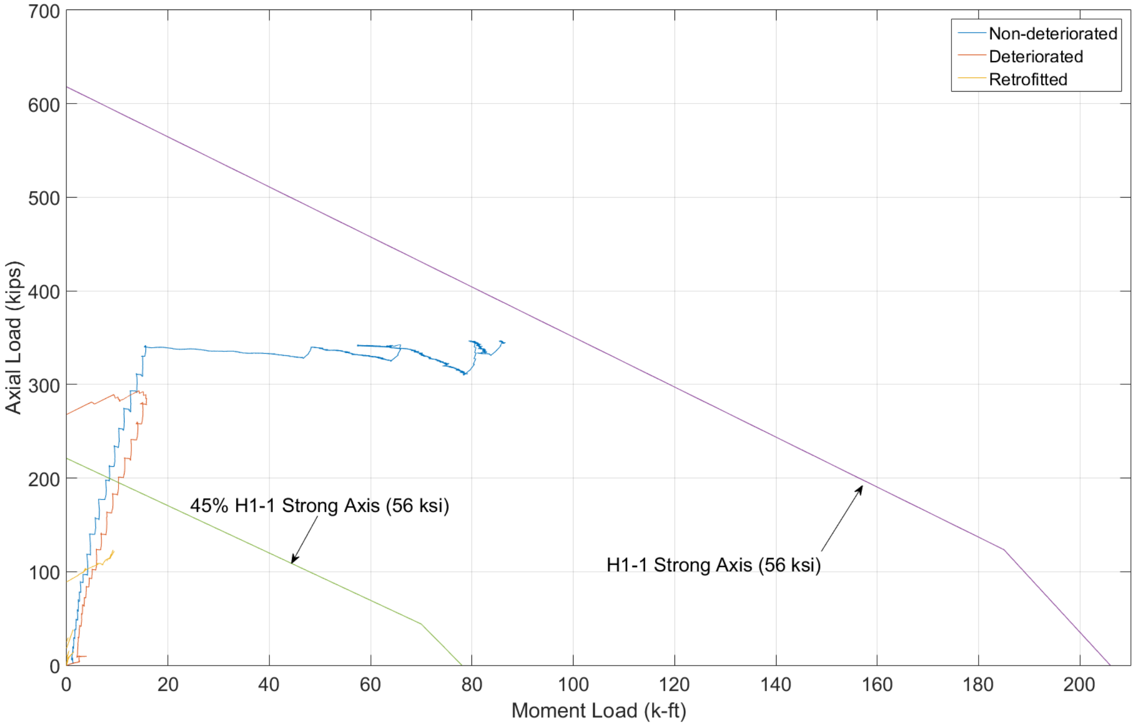

Figure 5.47 Pile bent deteriorated section axial vs. moment comparison

CHAPTER 6 COMPUTATIONAL MODELING

6.1 INTRODUCTION

The experimental study investigated one geometric configuration, and single concrete and steel material strengths. A computational study allowed for further considerations of reduced geometry and varied material strengths. Further development of the bond behavior between the steel and concrete is needed to improve the validity of the computational results. The following sections will present the procedure used to develop the models and the results.

6.2 COMPUTATIONAL MODELING PROCEDURE

Abaqus CAE was utilized to construct models representative of the retrofitted abutment test specimen from the experimental study. An initial model (Model 1) simulated the experimental specimen. This model was used for validation and calibration of the modeling methodology prior to investigating alternate configurations and parameters in three subsequent models.

The concrete was modeled with solid elements and a three inch mesh size in all dimensions, and the pile was modeled with shell elements, meshed at one inch by one inch. Concrete material properties were characterized with a smeared cracking model with tension stiffening (stress fraction, σ/σ_c of 1 and direct strains difference, ε-ε_c of 0). Model 1 material strengths were defined by values from the experimental results (concrete compressive stress, f_c‘ of 6.45 ksi and steel yield stress, f_y of 56 ksi). The subsequent model material strengths were defined using historic nominal design values for NDOR’s retrofit (concrete compressive stress, f_c‘ of 3 ksi and steel yield stress, f_y of 36 ksi). Figures 6.1 through 6.4 present the constitutive models utilized for the concrete and steel materials. The “Maximum Observed Stress” indicates the maximum stress recorded for any one of the models with that particular material stress. The concrete only exceeded the 70% f_c’ value in three of the four models (6% max exceedance) under the full axial load (690 k and 446 k respectively). By remaining nearly linear, the model did not need to consider nonlinearity of the concrete and cracking.

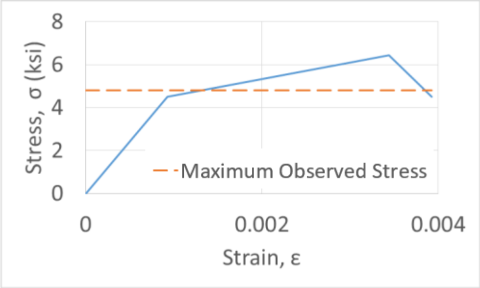

Figure 6.1 6.4 ksi concrete stress vs. strain

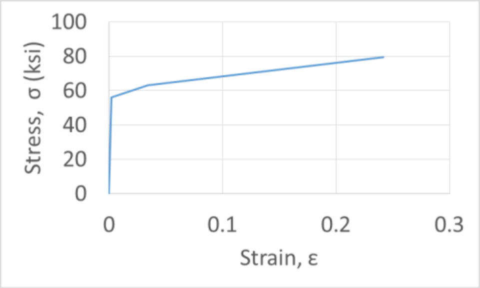

Figure 6.2 56 ksi steel stress vs. strain

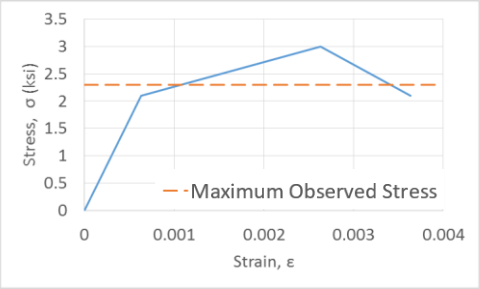

Figure 6.3 3 ksi concrete stress vs. strain

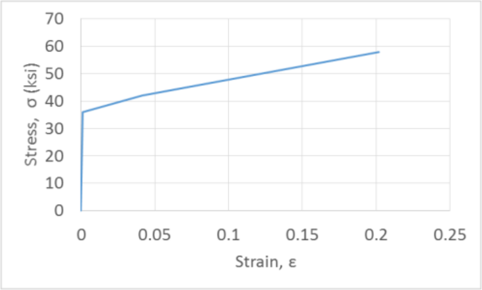

Figure 6.4 36 ksi steel stress vs. strain

The loading was applied using pressures at the shear and the axial loading locations. Figure 6.5 shows the axial load being applied to the end bearing plate (red arrows), and the shear load being applied to the bottom flange of the pile for three inches on either side of the stiffeners (black arrows), similar to the experimental test setup. The pile was restrained at the tie down points by fixing all degrees of freedom, except for the major axis bending rotation, along the bottom of the bottom flange at the nodes in line with the stiffeners.

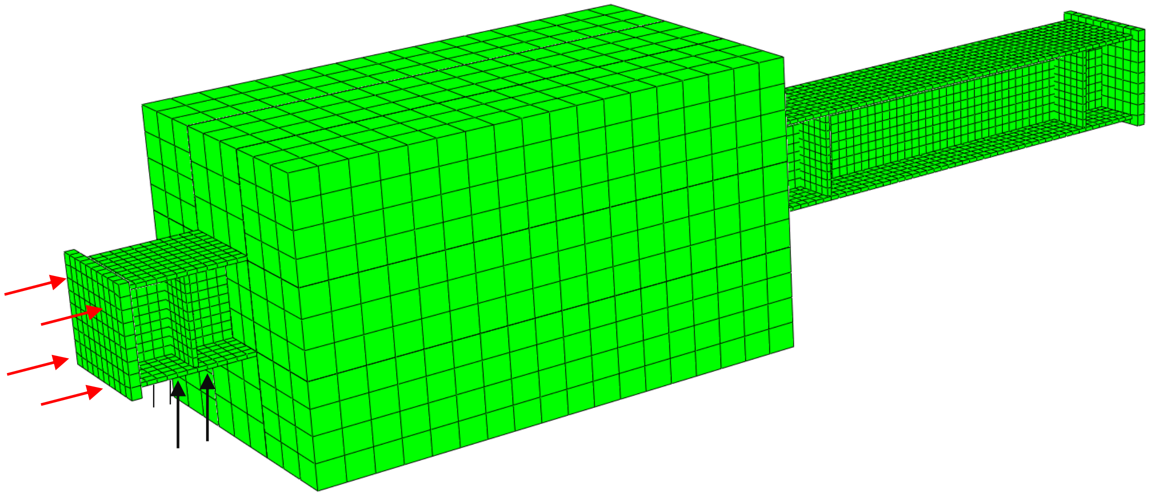

Figure 6.5 Axial and shear loading locations

For Model 1, the objective was to determine a contact and/or interaction that gave comparable results to the experimental test for axial load in the deteriorated steel and the base section. The steel-concrete bond was modeled with a combination of tied contact, and a normal and tangential interactions. Proportions of contact surfaces modeled with constraints versus interactions were iterated until acceptable agreement with experimental results was achieved. This resulted in a tied contact along the web, one inch past the ends of the web deterioration holes on both ends, and one inch strips of the flange along the edge of the deteriorated section, called Bond 1 and indicated by the blue color in Figure 6.6. The red portions of the pile represent the interaction portion of the pile. The interaction was defined with a normal and tangential set of parameters. The normal interaction applied a “hard” contact with separation allowed after contact and the tangential interaction utilized a penalty friction with a coefficient of 1.0. The interactions induced a more gradual transfer of stresses between the steel and the concrete elements.

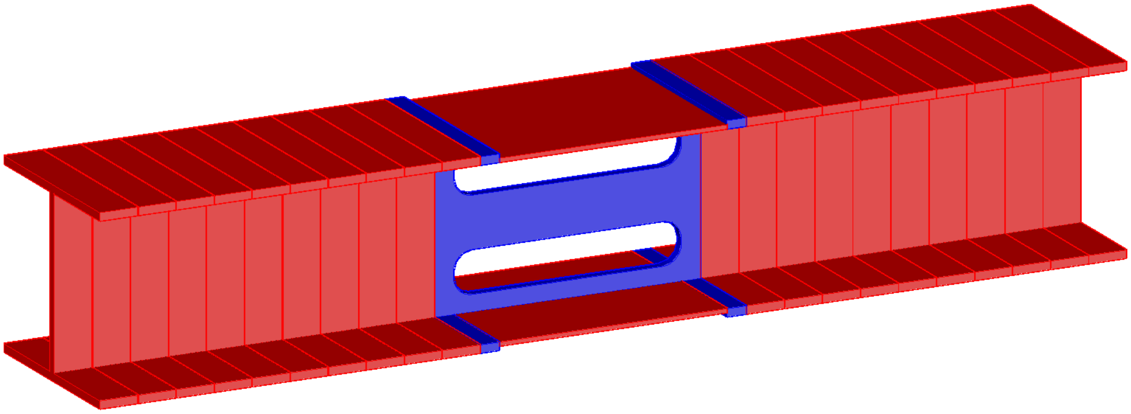

Figure 6.6 Location of contact and interaction definitions (Bond 1)

For Model 2, the material strengths were reduced to 3 ksi compressive stress for the concrete and 36 ksi yield stress for the pile steel. These values a representative of the historic nominal design material strengths consistent with past repair specifications. Bond was modeled identically in Models 1 and 2.

Model 3 was an extension of Model 2, having a reduced retrofit cross section. The experimental test cross section, simulated in Models 1 and 2, was 30”x30”. The concrete cross section was reduced in Model 2 to 20”x20”. These dimensions were selected to represent the smallest size that would permit installation of a reinforcement cage, while maintaining required clearances to the pile and cover to the exterior concrete surface. The same bond representation was originally applied to this model, as was applied to the previous two, but had to be changed due to convergence issues with severe plastification of steel elements tied to the concrete (non-convergent stress concentrations). After a few iterations, the minimum amount of tied contact was determined, as shown in Figure 6.7. This constituted about 30% of the non-deteriorated portion of the encased pile and 100% of the deteriorated portion (Bond 2).

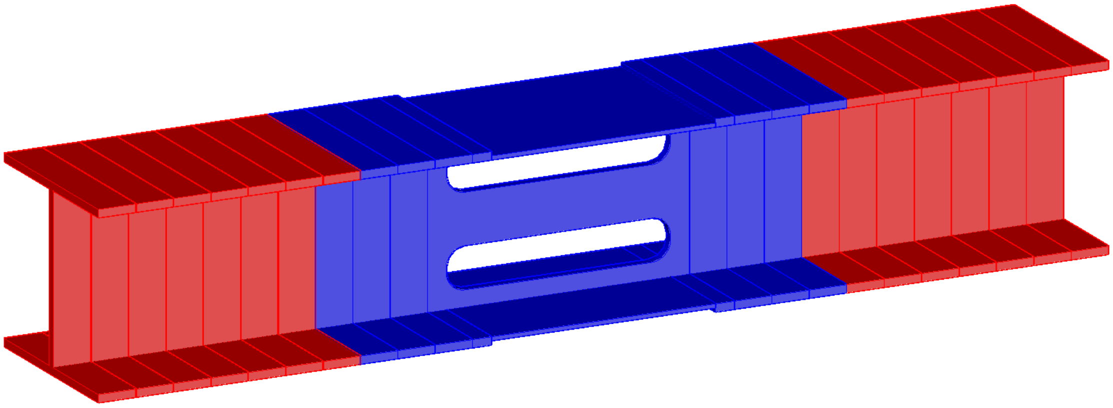

Figure 6.7 Location of contact and interaction definitions (Bond 2)

The final model, Model 4, represented the minimum amount of concrete that could effectively be used, filling the void between the flanges for a length of 4.5 feet centered on the deteriorated region. The bond representation (Bond 3) was tied for the length of the retrofit to the interior faces of the flanges and both sides of the web. The grey colored portion, as shown in Figure 6.8, represents the parts of the pile not defined with a contact or interaction property. Table 6.1 contains a summary of the computational models and their properties.

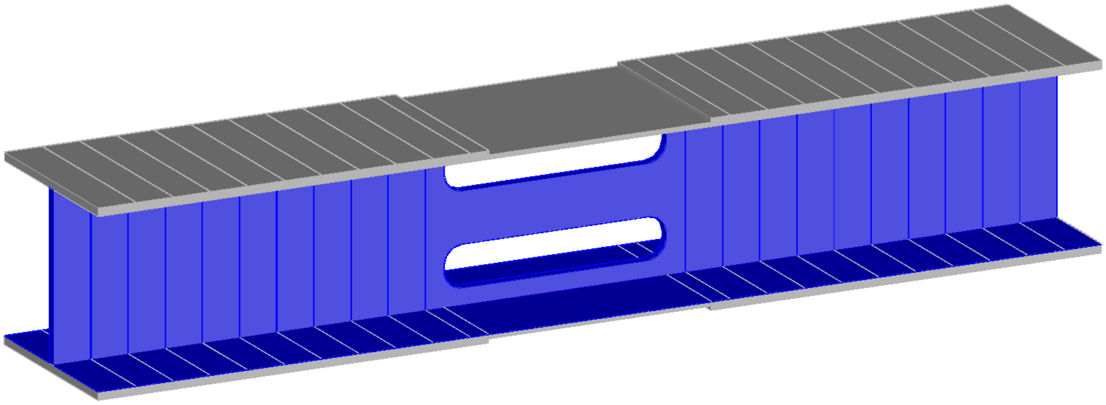

Figure 6.8 Location of contact and interaction definitions (Bond 3)

Table 6.1 Model properties

Model	Bond	Concrete Strength (ksi)	Steel Strength (ksi)	Retrofit Cross Section
1	1	6.4	56	30” x 30”
2	1	3.0	36	30” x 30”
3	2	3.0	36	20” x 20”
4	3	3.0	36	Infilled

6.3 COMPUTATIONAL MODELING RESULTS

The results presented in the following sections include the axial force and moment for the deteriorated and base section, and the bond that would be required to achieve those loads. Each model was subjected to five fixed ratios of combined axial and shear loads, creating axial and moment combined internal loading within the structural assembly. The ultimate capacity for each axial-shear ratio was plotted to form an approximate combined loading capacity envelope. The results of each analysis are presented in tabular form, graphically, and illustratively. Von Mises stress contours are shown to illustrate the stress distribution and flow between the pile and the concrete.

Model 1 Results

Results for Model 1, shown in Figure 6.9, closely match those observed in the experimental test when analyzed under the same loads. The pile shown in Figure 6.10, with a 360 k axial load and 1572 k-in moment (23.6 k shear load), yielded across a large portion of the cross section at the base near the tie down point from the top flange to the mid depth of the web. These are similar to the results that were encountered when reviewing the experimental data. It was also observed that the displacement for the model was 1.58 inches, which is comparable to 1.5 inches for the experimental results. Figure 6.11 and 6.12 show comparisons of the results of the experiments to that of the model. From 1.4 to 1.5 inches the error in reduces to an average of 5% in the displacement and 0.25% in the shear.

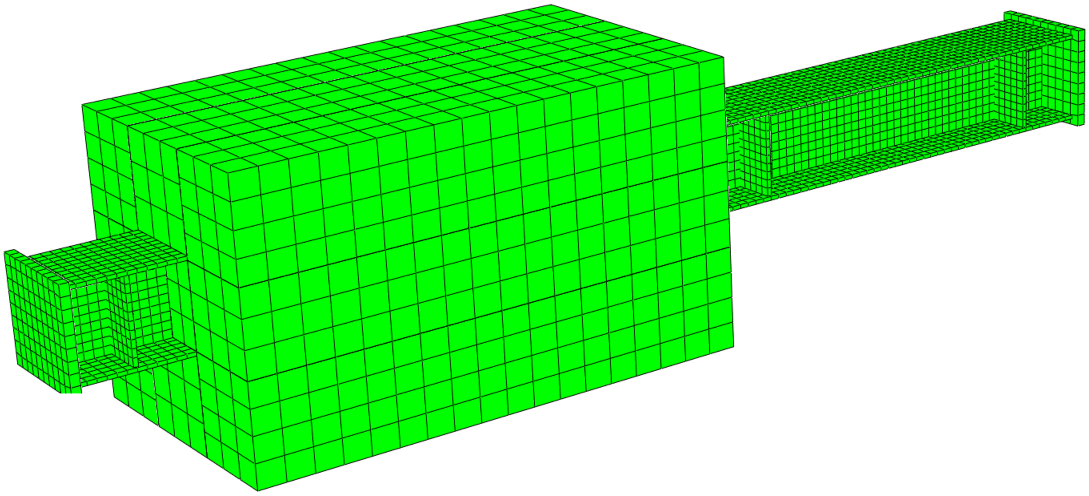

Figure 6.9 Model 1 3-D rendering

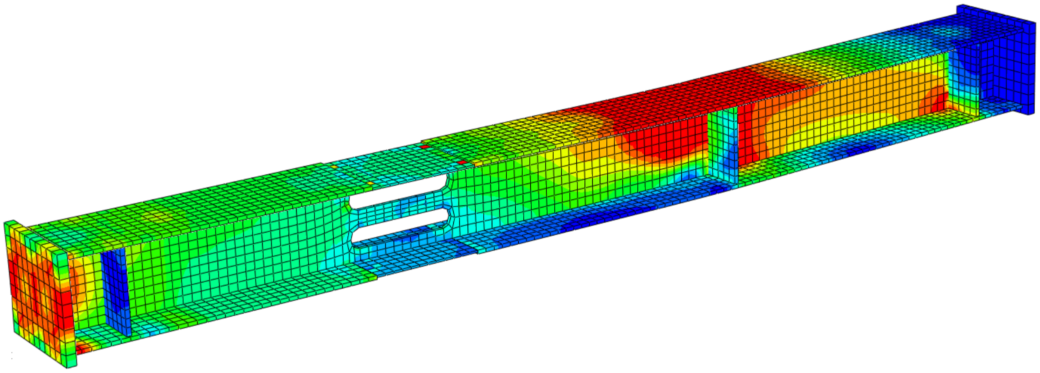

Figure 6.10 Model 1 pile stress distribution

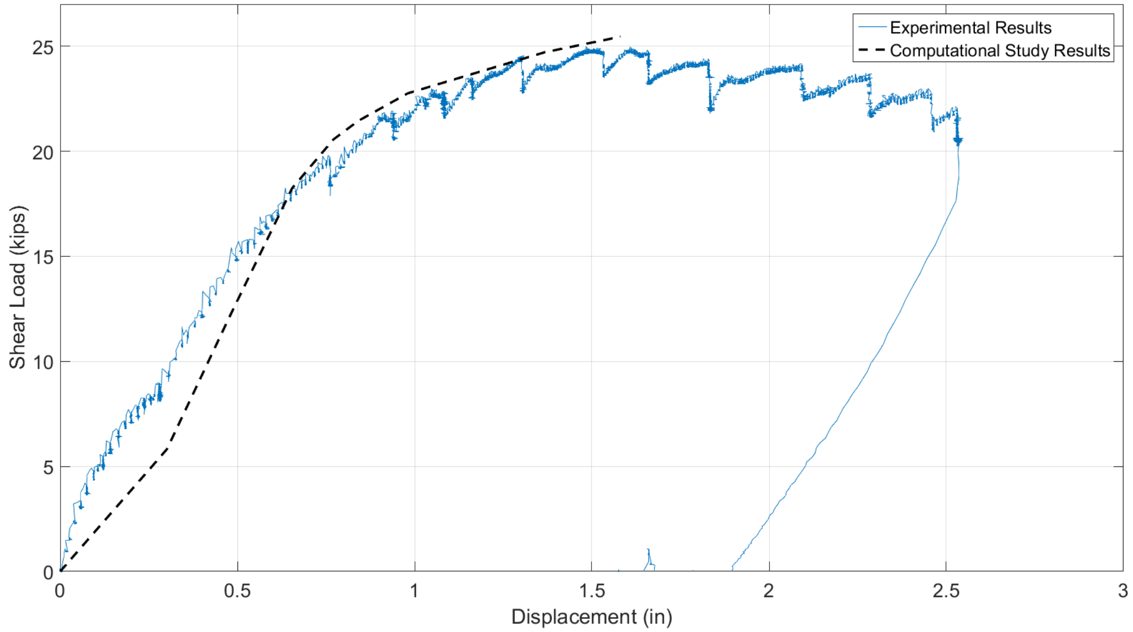

Figure 6.11 Comparison of experimental and computational shear vs. displacement results

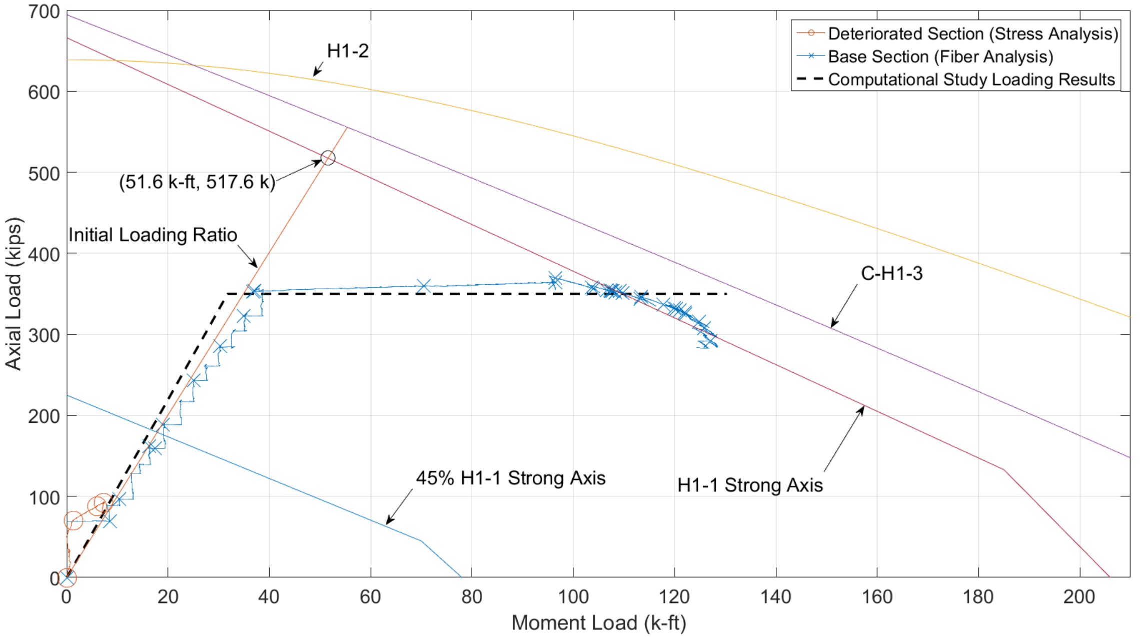

Figure 6.12 Comparison of experimental and computational axial vs. moment results

The computational study allowed for further investigation of the stress distribution and load flow through the retrofit. The point of most interest is the areas located towards the ends of the retrofit jacket shown in Figure 6.13. With the induced moment from this test, the concrete along the upper side of each flange experiences a noticeable stress concentration. With improvements to the bond representation, it would be expected that the stress would increase uniformly approaching the deteriorated section, gradually pulling more stress from the steel into the concrete.

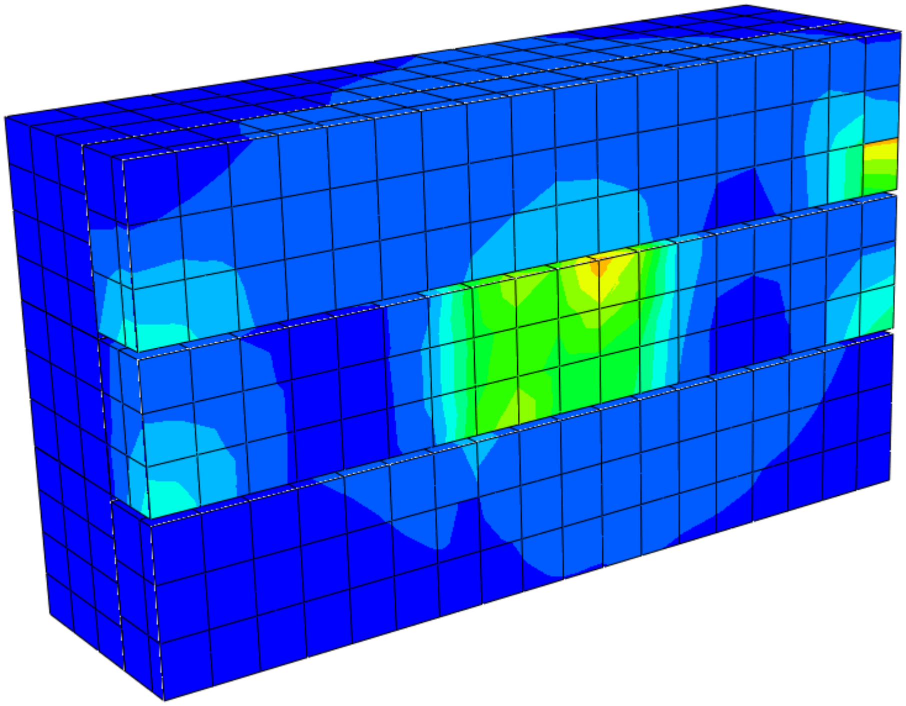

Figure 6.13 Model 1 concrete jacket cross section stress distribution

The computational study also allowed for the load to be varied, and the retrofitted pile was tested at five different locations along the pile's P-M interaction diagram. The results of the five different analyses, as presented in Table 6.2 and Figure 6.14, show that with the given bond representation, the pile is capable of reaching its plastic limit without failing in the concrete. It was also of interest to see the bond required to reach the desired loads. As the load increasingly becomes more axial and less moment based, the bond need increases. For a load of 690 k and 0 k-ft, the bond required is nearly two times the value determined for the experimental test. This is likely a result of using the tied contact for part of the bond. This also shows that with the higher moment values the bond is not as large, the load is transferred through a normal interaction at the interface of the steel and concrete, or direct bearing of the pile on the concrete and less by the bond.

Table 6.2 Model 1 loading ratios and results

Load Point		Base Section		Deteriorated Section		Bond* (ksi)
Axial (k)	Moment (k-in)	Axial (k)	Moment (k-in)	Axial (k)	Moment (k-in)	
690	0	690	0	215	0	0.402
560	648	560	626	165	50	0.334
360	1572	361	1541	98	107	0.223
180	2352	183	2306	45	131	0.117
0	2700	0	2621	0	135	0

*Based on difference of Base and Det. section axial loads divided by the embedded length.

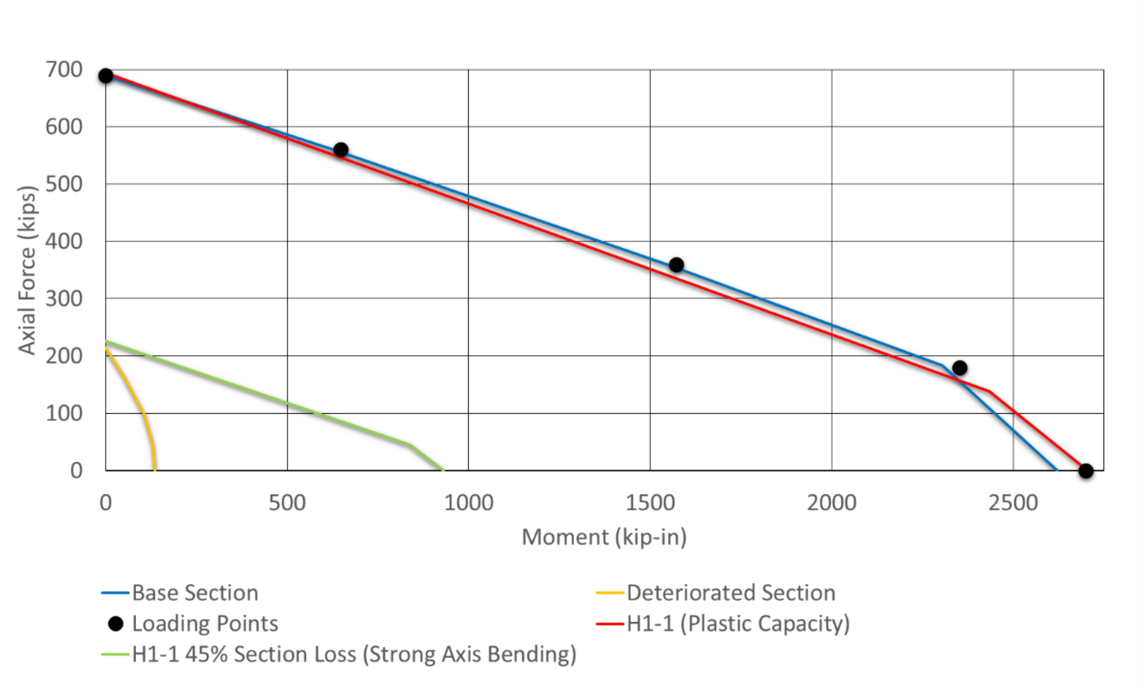

Figure 6.14 Model 1 interaction diagram with loading ratios and results

Figure 6.15 through 6.19 shows the stress contour results for the five loading ratios. The 690 k and 560 k loading ratios required three inch thick bearing plates to eliminate failure of the bearing plate prior to reaching the desired load. The cross sectional cuts of the retrofit show in Figures 6.15 through 6.19 provide a view of the stresses local to the pile in the concrete and gives a better sense of how the bond representation is acting. The remaining model results present the stress contours in the concrete in the same manner.

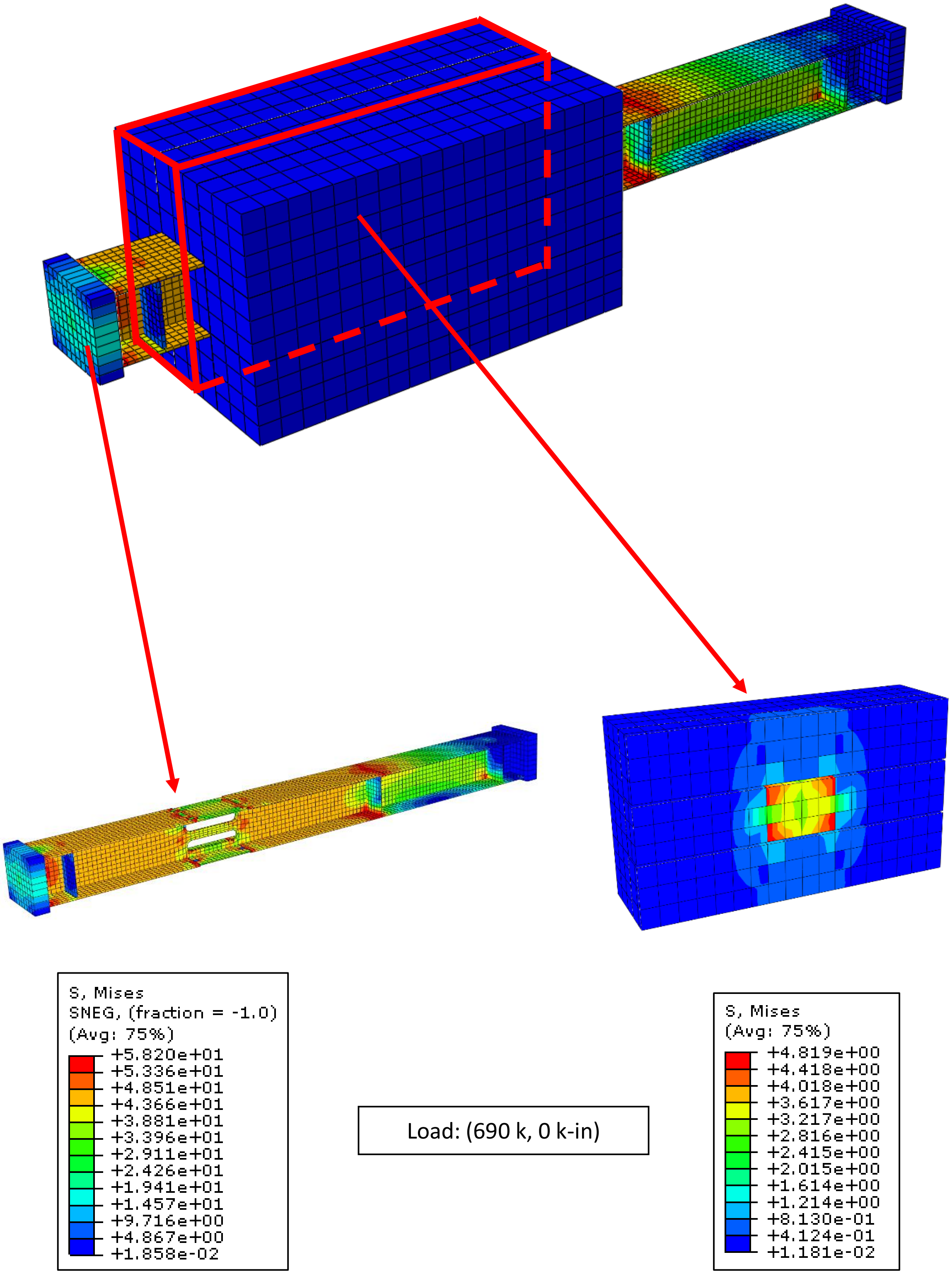

Figure 6.15 (690 k, 0 k-in) Model 1 stress contours

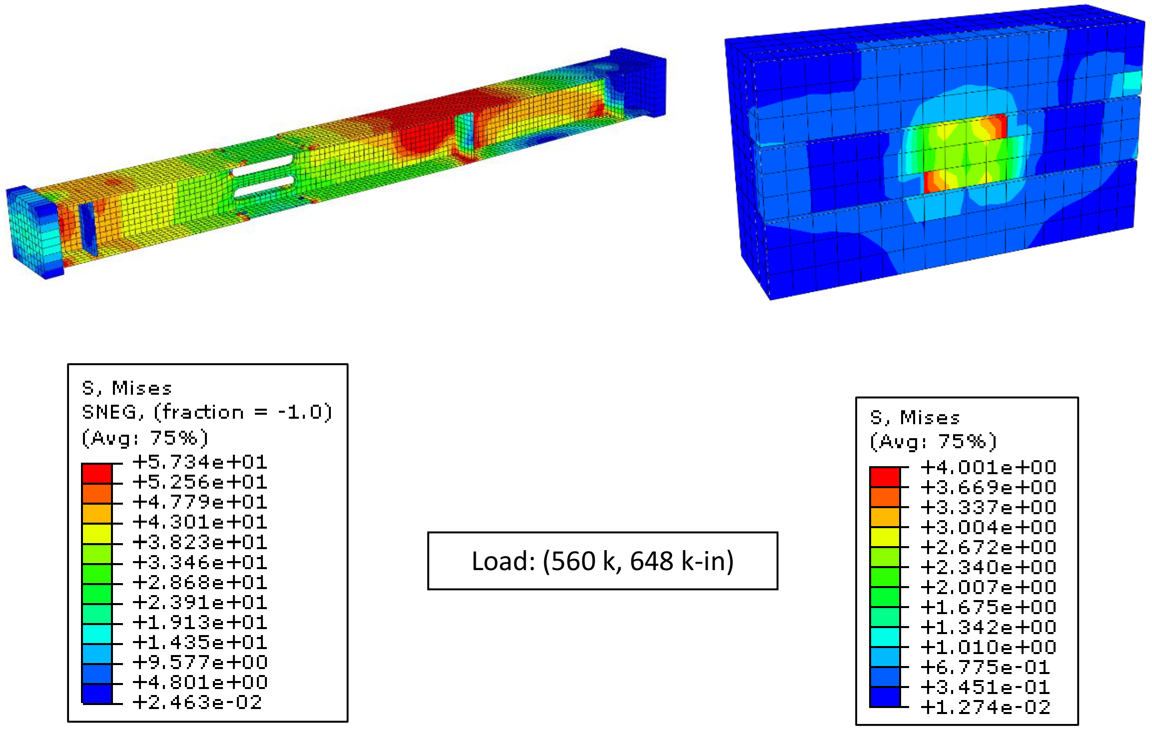

Figure 6.16 (560 k, 648 k-in) Model 1 stress contours

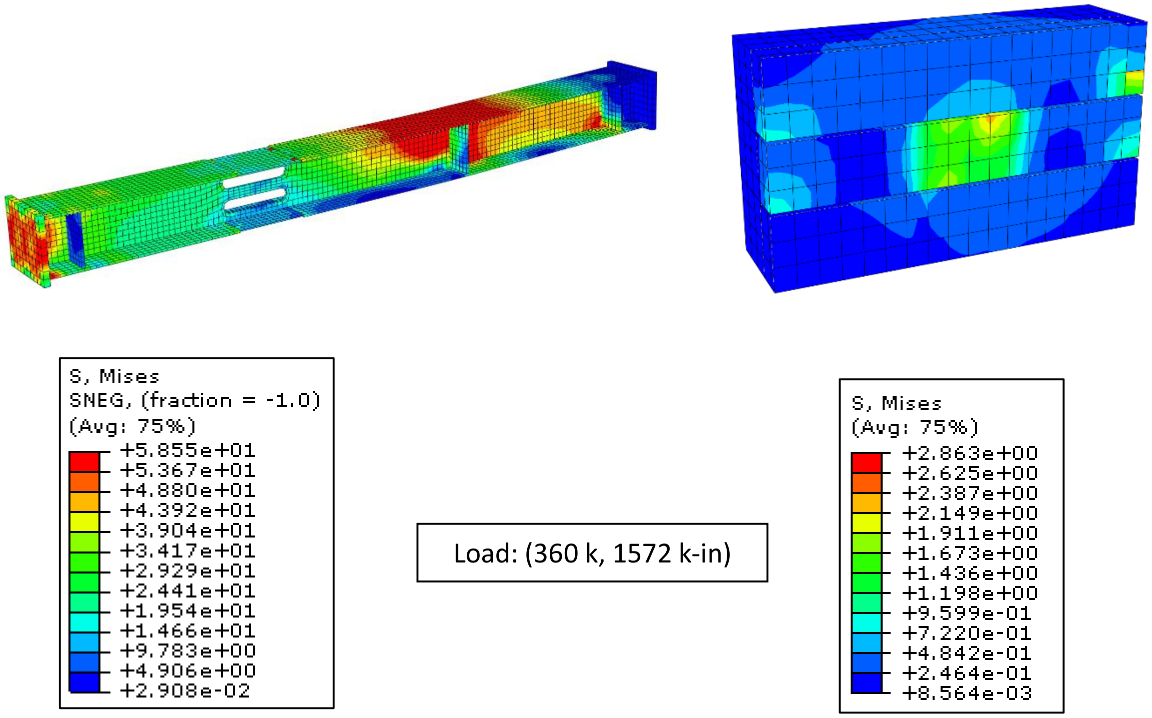

Figure 6.17 (360 k, 1572 k-in) Model 1 stress contours

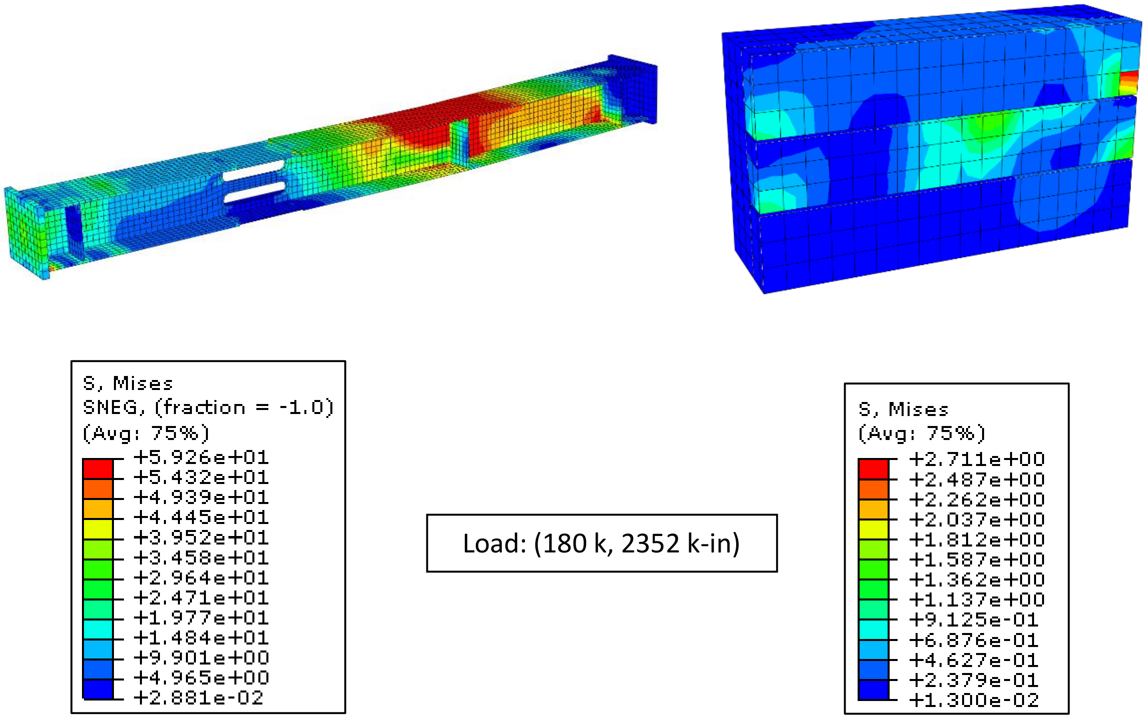

Figure 6.18 (180 k, 2352 k-in) Model 1 stress contours

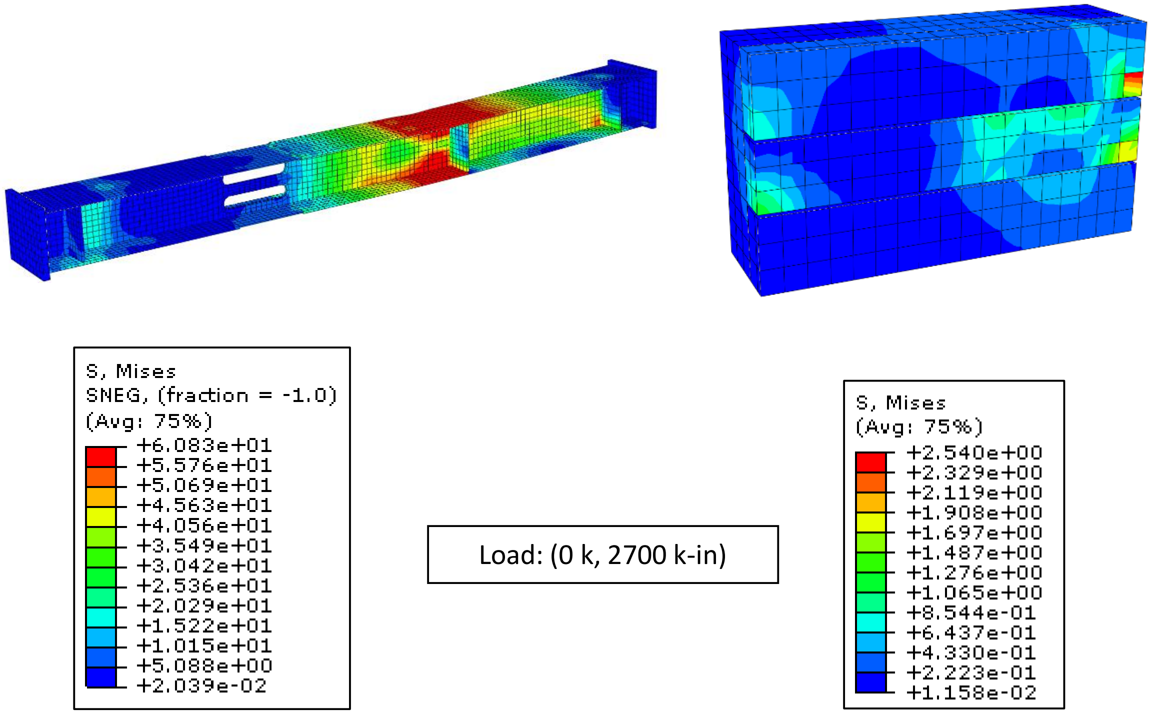

Figure 6.19 (0 k, 2700 k-in) Model 1 stress contours

Model 2 Results

Model 2 was an extension of Model 1 with the same geometry and bond representation, but reduced material strengths for the pile and concrete. The concrete was reduced to 3 ksi and the steel to 36 ksi. Analyses were conducted for five load ratios along the pile's P-M interaction diagram in a similar fashion as was done for Model 1.

The results of the five different analyses, as presented in Table 6.3 and Figure 6.20, show that again with the given bond representation (Bond 1), the pile is capable of reaching its plastic limit without failing in the concrete. The bond required for Model 2 was approximately half of the bond observed in Model 1, and again, for a pure axial load, the bond required is nearly two times the bond required of the third load point.

Table 6.3 Model 2 loading ratios and results

Load Point		Base Section		Deteriorated Section		Bond* (ksi)
Axial (k)	Moment (k-in)	Axial (k)	Moment (k-in)	Axial (k)	Moment (k-in)	
446	0	448	0	178	0	0.229
357	432	357	432	133	40	0.190
236	996	237	990	82	81	0.131
90	1560	93	1555	28	107	0.0550
0	1680	0	1680	0	114	0

*Based on difference of Base and Det. section axial loads divided by the embedded length.

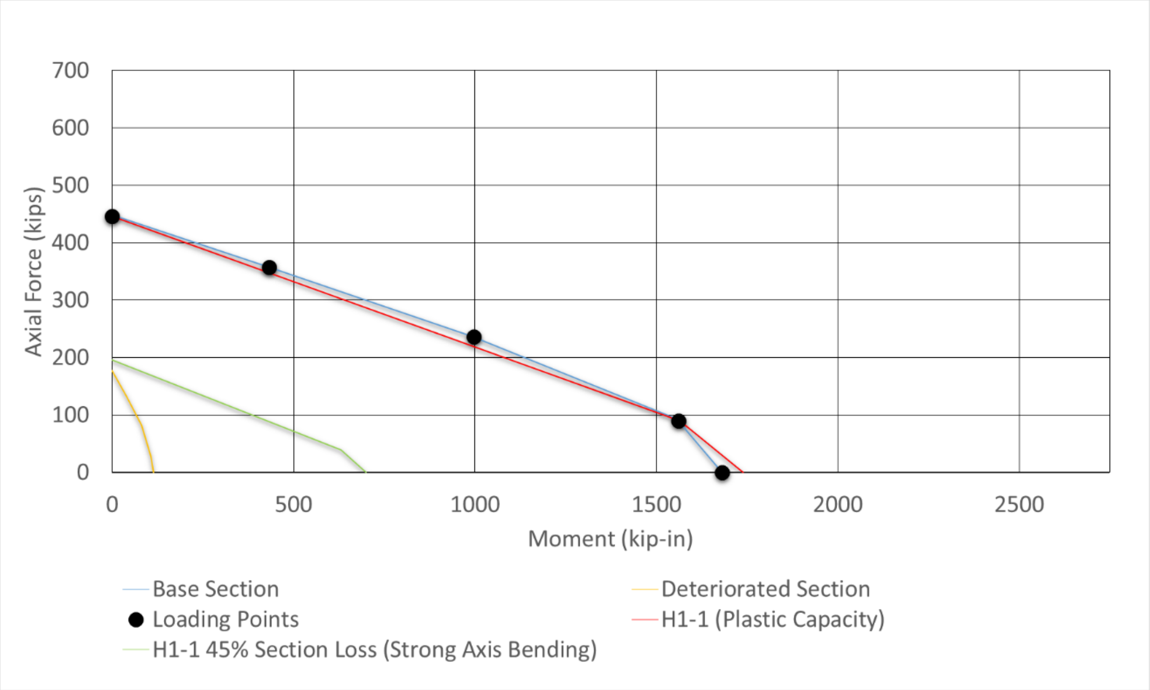

Figure 6.20 Model 2 interaction diagram with loading ratios and results

Figures 6.21 through 6.25 show the stress contour results for the five loading ratios. As was required for Model 1, the first two loading ratios required three inch thick bearing plates to eliminate failure of the bearing plate prior to reaching the desired load.

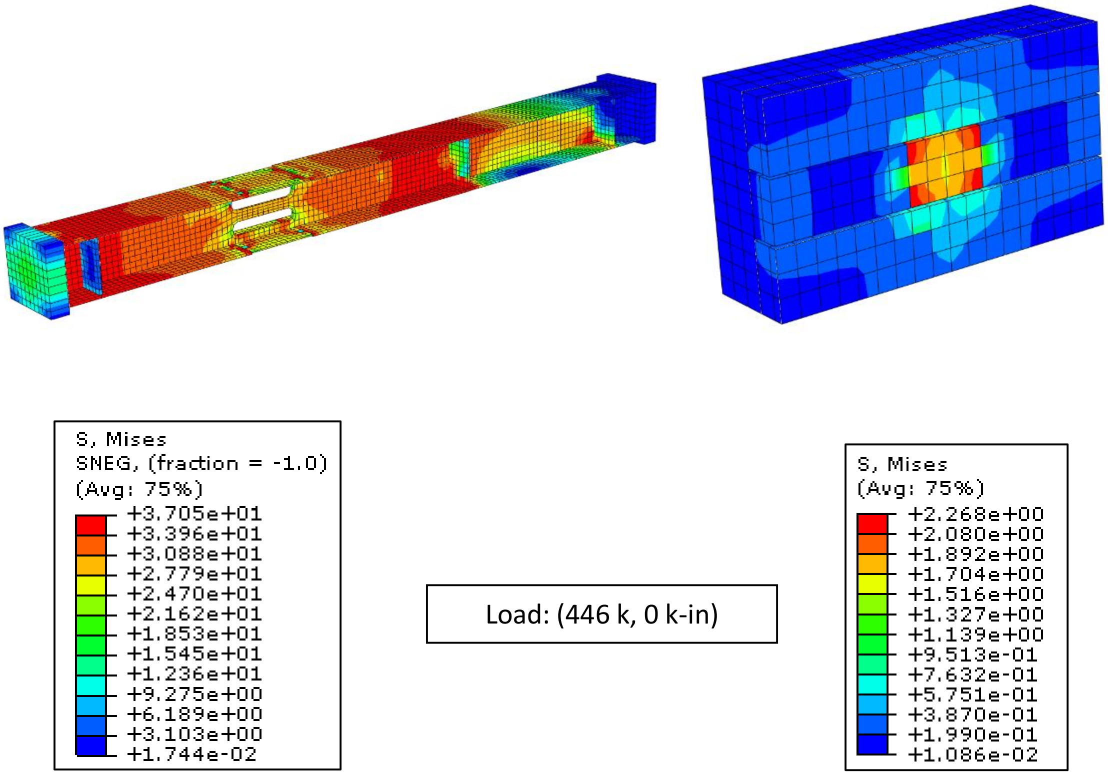

Figure 6.21 (446 k, 0 k-in) Model 2 stress contours

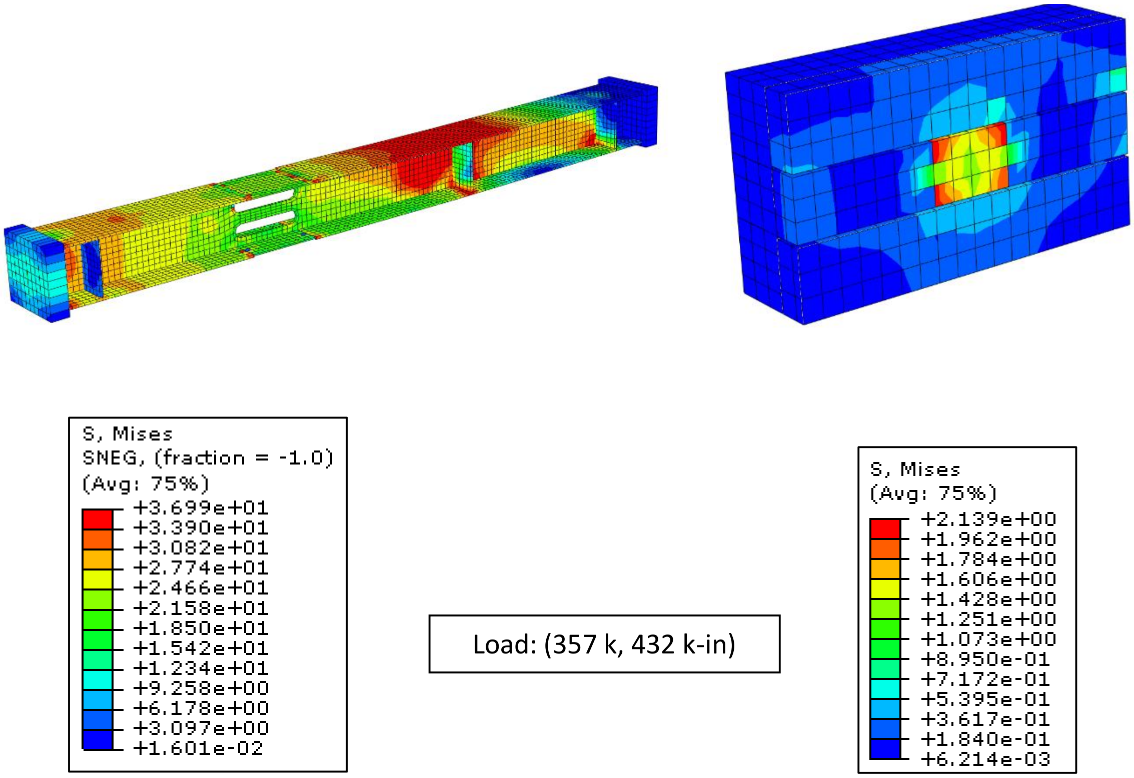

Figure 6.22 (357 k, 432 k-in) Model 2 stress contours

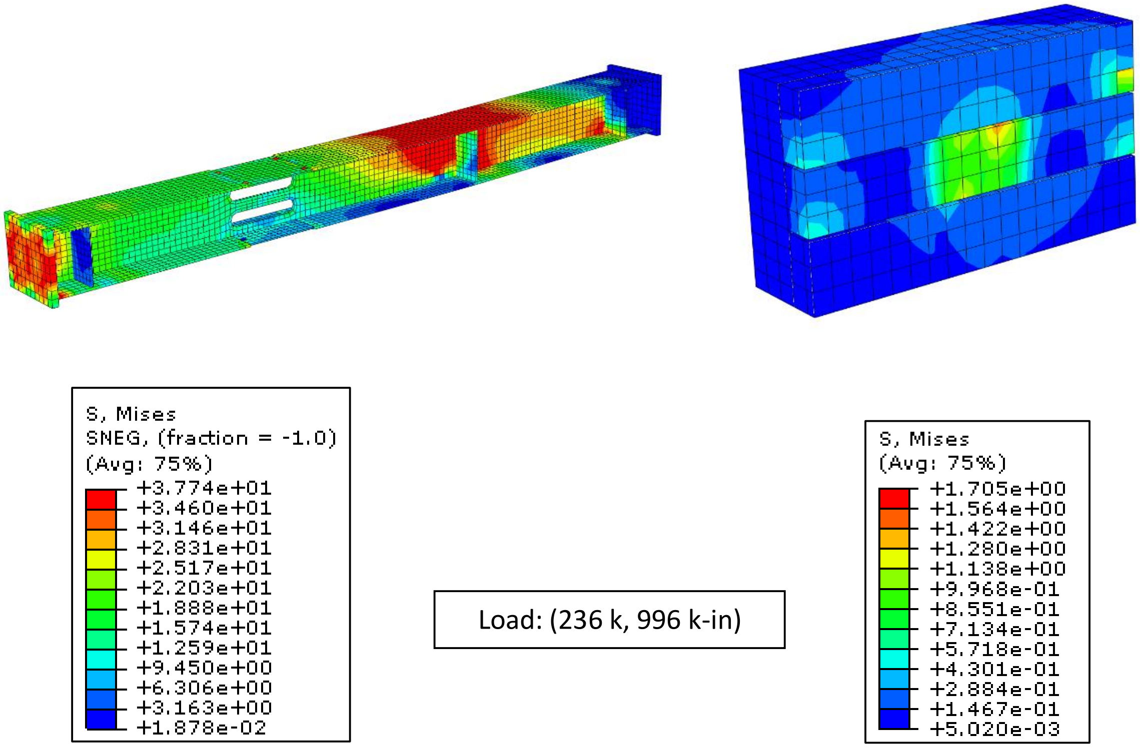

Figure 6.23 (236 k, 996 k-in) Model 2 stress contours

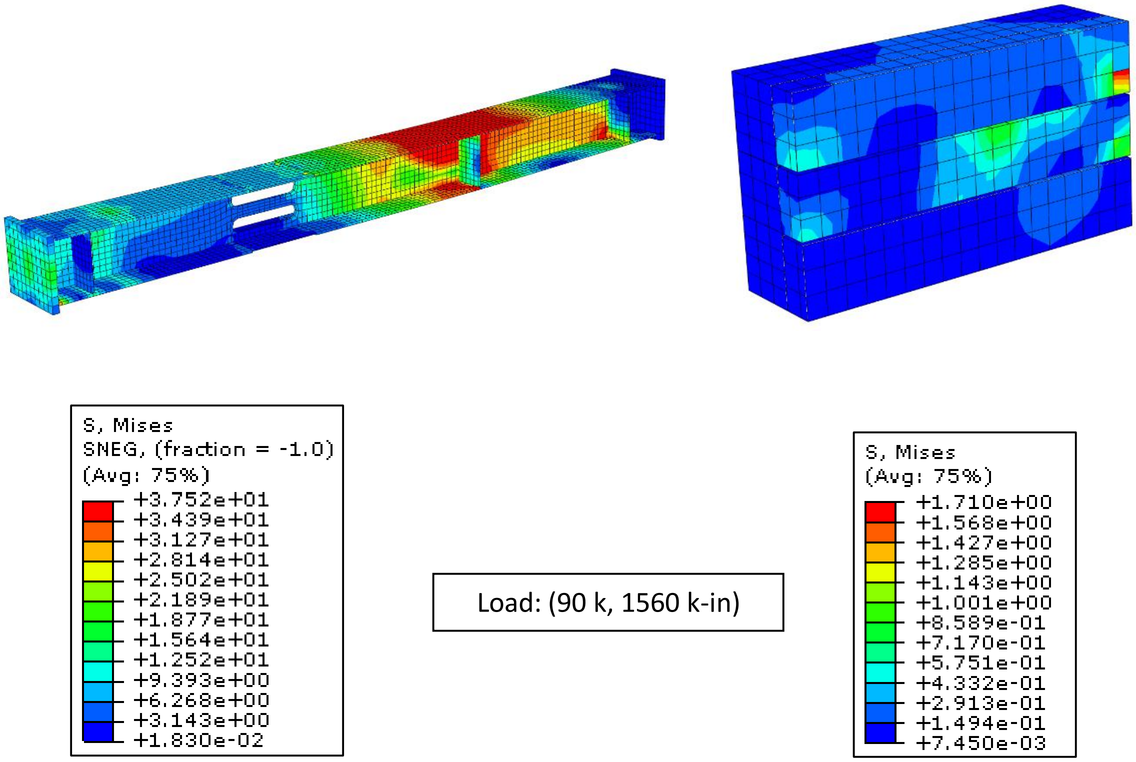

Figure 6.24 (90 k, 1560 k-in) Model 2 stress contours

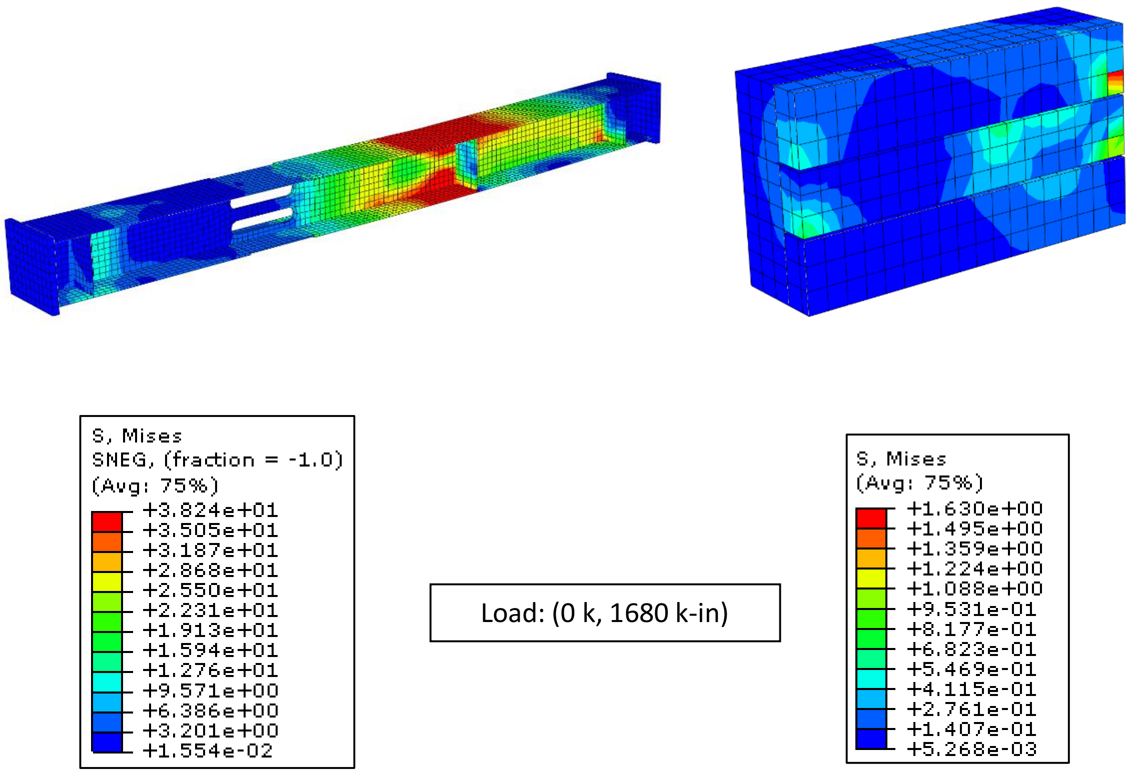

Figure 6.25 (0 k, 1680 k-in) Model 2 stress contours

Model 3 Results

Model 3 consisted of the same material properties of Model 2, but varied in geometry with a reduced retrofit cross section, as shown in Figure 6.26. The cross section was reduced by 10 inches in width and height over the experimental test cross section of 30”x30”. The same five loading ratios were used from Model 2 to analyze Model 3.

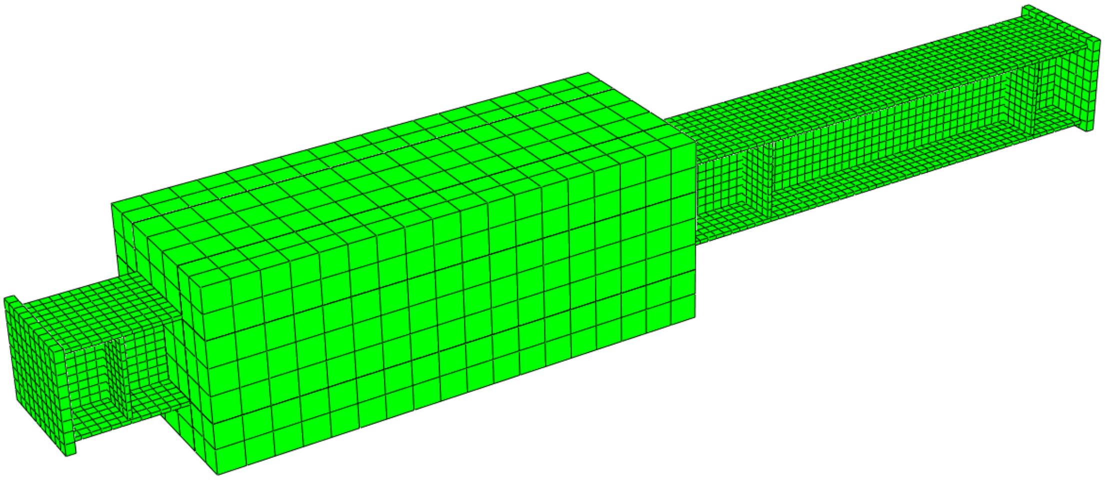

Figure 6.26 Model 3 3-D rendering

The results of the five different analyses are presented in Table 6.4 and Figure 6.27. For this model, Bond 2 was utilized to reach the plastic limit of the pile. The bond required for Model 3 fell between the bonds observed in Model 1 and Model 2.

Table 6.3 Model 3 loading ratios and results

Load Point		Base Section		Deteriorated Section		Bond* (ksi)
Axial (k)	Moment (k-in)	Axial (k)	Moment (k-in)	Axial (k)	Moment (k-in)	
446	0	448	0	178	0	0.308
357	432	357	432	133	40	0.248
236	996	237	990	82	81	0.165
90	1560	93	1555	28	107	0.066
0	1680	0	1680	0	114	0

*Based on difference of Base and Det. section axial loads divided by the embedded length.

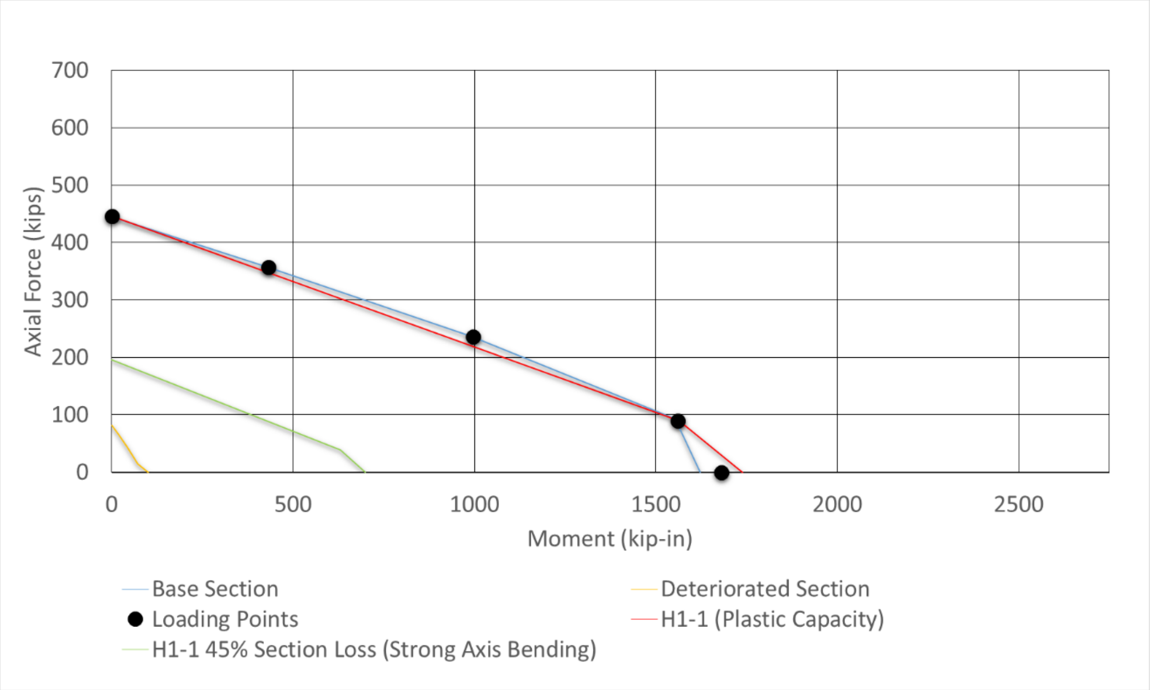

Figure 6.27 Model 3 interaction diagram with loading ratios and results

Figures 6.28 through 6.32 shows the stress contour results for the five loading ratios. As with Model 1 and Model 2, the first two loading ratios required three inch thick bearing plates to eliminate failure of the bearing plate prior to reaching the desired load.

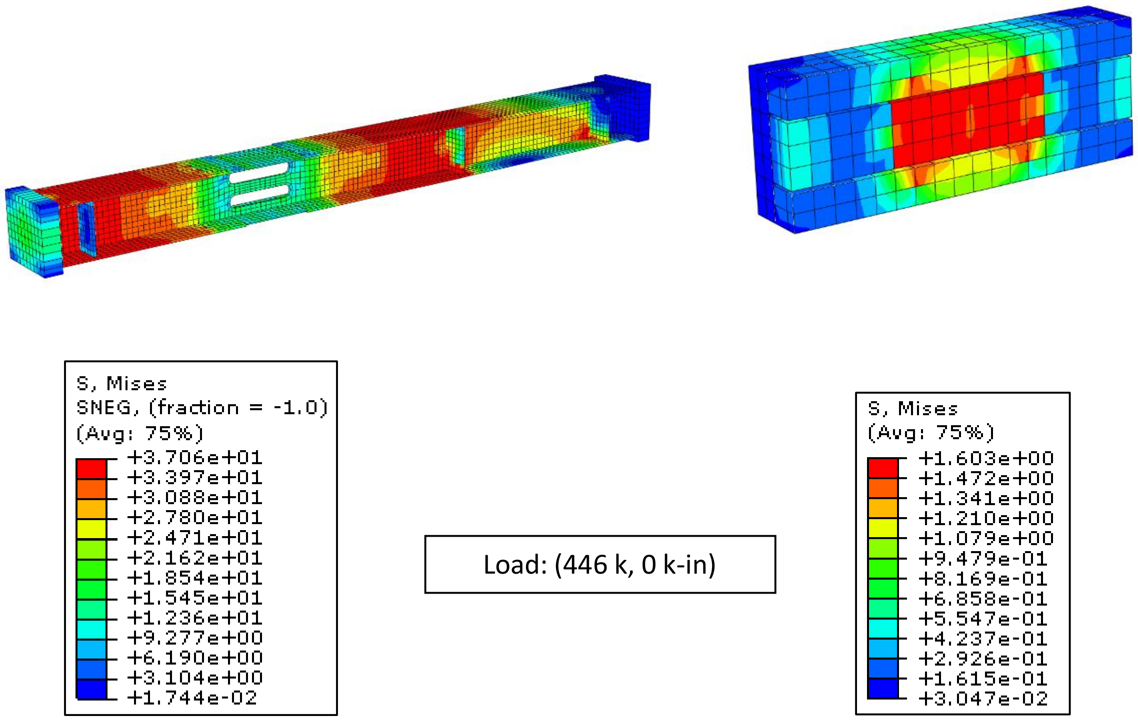

Figure 6.28 (446 k, 0 k-in) Model 3 stress contours

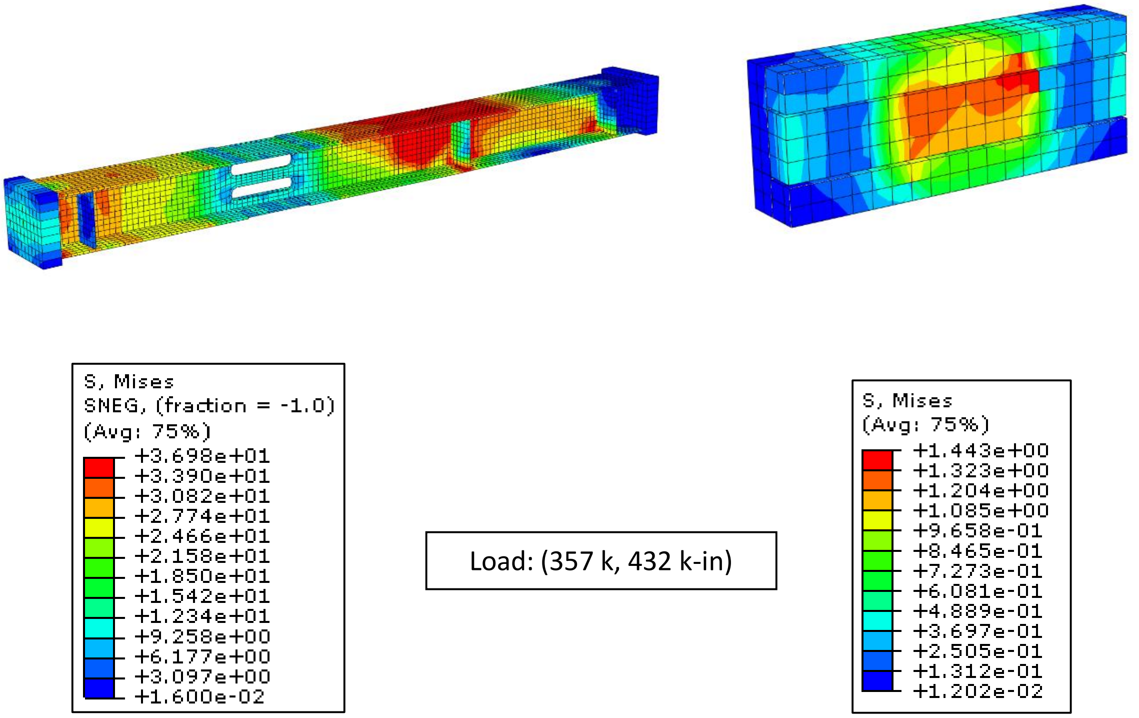

Figure 6.29 (357 k, 432 k-in) Model 3 stress contours

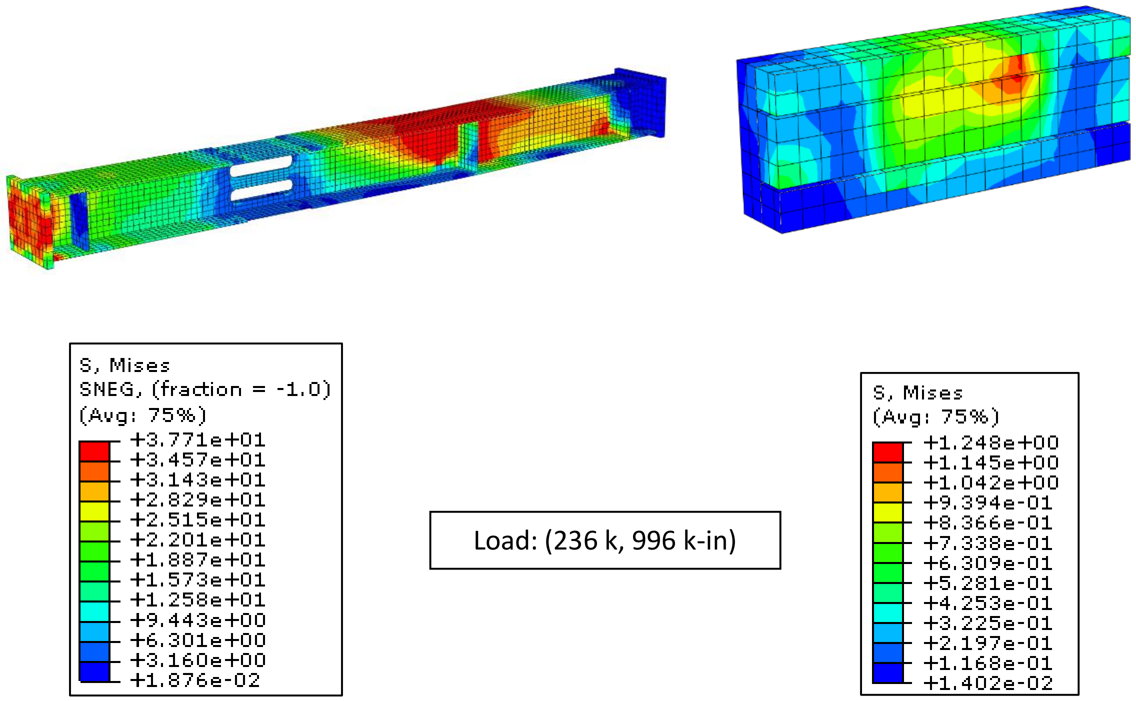

Figure 6.30 (236 k, 996 k-in) Model 3 stress contours

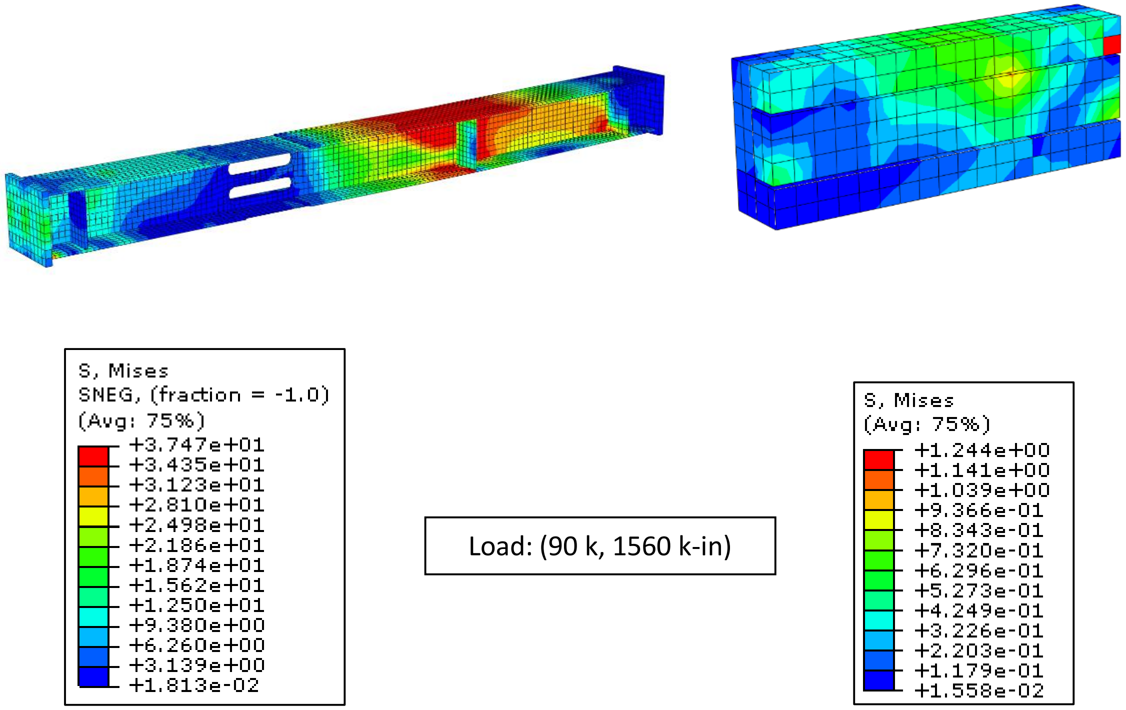

Figure 6.31 (90 k, 1560 k-in) Model 3 stress contours

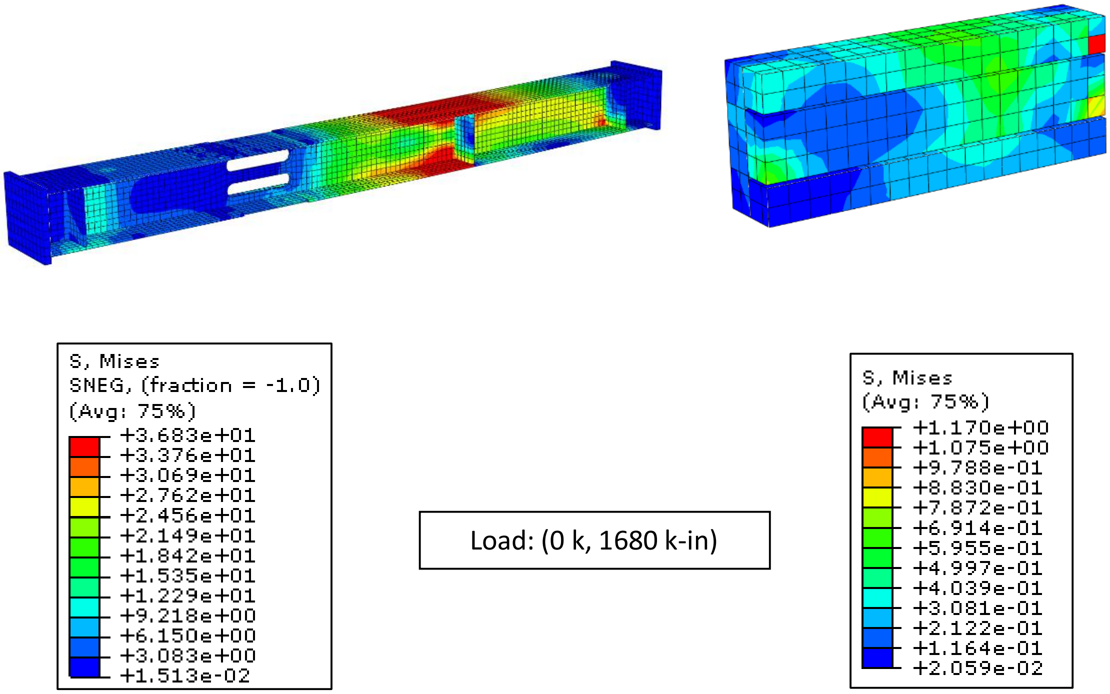

Figure 6.32 (0 k, 2700 k-in) Model 3 stress contours

Model 4 Results

Model 4 (Figure 6.33) further reduced the cross section of the retrofit from Model 3. The concrete was placed in the void between the flanges of the pile. This infilled model was developed to determine what sort of interaction would be required between the steel and concrete if the minimum amount of concrete was applied for the same length of retrofit as in the other models.

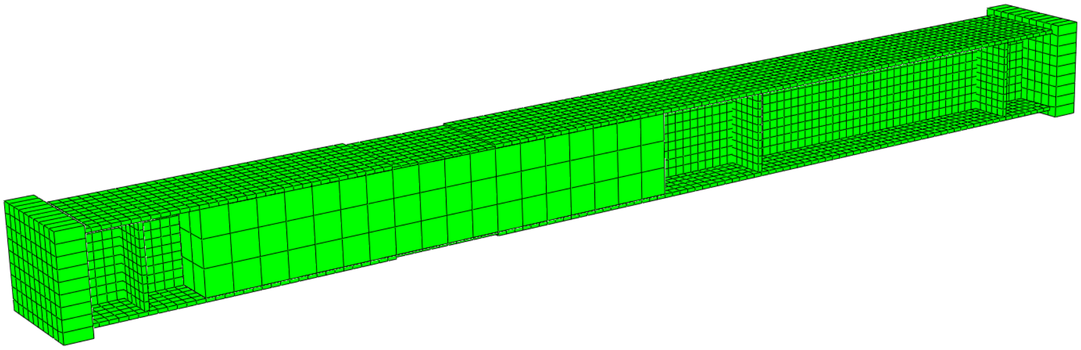

Figure 6.33 Model 4 3-D rendering

Model 4 required Bond 3 for its bond representation, Bond 3 used a tied contact for the length of the retrofit. The results, as presented in Table 6.5 and Figure 6.34, show that the bond representation is sufficient to transfer the load around the deteriorated section for all but the first loading point.

Table 6.5 Model 4 loading ratios and results

Load Point		Base Section		Deteriorated Section		Bond* (ksi)
Axial (k)	Moment (k-in)	Axial (k)	Moment (k-in)	Axial (k)	Moment (k-in)	
446	0	414	0	216	0	0.168
357	432	357	417	169	196	0.159
236	996	237	973	108	356	0.109
90	1560	93	1544	29	576	0.054
0	1680	0	1680	-32	686	0.027

*Based on difference of Base and Det. section axial loads divided by the embedded length.

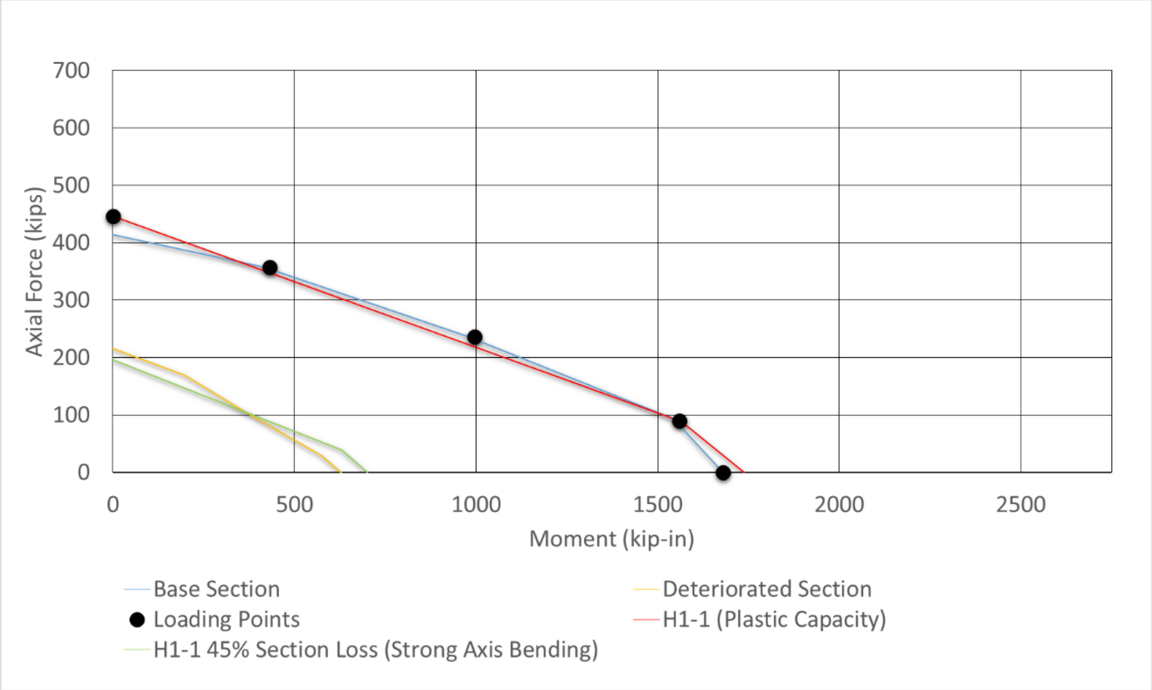

Figure 6.34 Model 4 interaction diagram with loading ratios and results

The bond was modeled with a contact that assumed no slip, and did not allow separation. This is unrealistic as the deteriorated section would likely buckle outward with insufficient load transfer and the concrete would provide limited restraint against that failure. As can be seen in Figures 6.35 through 6.39, the deteriorated section flanges experience a significant amount of stress indicating a low stress transfer to the concrete. This was confirmed in looking at the required bond values, even with the tied condition, they were the lowest of all the models.

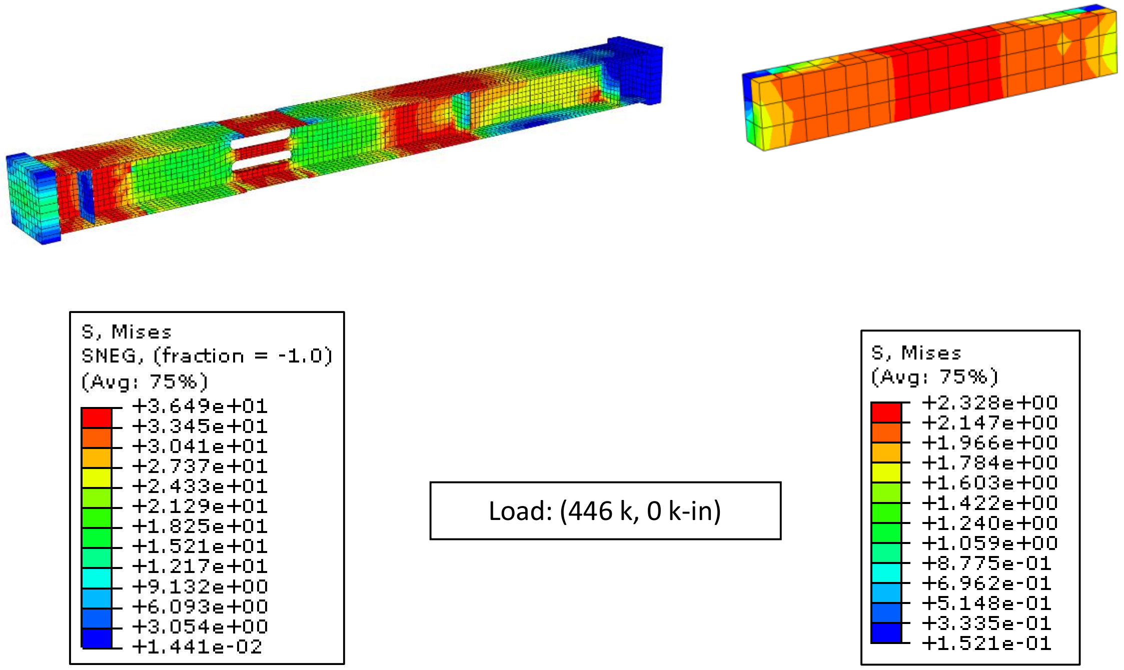

Figure 6.35 (446 k, 0 k-in) Model 4 stress contours

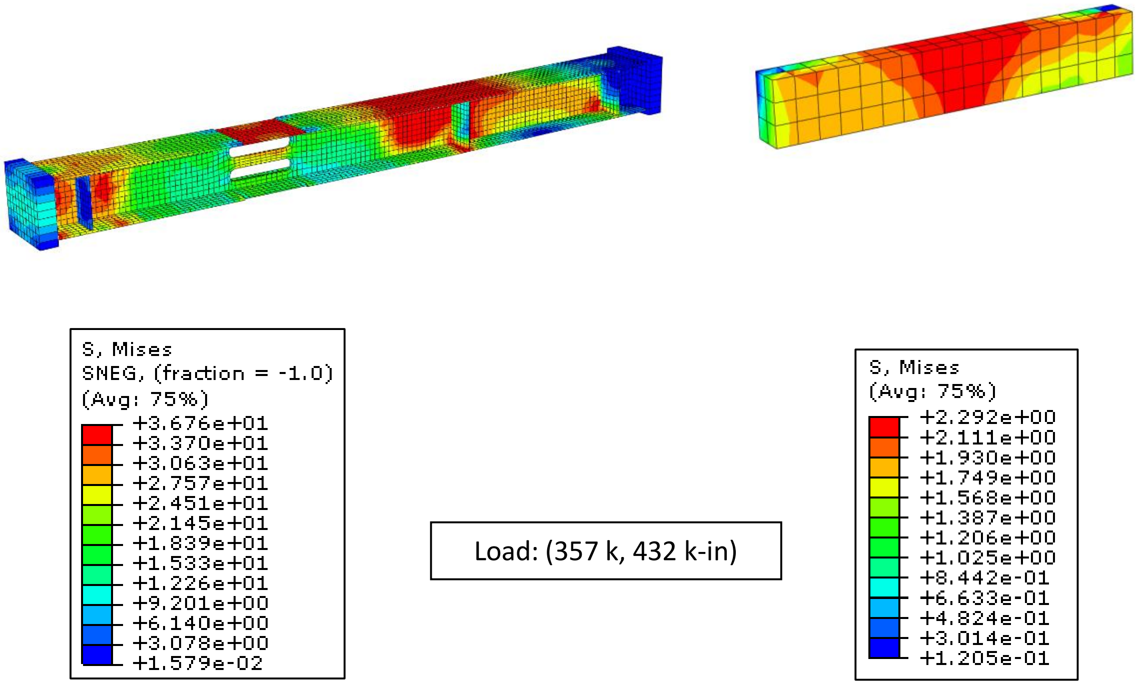

Figure 6.36 (357 k, 432 k-in) Model 4 stress contours

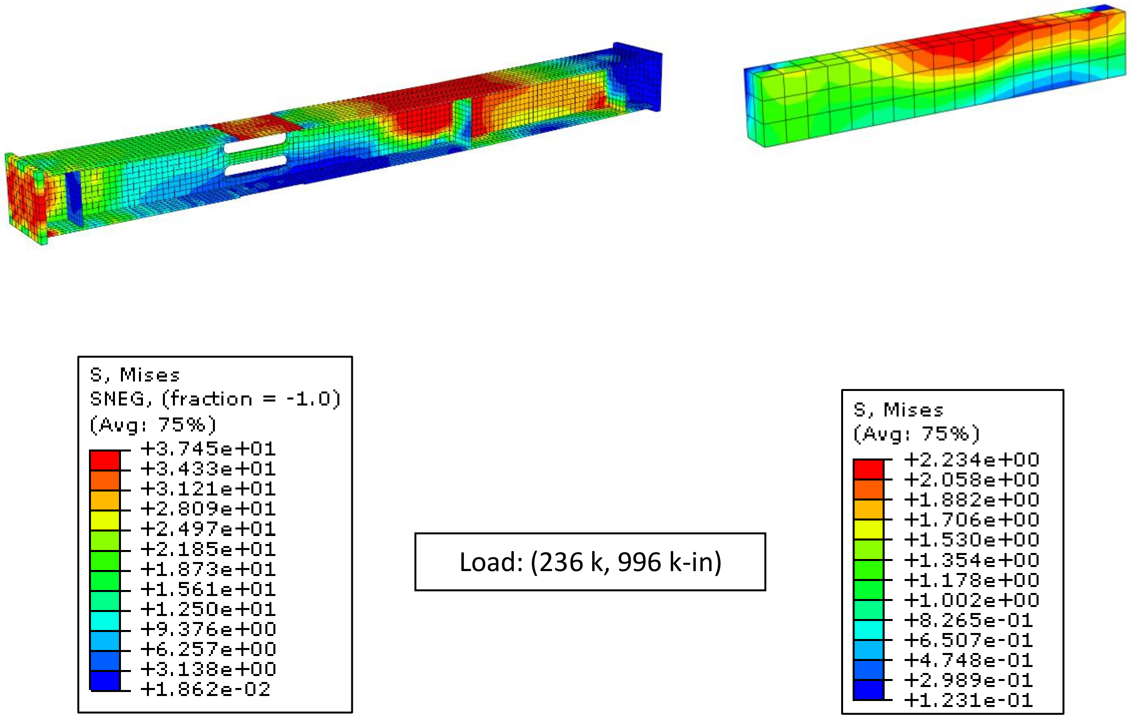

Figure 6.37 (236 k, 996 k-in) Model 4 stress contours

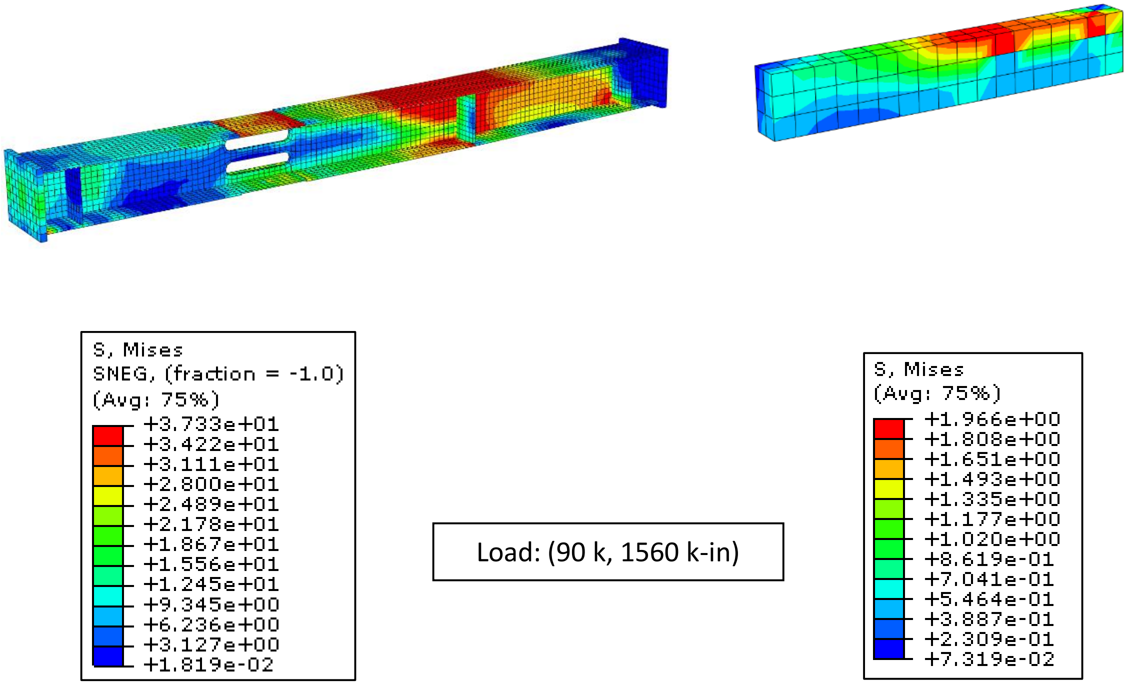

Figure 6.38 (90 k, 1560 k-in) Model 4 stress contours

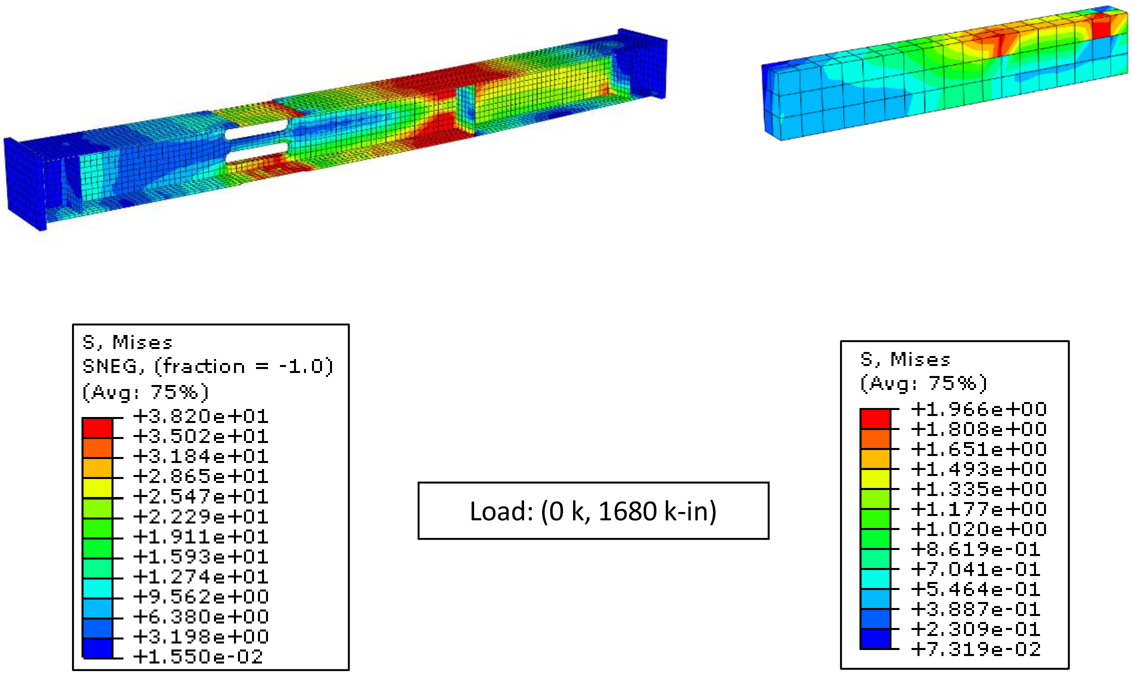

Figure 6.39 (0 k, 1680 k-in) Model 4 stress contours

6.4 COMPUTATIONAL MODELING SUMMARY

The results from the computational study provided greater insight into the bond required to reach the capacity of the steel at each loading ratio, as well as the need for improvement on bond representation. The bond strength required varies based on the ratio of axial to moment loading. As the axial share of the combined loading increases, more bond is needed to transfer the load. The bond value also increased in the models with higher strength concrete and steel, this was due to the increase loading that was applied.

From the analyses, with the same retrofit cross section, the reduced material strength would still be sufficient to transfer the load and reach the plastic limit of the pile. Model 3 was also capable with an increased tied contact. Model 4 would likely require shear studs or a type of anchor to secure the flanges to the concrete and eliminate buckling, specifically at the deteriorated section.

The bond is the largest concern in these analyses and as discussed in previous sections, a parameter with limited confidence when consulting AISC (2011) and AASHTO (2012). Bond behavior will ultimately govern the capacity of the retrofit, so additional testing is needed to establish typical expected and dispersions of bond values.

CHAPTER 7 DISCUSSION/CONCLUSION

The experimental portion of this research validated the restoring capacity of the Nebraska Department of Roads' (NDOR) reinforced concrete encasement retrofit for corroded steel HP piles, for the material strengths tested. Further investigation into the bond interaction of the concrete to the steel as well as further refinement of the design capacity are recommended. Below are the bulleted conclusion highlights, followed by more detailed discussion.

- The NDOR concrete encasement retrofit proved to be sufficient in restoring the capacity of the pile
- A greater than anticipated steel-concrete bond stress was observed.
- The computational study suggest that a smaller retrofits could provide similar benefits with reduced material strengths
- Additional testing is needed to establish typical expected and dispersions of bond values.
- The use of installed shear studs, or welded angles as load transferring mechanisms could greatly improve the reliability of the repair.

In both the abutment and pile bent cases, the retrofitted piles were restored to full capacity and experienced similar limit states to those of the non-deteriorated piles. The local failures seen in the deteriorated sections under the deteriorated cases were eliminated in the retrofitted test. Additionally, bond stresses were calculated at values much higher than anticipated encouraging further investigation.

In comparison to the other retrofits mentioned in the literature review, NDOR provides a retrofit that is capable of restoring full capacity to the pile and is relatively simple to implement. Maintenance personnel are familiar with concrete, and the installation process currently employed for this retrofit does not require additional training over what is already required of the crews. A closer look at cost-efficiency and further efforts to improve the design could yield a competitive alternative to the newer FRP materials that are being advertised.

The bonding mechanism between the steel and concrete was further explored with a computational study. The bond representation provided a better understanding of the influence of the type of loading on the concrete and the pile. From the models, as the moment increases the normal pressure interaction developed between the steel and concrete at the slip interface, or bearing, is significant in transferring load. This normal interaction between the materials is a simple and largely understood means of transferring load. The bond is subject to many circumstances and is likely to vary from one retrofit to the next. Consideration should be given to making use of an installed bearing mechanism (i.e. welded channels or angles, or shear studs) to improve load transfer for the loading ratios with higher axial demand. The use of such a bearing mechanism could greatly improve the reliability of the repair. This could also lead to reductions in the cross section of the retrofit, reducing unnecessary dead load and material. Further studies would be required to investigate the best way to implement such improvements.

The current retrofit employed by NDOR proved to be sufficient in restoring the capacity of the pile in the experimental study with the given material strengths. The computational study showed that smaller, retrofits could provide similar benefits, if sufficient bonds strength at the steel-concrete shear interfaces are achieved in the field. Further information and studies are needed to improve the understanding of the bond between steel encased by concrete. With an improved understanding of the bond capacity and its reliability, the current retrofit design can potentially be simplified for future applications.

CHAPTER 8 REFERENCES

Ainge, Steven W. (2012) "Repair and Strengthening of Bridge Substructures" Master's Theses (2009 -).Paper 173. http://epublications.marquette.edu/theses_open/173

American Association of State Highway and Transportation Officials. (2012). *AASHTO LRFD bridge design specifications, customary U.S. units.*

American Institute of Steel Construction. (2011). *Steel construction manual.*

Delaware Department of Transportation. (2012). *Bridge Manual.*

Florida Department of Transportation, Office of Maintenance. (2011) *Bridge Maintenance and Repair Handbook.*

Georgia Department of Transportation, Office of Bridge and Structural Design Bridge Maintenance Unit. (2012). *Bridge Structure Maintenance and Rehabilitation Repair Manual.*

Liu, Xiangdong. (2003). Rehabilitation of steel bridge members with FRP composite materials.

National Cooperative Highway Research Program, A.G.Lichtenstein and Associates. (1998). *Manual for bridge rating through load testing.* Washington, D.C.: Transportation Research Board, National Research Council.

Nebraska Department of Roads, Bridge Division. (2014). *Bridge Office Policies and Procedures.*

Shama, A.A., Mander, J.B., Blabac, B.B., & Chen, S.S., Multidisciplinary Center for Earthquake Engineering Research (U.S.). (2001). *Experimental investigation and retrofit of steel pile foundations and pile bents under cyclic lateral loading*. Buffalo, N.Y.: Multidisciplinary Center for Earthquake Engineering Research.

Shi, C. (2014). Numerical investigation of H-shaped short steel piles with localized severe corrosion. *Engineering Structures, 73*, 114-124.

United States, Department of the Army. (1991). *Pile construction.* Washington, DC: Headquarters, Dept. of the Army.

U.S. Department of Transportation, Federal Highway Administration. (2013). *National Bridge Inventory.*

Vijay, P.V., Clarkson, J. D., GangaRao, H. V., Soti, P. R., & Lampo, R. (2014). *FRP Composites for Rehabilitation of Hydraulic Structures*. Department of Civil and Environmental Engineering and Constructed Facilities Center, West Virginia University, and US Army Corps of Engineers.

Wan Baolin, Wisconsin Department of Transportation, Research Coordination Unit, Wisconsin Highway Research Program, Marquette University, Department of Civil, Construction and Environmental Engineering. (2013). *Procedures, cost and effectiveness for deteriorated bridge substructure repair*. Madison, WI: Wisconsin Highway Research Program.

Wipf, T. J., Iowa Highway Division, Iowa Highway Research Board, Iowa State University, Department of Civil & Construction Engineering. (2003). *Evaluation of appropriate maintenance, repair and rehabilitation methods for Iowa bridges*. Ames, Iowa: Dept. of Civil & Construction Engineering, Iowa State University.

APPENDIX A OTHER LOADING RATIOS CONSIDERED

A major component of the experimental design was determining the loading that the piles would be subjected to during the test. Bridges are unique, and the load transferred to the substructure depends on the geometry, material, and location. Determination of the loading could be based on any number of parameters. Through discussions with the TAC, it was decided to use an internal loading combination comprised of 80% axial and 20% moment. For completeness though, the remainder of this section will explain the other scenarios that were developed and considered.

The first loading ratio was based on the U.S. Department of Transportation, Federal Highway Administration’s National Bridge Inventory (NBI, 2013) data for Nebraska. The NBI (2013) data was filtered to bridges with a length less than 160 feet and greater than 20 feet. From discussions with senior faculty, most bridges of interest to this project would likely be less than 160 feet. Nebraska has a large number of box culverts, therefore anything less than 20 feet was filtered from the data. With this range extracted from the database, other details of these bridges were considered. This included number of spans, maximum span length, and bridge width. A worst case bridge scenario was developed from the data using maximums for width, length, and maximum span. Table A-1 indicates that most bridges were built around 1979 with two lane. The average number of spans was used to meet the length and maximum span selected. The remaining geometry of the bridge was determined by assuming a typical bridge deck thickness of eight inches and unit weight of 150 pounds per square foot for concrete. With the geometry determined, the dead load of the deck was calculated. From the NBI (2013) data for Nebraska, 92% of bridges are either constructed with steel or concrete girders. Both were considered when calculating the total dead load. The remaining loads considered were thermal expansion/contraction and live load.

Table A - 1 Nebraska bridge data summary (NBI, 2013)

	Average	Maximum	Minimum	Std. Dev.
Width (ft)	14	70	10	6
Length (ft)	53	160	20	29
Spans	3	10	1	1
Max span (ft)	22	90	5	11
Year built	1979	2012	1914	20
Traffic Lanes	2	12	1	1

With all loads determined, a spreadsheet was developed to allow for iteration on the number of girders and piles. Assumed girder sizes were used and pile spacing was limited to 10 feet. With a few iterations of these parameters, the expected loading was anywhere from 100 kips to 180 kips of dead load per pile. The largest thermal displacement was expected to be approximately half an inch and would likely cause about 15 k-ft in moment for the abutment case. From the end of the thermal load, the live load was applied. Based on AASHTO (2012) guidance, the live load (braking force included) was taken as a lower bound slope of 3.75 k-ft per kip. The live load was also considered without the thermal load as another option, and also without the braking forces. This resulted in a fairly target large area, shown in Figure A-1 as the grey highlighted area, along the pile’s interaction curve to choose the targeted loading from.

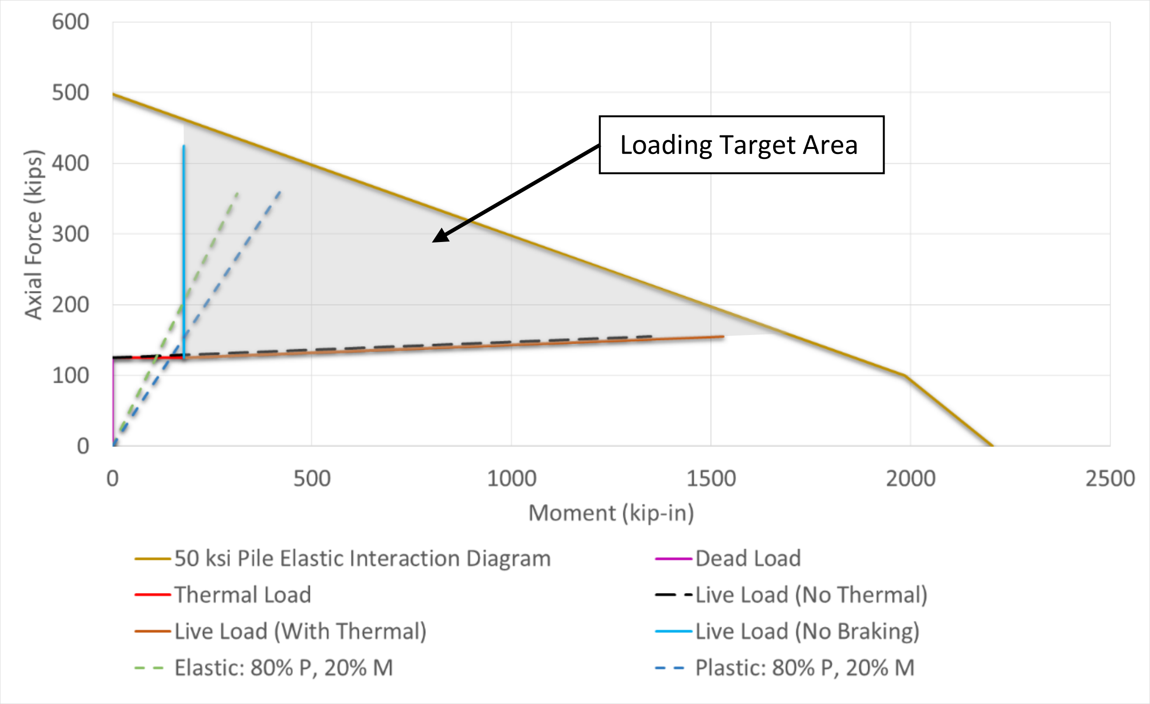

Figure A - 1 Axial vs. moment loading scenarios

The second loading scenario was based on the yield stress of the section being split 20% moment and 80% axial. This resulted in a moment that was slightly less than the 80/20 calculations done based on area, but yielded the same axial force. This becomes apparent when looking at the equations below as the axial force equation simplifies to the same equation for both cases

80/20 based on stress

$$Moment = 20\% * f_y * \frac{I_x}{d/2}$$

$$Axial\ Force = 80\% * f_y * A_g$$

80/20 based on area

$$Moment = f_y * t_m * b_f * (d - t_m)$$

$$t_m = \frac{A_g * 20\%}{b_f * 2}$$

$$Axial\ Force = f_y * \left(A_g - t_m * b_f * 2\right) = 80\% * f_y * A_g$$

As was stated before, the loading was based on the area being divided to handle 80% axial force and 20% moment. This loading ratio was within the range presented from the NBI (2013) data and closer to a middle ground in comparison to the stress based 80/20 loading scenario.

APPENDIX B REINFORCEMENT DETAILS

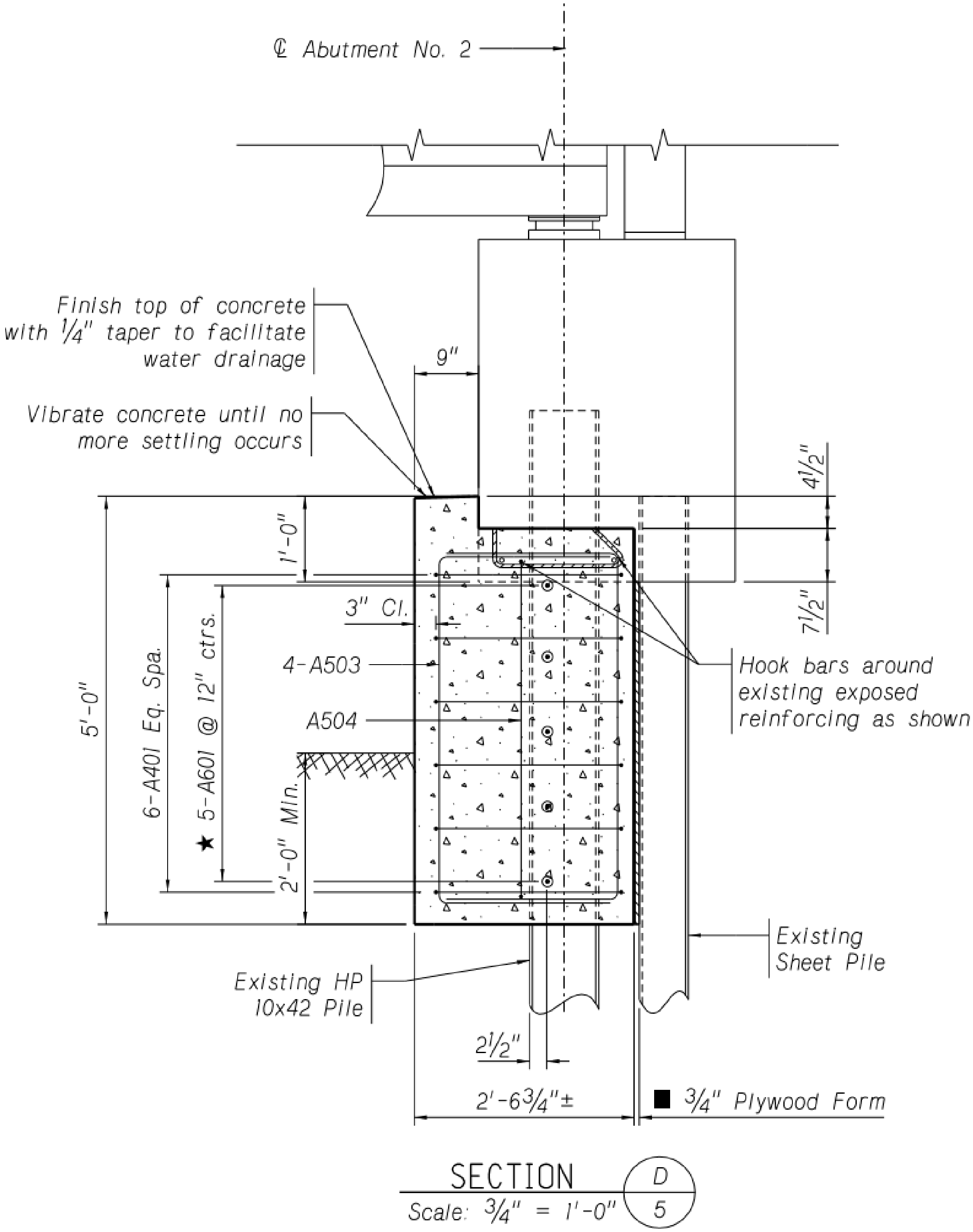

Figure B-1 Section view detail of NDOR concrete retrofit

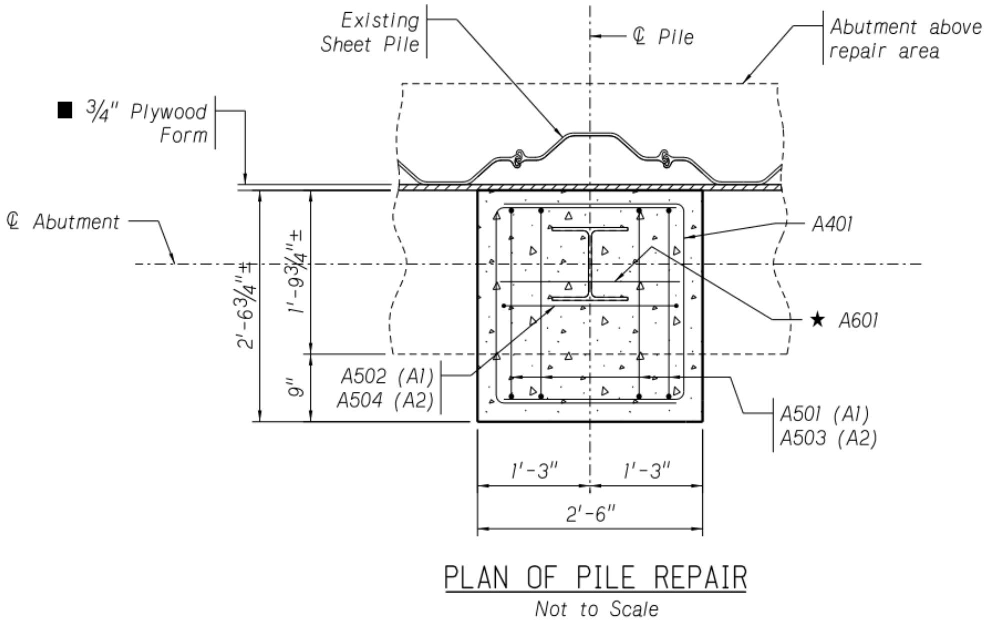

Figure B-2 Plan view of NDOR concrete retrofit

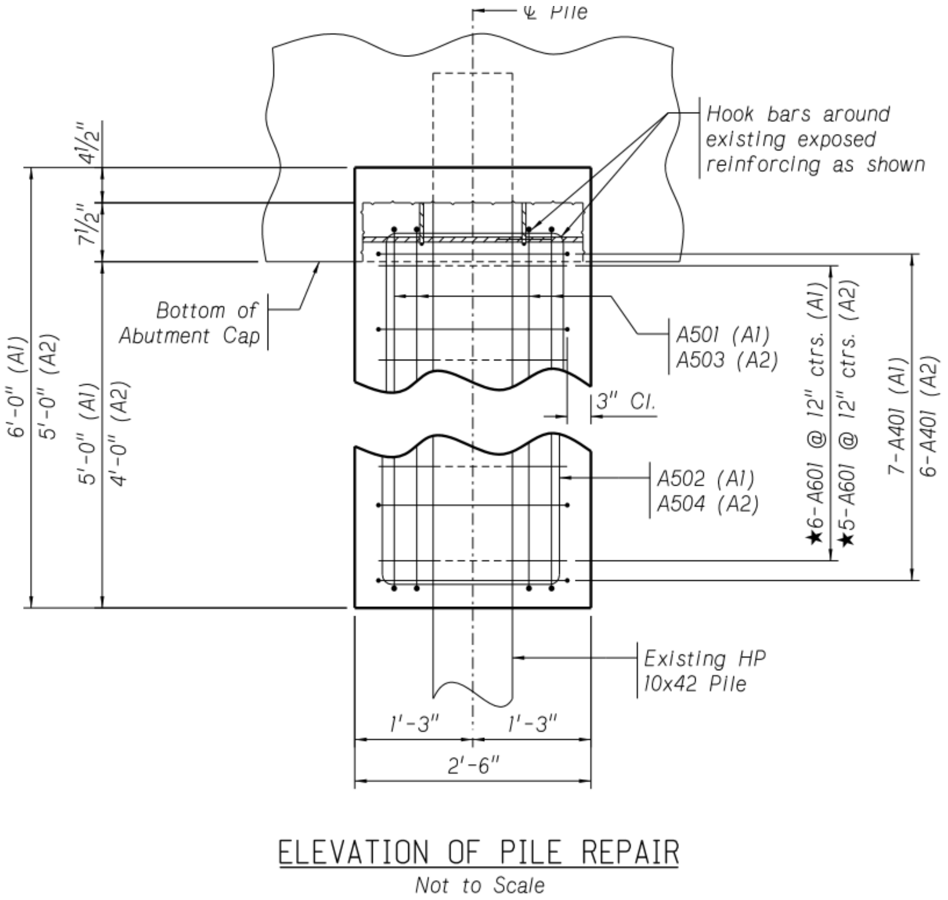

Figure B-3 Elevation view of NDOR concrete retrofit

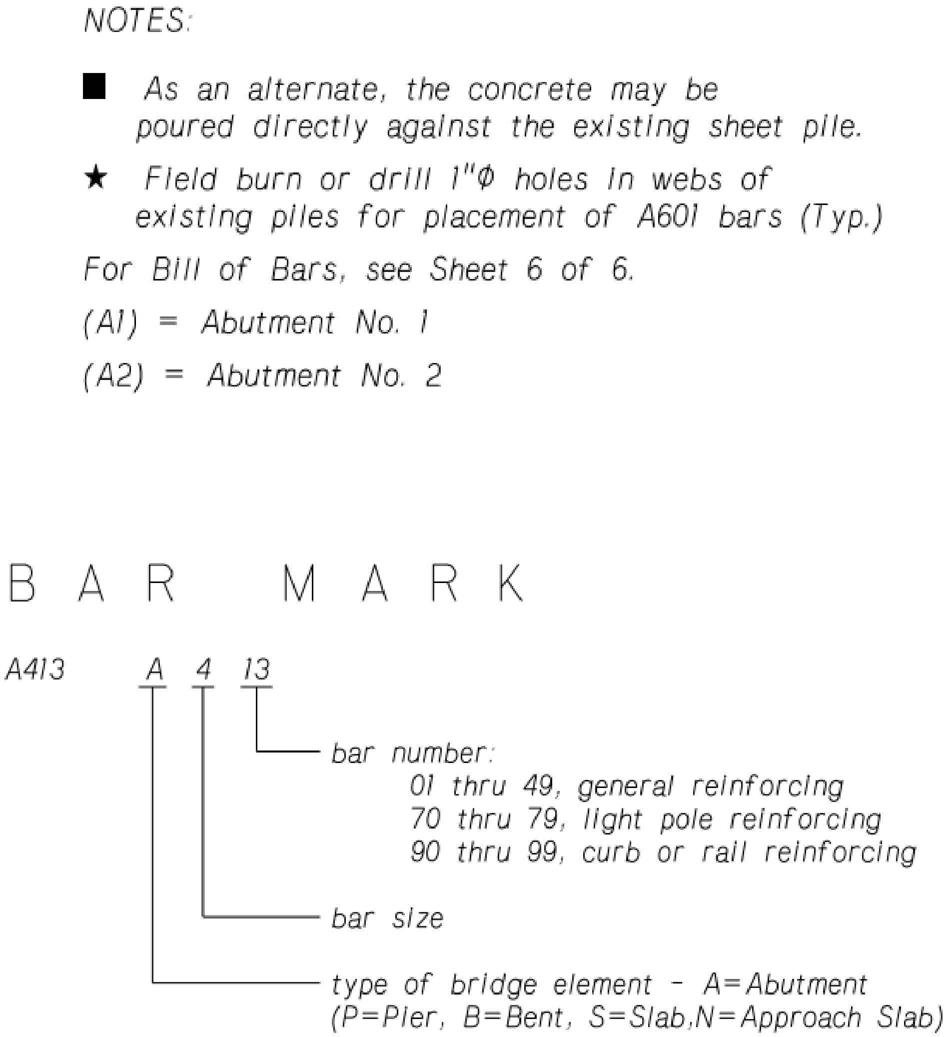

NOTES:

■ As an alternate, the concrete may be poured directly against the existing sheet pile.

★ Field burn or drill 1"Φ holes in webs of existing piles for placement of A601 bars (Typ.)

For Bill of Bars, see Sheet 6 of 6.

(A1) = Abutment No. 1

(A2) = Abutment No. 2

BAR MARK

Figure B-4 NDOR rebar notes

APPENDIX C ADDITIONAL PLATE STEEL DETAIL

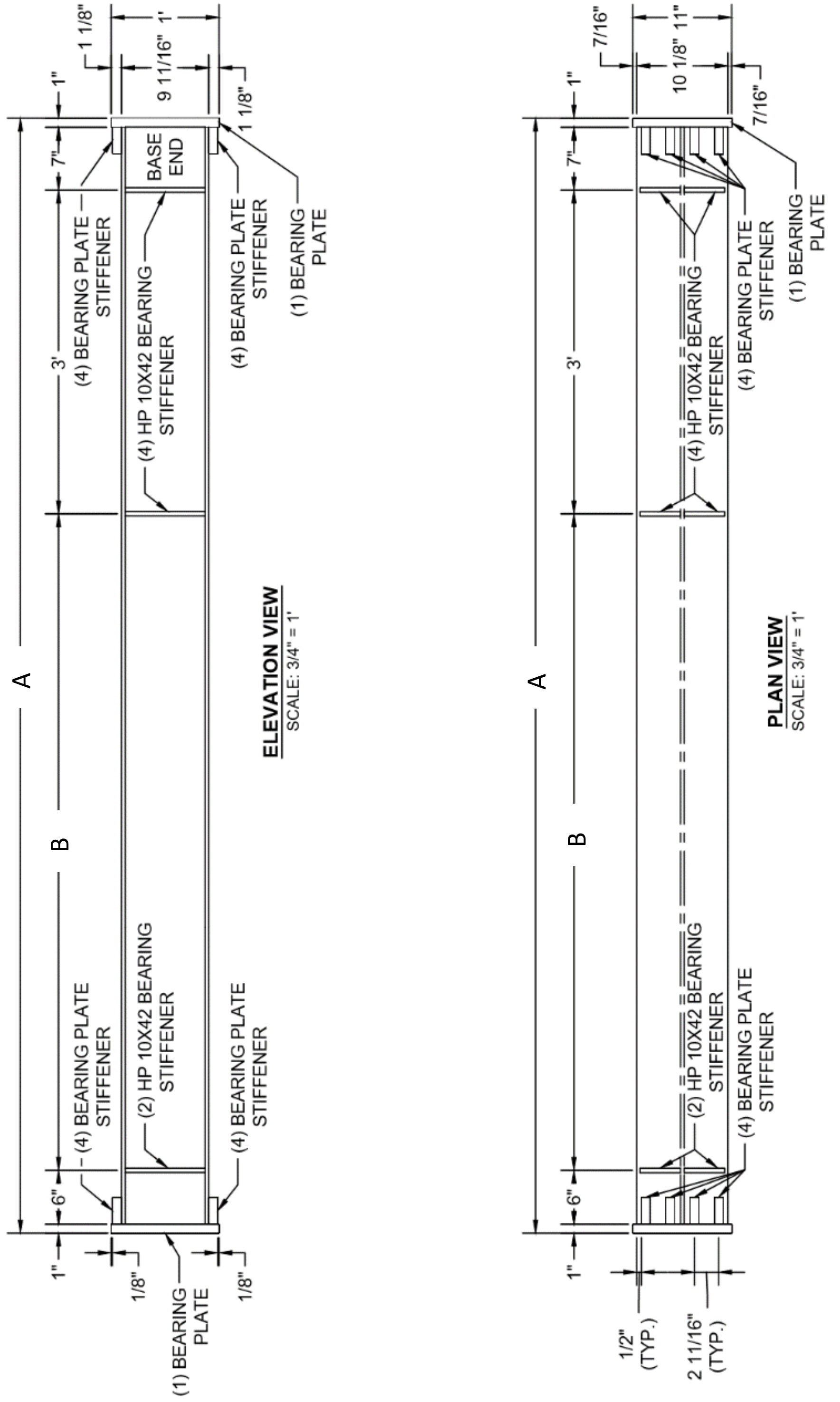

Note:

	Abutment	Pile Bent
A	10’-4”	19’-4”
B	6’-1”	15’-1”

Figure C-1 Additional plate steel detail